博士 (工学) 学位論文

Study on Green Monopropellant Propulsion with Discharge Plasma System

(放電プラズマシステムを用いた低毒性一液式宇宙推進機に関する研究)

首都大学東京大学院
システムデザイン研究科
システムデザイン専攻 航空宇宙システム工学域

Asato Wada
和田 明哲

平成 30 年 (2018 年) 3 月

Study on Green Monopropellant Propulsion with Discharge Plasma System

by

Asato Wada

M.Eng., Aerospace Engineering,
Tokyo Metropolitan University, 2015
B.Eng., Aeronautical and Astronautical Engineering,
Tokyo Metropolitan College of Industrial Technology, 2013

A DISSERTATION
SUBMITTED TO THE DEPARTMENT OF AEROSPACE ENGINEERING
IN PARTIAL FULFILLMENT OF THE REQUIREMENTS
FOR THE DEGREE OF
DOCTOR OF PHILOSOPHY IN ENGINEERING
AT THE
TOKYO METROPOLITAN UNIVERSITY

March 2018

Signature of Author_____

Department of Aerospace Engineering

February 2, 2018

Certified by_____

Haruki Takegahara, Ph.D.

Professor, Tokyo Metropolitan University

Chair, Thesis Committee

Certified by_____

Hironori Sahara, Ph.D.

Professor, Tokyo Metropolitan University

Member, Thesis Committee

Certified by_____

Takashi Sakurai, Ph.D.

Associate Professor, Tokyo Metropolitan University

Member, Thesis Committee

Certified by_____

Keiichi Hori, Ph.D.

Professor, Institute of Space and Astronautical Science,

Japan Aerospace Exploration Agency

Member, Thesis Committee

Study on Green Monopropellant Propulsion with Discharge Plasma System

by

Asato Wada

Submitted to the Department of Aerospace Engineering

in Partial Fulfillment of the Requirements for the Degree of

Doctor of Philosophy in Engineering

at the Tokyo Metropolitan University

Abstract

Green monopropellants for space propulsion system of spacecraft have been continuously developed and researched in the world. Replacements of conventionally used hydrazine have been called green monopropellant because they have lower toxicities than hydrazine. In Japan, one green monopropellant, called hydroxylammonium-nitrate (HAN) based monopropellant SHP163, has been developed by ISAS/JAXA. This monopropellant is thus storable as a liquid under a vacuum condition and has higher density specific impulse than hydrazine. Additionally, the mass of a propulsion system can be reduced while maintaining the same delta-V. However, when employing HAN based monopropellants in a conventional solid catalyst thruster (reaction control system, RCS), there are technical problems in environments with higher operating temperatures and atmospheric oxidation such that the catalyst sinters, reduces, and then deactivates. To solve these problems, this research is an effort to develop a HAN-based monopropellant thruster with an alternative ignition system that uses discharge plasma. The objective of this thesis is to design and build the laboratory model thruster for the HAN-based monopropellant, and to evaluate the performance characteristics of the thruster.

First, an ignition system that uses discharge plasma of noble gas, called discharge plasma system has been proposed. To evaluate the SHP163 ignition characteristics of discharge plasma system, the effects of geometric swirl number on the ignition characteristics were evaluated under atmospheric conditions. It is concluded that the geometric swirl number has strong effects on the plasma distribution, the propellant ignition probability, and the ignition delay time. At an argon mass flow rate of 0.15 g/s and SHP163 mass flow rate of 0.3 g/s, the continuity of the exhaust flame from downstream of the discharge plasma system with a geometric swirl number of 6.7 was confirmed at sea level condition.

Next, to design and build of the HAN-based monopropellant thruster, the effects of the SHP163 mass flow rate and combustion chamber characteristic length (L-star) on combustion characteristics were experimentally evaluated by measuring thrust and pressure under ambient pressure of 1.2 kPa. As a result, it was observed that a

shorter L-star increased the characteristic exhaust velocity efficiency (i.e. reactivity). Additionally, for all SHP163 feed pressure (i.e. SHP163 mass flow rate of 1N-class), there were no failed ignition cases with a single-hole injector. It was found from the result that a maximum thrust of 0.37 N at nozzle expansion ratio of 1 was achieved with power consumption of 527 W and an SHP163 mass flow rate of 0.34 g/s, in conjunction with characteristic exhaust velocity (C-star) efficiency of 98%. In this experiment, it was obtained the consumed power at combustion of SHP163 for 15 s was similar to preheating energy of catalyst, and the hot firing tests of the thruster was demonstrated the operation successfully under vacuum condition.

Finally, to evaluate the performance characteristics of the thruster and spectra of exhaust plume, the vacuum firing tests of a laboratory model thruster with discharge plasma system using SHP163 have been conducted. Additionally, the reactivity evaluation of SHP163 by the discharge plasma has been proposed using C-star efficiency. As a result, at the feed pressure of 0.6 MPa, a maximum thrust of 0.50 N was achieved with power consumption of 564 W and SHP163 mass flow rate of 0.31 g/s, in conjunction with specific impulse of 109 s, C-star efficiency with argon plasma of 41%, and thrust efficiency of 47%. In addition, it was confirmed that measured thrust was varied from 0.25 N to 0.50 N in a range of SHP163 mass flow rate from 0.09 g/s to 0.31 g/s. Here, at these experiments, the mass flow rate of argon gas is set at 0.15 g/s for plasma generation. Furthermore, in terms of the combustion products of SHP163, the emission spectrums of carbon monoxide, swan band, hydroxyl radical, hydrogen atom, and oxygen atom were observed under vacuum condition. It was confirmed that the characteristic exhaust velocity efficiency tends to be higher at higher spectral intensity (e.g. OH). Moreover, as a result of thruster lifetime-evaluation, at an accumulated firing time of 1646 s, no effect of electrode degradation on the performance of the thruster was observed. Since this study, the green monopropellant propulsion with discharge plasma system has been proposed, and demonstrated under vacuum condition, and the performances of thruster were evaluated.

Acknowledgments

Firstly, I would like to express his sincere gratitude and appreciation to my academic supervisor, Prof. Dr. Haruki Takegahara, for valuable discussion and encouragement in pursuing this study. I would also like to thank my thesis committee members, Prof. Dr. Keiichi Hori (Institute of Space and Astronautical Science, Japan Aerospace Exploration Agency), Prof. Dr. Hironori Sahara (Tokyo Metropolitan University), and Prof. Dr. Takashi Sakurai (Tokyo Metropolitan University), for constructive discussions and encouragement. Without their helpful suggestions and discussions, I could not have accomplished good results throughout the academic program.

To Prof. Dr. Kyoichi Kuriki (Institute of Space and Astronautical Science), Prof. Dr. Junichiro Aoyagi (University of Yamanashi), and Dr. Hiroki Watanabe (Tokyo Metropolitan University), I would like to thank for helpful discussions and technical support throughout this research. I would also like to thank Prof. Dr. Masakatsu Nakano (Tokyo Metropolitan College of Industrial Technology), for valuable guidance and encouragement throughout my student life at the technical college.

I would like to thank Mr. Ryuichi Komatsu for technical support of machine tool. I am also grateful for the cooperation in the laboratory, especially Dr. Toshiaki Iizuka, Dr. Takahiro Shindo, Mr. Yuta Sato, Mr. Sunsuke Kawabata, and Mr. Hiroshi Maeda.

Finally, to my family, Ayako W., Imayo O., Yukari O., Mitsunobu A., Koumei W., Asami W., and Luna W., I would like to thank for supporting me. Without their invaluable support and encouragement, I could not have accomplished this thesis.

Table of Contents

List of Tables

List of Figures

Chapter 1
Introduction

1.1. Conventional Chemical Thruster

A propellant for reaction control system (RCS) thruster has been generally used a hydrazine-based monopropellant or a hydrazine-based bipropellant because the RCS thrusters with the hydrazine-based propellant have a high reliability and a space flight-proven capability [1]. In terms of the bipropellant thruster, monomethyl-hydrazine (CH_3NHNH_2) / nitrogen-tetroxide (N_2O_4) thrusters have the characteristics of specific impulse of 300 s and above, and self-ignition [2]. In contrast, in terms of the monopropellant thruster, hydrazine (N_2H_4) thrusters have been required the use of ignition system (solid catalyst) at the preheating temperature of > 300 °C [3]. However, these hydrazine-based propellants have the characteristics of a high toxicity and a low vapor pressure. Recently, the replacements of conventional hydrazine, called “green propellants”, have been developed because they have lower toxicities than the hydrazine.

1.2. Development Status of Green Monopropellant Thrusters

Since the late 1950s, the replacements of conventional hydrazine have been continuously developed and researched in the United States, Russia, Europe and Asia [4-9]. These replacements for the monopropellant thruster are included a hydrogen peroxide (H_2O_2/H_2O blends), nitrous oxide (N_2O), NOFBX (Nitrous Oxide/Hydrocarbon blends), ammonium Di-nitramide (ADN, $NH_4N(NO_2)_2$) based blends and hydroxylammonium (or hydroxylamine)-nitrate (HAN, NH_3OHNO_3) based blends [5, 6]. The HAN based blends and ADN based blends are the ionic liquid. The ionic liquid (IL) is defined as salts with melting temperatures (i.e. freezing point) below 373.15 K [10]. The characteristics of these monopropellants are a high specific impulse and a high density.

1.2.1. Ammonium Di-Nitramide Based Thrusters

Since the 1970s, ADN was developed by the Zelinsky Institute of Organic Chemistry in Moscow (Russia), and there is a report that one ADN-based propellant was used for Topol-M intercontinental ballistic missile (ICBM) [11].

Since the 1997, ADN-based monopropellants have been developed by the Swedish Space Corporation (SSC), the Swedish Defense Research Establishment (FOA) and the Chalmers University of Technology [12]. In

Sweden, one ADN-based monopropellant, called LMP-103S (Liquid Mono-Propellant-103S), has been developed by SSC. LMP-103S is a liquid mixture of ADN ($NH_4N(NO_2)_2$)/ammonia (NH_3)/water (H_2O)/methanol (CH_3OH) in a ratio of 63/18.4/4.6/14 by weight percentages [13]. To prove the space flight of a 1N-calss ADN based monopropellant thruster with catalyst (HPGP, high performance green propulsion), PRISMA-satellites was launched at Dnepr-1 in June 2010. In PRISMA mission, the operating tests of two 1N-class HPGP thruster was demonstrated by formation flight and rendezvous in space [14, 15]. Recently, one ADN-based monopropellant, called FLP-106 (FOI Liquid Propellant number 106) has been developed by the Swedish Defense Research Agency (FOI) as the candidate of monopropellant thruster for further development [16-18].

1.2.2. Hydroxylammonium-Nitrate Based Thrusters

In United States, One HAN based propellant, called LGP1845 (Liquid Gun Propellant), was developed and researched by the U.S. Army, and then the Integrated High Payoff Rocket Propulsion Technology (IHPRPT) program was initiated at NASA [4, 19]. In the late 1980, LP1846 (XM46), LP1845 and LP1898 were developed for the propulsion system of the satellite [4]. In the late 1990, RK-315E (AF-M315E), RK-618A and RK-315A were developed by the U.S. Air Force Research Laboratory (AFRL) [20, 21]. Since then, the monopropellant thrusters using AF-M315E, called GR-1 (1N-class Green Monopropellant Rocket Engine) and GR-22 (22N-class Green Monopropellant Rocket Engine) have been continuously developed by the Aerojet Rocketdyne [22, 23]. Here, AF-M315E is a liquid mixture of HAN / Water / Hydroxyethylhydrazinium nitrate ($HOCH_2CH_2NH_2NH_2^+NO_3^-$, HEHN [24]) in a ratio of 44.5/11/44.5 by weight percentages [21]. In the Green Propellant Infusion Mission (GPIM) project, the LCH-240 catalyst thrusters (i.e. GR-1 and GR-22) are due to integrate on the payload deck of a Ball Aerospace BCP-100 (Ball Configurable Platform-100) spacecraft bus [25]. Additionally, a 0.5 N-class AF-M315E thruster (BGT-X5) for 1U CubeSat has been developed by the Busek Company, and then the thrusters in a range of thrust-scale from 0.5 N to 5 N have been demonstrated the scalability of catalyst [26].

In Japan, one HAN based monopropellant, called SHP163 (Solution Hori Propellant with methanol of 16.3%), has been developed by the ISAS/JAXA (Institute of Space and Astronautical Science/Japan Aerospace Exploration Agency). SHP163 is a liquid mixture of HAN (NH_3OHNO_3)/ammonium nitrate (NH_4NO_3)/water (H_2O)/methanol (CH_3OH) in a ratio of 73.6/3.9/6.2/16.3 by weight percentages [27]. The 20 N-class catalyst thruster using SHP163 has been developed by ISAS/JAXA [7, 28].

Table 1-1 Characteristic properties of monopropellants.

Propellant	Hydrazine	SHP163	AF-M315E	LMP-103S	FLP-106
Compositions	N_2H_4	NH_3OHNO_3/ NH_4NO_3/ H_2O/CH_3OH (=73.6/3.9/6.2 /16.3wt.%) [27]	NH_3OHNO_3/ H_2O/ $C_2H_9N_3O_4$ (=44.5/11.0/4 4.5wt.%) [3, 21]	$NH_4N(NO_2)_2$/ NH_3/H_2O/ CH_3OH (=63/18.4/4.6/ 14wt.%) [6, 13]	$NH_4N(NO_2)_2$/ H_2O/ CH_3NHCHO (=64.6/11.5/2 3.9wt.%) [16, 17]
Combustion Products [a)]	H_2(67%), N_2(33%), NH_3(<1%)	H_2O(68%), N_2(18%), CO_2(11%), H_2(1%), CO(1%), O_2(1%)	H_2O(59%), N_2(21%), CO_2(9%), H_2(6%), CO(5%)	H_2O(50%), N_2(23%), H_2(16%), CO(6%), CO_2(5%),	H_2O(42%), N_2(26%), H_2(15%), CO(10%), CO_2(7%),
Freezing Point, °C	1.4~2.0 [6, 7]	< − 37 [7]	0 [22]	− 90 [32]	< 0 [6, 16]
Vapor Pressure at 25 °C, kPa	< 1.9 [5, 6]	5.0~6.0(20°C) [33]	1.4 [29, 31]	9.1~13.6 [6, 32]	< 2.1 [6]
Viscosity at 20 °C, mPa·s	1.0 [1]	11.9 [7]	27 [26]	3.9 [32]	3.7 [16]
Density at 25 °C, g/cm^3	1.004 [6]	1.411 [7]	1.465 [31]	1.238 [6]	1.357 [6]
LD50 Oral, mg/kg	60 [7]	500 [7, 33]	550 [30]	750-800 [6]	1270 [6]
LD50 Skin, mg/kg	91 [7]	> 2000 [7, 33]	N/A	N/A	N/A
Adiabatic Flame Temperature [a, b)], °C	596	2043	1982	1599	1727
Characteristic Exhaust Velocity [a, b)], m/s	1209	1417	1423	1356	1355
Specific Impulse [a, b)], s	235	277	275	257	257

a) Value calculated at the following conditions: combustion chamber pressure of 0.4 MPa, ambient pressure of 0 Pa, expansion ratio of 100 under a frozen flow condition.

b) Heat of formation: HAN, −366.5 kJ/mol [34]; ADN, −148.0 kJ/mol [34]; MMF (monomethylformamide, CH_3NHCHO), −247.4 kJ/mol [17]; HEHN, −373.0 kJ/mol.

1.2.3. Characteristics Properties of Monopropellants

The characteristic properties of monopropellants are given in Table 1-1. The values of (a) in Table 1-1 were calculated using NASA computer program CEA (Chemical Equilibrium with Applications) [35]. SHP163 has a glass transition at −37 ºC and density of 1.411 g/cm^3. This monopropellant is thus storable as a liquid under a vacuum condition and has approximately 66% higher density specific impulse than hydrazine. Additionally, the mass of a propulsion system can be reduced while maintaining the same delta-V.

1.2.4. Ignition Methods for Green Monopropellants

The conventional RCS thrusters with hydrazine have been used the solid catalyst (such as S405, Shell405, LCH-207, and LCH-210) [1, 3]. However, the HAN based monopropellants have at the flame temperature above 2000 K, and it is necessary to improve the thermostability of conventional catalyst. Since then, to improve the performance of catalyst, the catalyst for a HAN-based monopropellant AF-M315E, called LCH-240 (5% iridium on hafnium oxide), has been developed by Aerojet-Rocketdyne [36, 37].

Recently, the alternative ignition methods of the catalyst for HAN-based monopropellant, such as spark plug, plasma torch and laser ignition, have been continuously developed and researched in the world. In the United States, the alternative ignition systems have been developed by the Pennsylvania State University, the Digital Solid State Propulsion (DSSP), and the AFRL. At the Pennsylvania State University, a microwave plasma torch ignition system for HAN based and ADN based monopropellant has been developed and researched, and the ignition of the monopropellant in a range of the mass flow rate from 2 to 6 mL/min was confirmed using helium plasma at input power of 500 W [38]. At the DSSP, a pulsed plasma thruster using HAN-based GEM propellant has been developed [29]. At the AFRL, an ignition system using resonant laser at wavelengths in the UV and IR for HAN/HEHN-blends have been developed [39]. In the Malaysia, an electrolytic micro-thruster using DC power supply has been developed and researched, and a maximum thrust of 197 mN was confirmed at the voltage of 45 V and the input energy of 14.7 J [40]. In Japan, the alternative ignition systems have been developed by the Kyushu Institute of Technology, the Nagaoka University of Technology and ISAS/JAXA. At the Kyushu Institute of Technology, 1 kW-class arc plasma torch thruster has been developed, and a maximum combustion chamber pressure of 0.3 MPa was confirmed [41]. At the Nagaoka University of Technology and the ISAS/JAXA, the laser ignition systems for SHP163 and ADN based monopropellant (ADN/MMAN/Urea = 40/40/20 wt.% [42]) have been developed and researched [43, 44]. However, these thrusters with alternative ignition system have not yielded practical applications.

1.3. Objectives of Thesis

When employing HAN-based monopropellants in a conventional reaction control system (RCS) thruster with solid catalyst, there are some technical problems in environments with higher operating temperatures (flame temperature) and oxidizing combustion atmosphere such that the iridium-based and platinum based solid

catalysts (such as S405, Shell405, LCH-207, and LCH-210) sinter and degrade [3, 7]. At lager hydrazine thruster, these similar problems are observed [45]. To solve these problems, in this laboratory, the alternative ignition systems using discharge plasma have been proposed and researched [46, 47]. However, in terms of the reactivity of monopropellant by discharge plasma, there are some technical such that these systems have not been evaluated the requirements for monopropellant thruster, and the reactivity is insufficient by the discharge plasma. In this study, to improve the reactivity of monopropellant, an alternative ignition system that uses discharge plasma of a gas (e.g. Ar, Xe, He and N_2), called discharge plasma system, has been proposed. A discharge plasma is generated from ionized gas using a direct current power supply, and a monopropellant is reacted by joule-heating and thermal decomposition when it comes into contact with the discharge plasma.

The objective of this thesis is to design and built the laboratory model thruster with discharge plasma system for HAN based monopropellant SHP163, and to evaluate the performance characteristics of the thruster. Additionally, the feasibility of HAN-based monopropellant thruster with the discharge plasma system is evaluated. For the stable ignition of monopropellant, it is necessary to evaluate and consider three factors that monopropellant species, input energy, and flow and pressure field. In terms of input energy, power supply was set with the minimum energy for plasma stable generation. In addition, one HAN-based monopropellant, SHP163, was prepared. Thus, in this study, a factor of flow and pressure field was evaluated for HAN-based monopropellant thruster with discharge plasma system. A factor of flow and pressure field is discussed in terms conditions that gas species, gas supply methods, monopropellant supply methods, and combustion chamber design. Additionally, to employ the ignition system for the monopropellants in space propulsion system, it is necessary to consider the requirements that combustion stability, multiple ignition (ignition repeatability), response time, power consumption, and thruster lifetime. To meet the requirements for monopropellant thruster, the following performance of this monopropellant thruster was evaluated in this study.

- Combustion Stability → Long Term Steady State Operation (>5 s)
- Multiple Ignition → Conditions of Ignition Repeatability
- Response Time → Thrust (or Pressure) Rise Time
- Power Consumption → Consumed power for Thruster Operations
- Thruster Lifetime → Electrodes Degradation

1.4. Outline of Thesis

The outline of thesis is organized as follows.

Chapter 2 provides the overview of ignition method using discharge plasma and the concept of chemical reaction by discharge plasma.

Chapter 3 presents the schematic of experimental apparatus and the specifications of measurements.

Chapter 4 presents the results of propellant ignition tests, the effects evaluation of gas injection methods

on generated plasma conditions and SHP163 ignition characteristics, and proposes the discharge plasma system. In terms of both the mass flow rate and the geometric swirl number of the gas injector, the effects on ignition characteristics are evaluated under sea-level.

Chapter 5 presents the experimental results of vacuum firing tests to design and build a thruster with discharge plasma system. In terms of both propellant injector and combustion chamber, the design of thruster is estimated.

Chapter 6 shows the thruster performances that are evaluated by the characteristics exhaust velocity and the emission spectra.

Finally, Chapter 7 summarizes this thesis in terms of a green monopropellant thruster with discharge plasma system.

1.5. Reference in Chapter 1

[1] Price, T. W., and Evans, D. D., "The Status of Monopropellant Hydrazine Technology," Jet Propulsion Laboratory, National Aeronautics and Space Administration Technical Report 32-1227, 15 February 1968.

[2] Butt, A., Propp, C. G., Pitts, H. M., and Sharp, D. J., "NASA Ares I Launch Vehicle Roll and Reaction Control Systems Design Status," AIAA 2009-5130, 2-5 August 1996.
doi: 10.2514/6.2009-5130

[3] Fokema, M. D., and Torkelson, J. E., U.S. Patent Application for a "Thermally Stable Catalyst and Process for the Decomposition of Liquid Propellants," No. 11/457, 985, filed Jul. 17, 2006.

[4] Jankovsky, R. S., "HAN-Based Monopropellant Assessment for Spacecraft," AIAA-96-2863, July 1996.
doi: 10.2514/6.1996-2863

[5] Sacheim, R. L., and Masse, R. K., "Green Propulsion Advancement: Challenging the Maturity of Monopropellant Hydrazine," Journal Propulsion and Power, published online 24 February 2014; Vol. 30, No. 2, 2014, pp. 265-276.
doi: 10.2514/1.B35086

[6] Gohardani, A. S., Stanojev, J., Demaire, A., Anflo, K., Persson, M., Wingborg, N., and Nilsson, C., "Green Space Propulsion: Opportunities and prospects," Progress in Aerospace Sciences, published online 17 September 2014; Vol. 71, 2014, pp. 128-149.
doi: 10.1016/j.paerosci.2014.08.001

[7] Amrousse, R., Katsumi, T., Azuma, N., and Hori, K., "Hydroxylammonium Nitrate (HAN)-based Green Propellant as Alternative Energy Resource for Potential Hydrazine Substitution: From Lab Scale to Pilot Plant Scale-Up," Combustion and Flame, published online 8 December 2016; Vol. 176, 2017, pp. 334-348.
doi: 10.1016/j.combustflame.2016.11.011

[8] Goza, D. A., "Application Investigation of a Hydroxylammonium Nitrate Thermocatalytic Thruster on "Green Propellant"," Procedia Engineering, published online 10 May 2017; Vol. 185, 2017, pp. 91-96.
doi: 10.1016/j.proeng.2017.03.297

[9] Chen, J., Li, G., Zhang, T., Wang, M., and Yu, Y., "Experimental investigation of the catalytic decomposition and combustion characteristics of a non-toxic ammonium dinitramide (ADN)-based monopropellant thruster," Acta Astronautica, published online 27 September 2016; Vol. 129, 2016, pp. 367-373.
doi: 10.1016/j.actaastro.2016.09.027

[10] Wiles, J. S., "A short history of ionic liquids-from molten salts to neoteric solvents," Green Chemistry, Vol. 4, 2002, pp. 73-80.
doi: 10.1039/B110838G

[11] Talawar, M. B., Sivabalan, R., Anniyappan, M., Gore, G. M., Asthana, S. N., and Gandhe, B. R., “Emerging Trends in Advanced High Energy Materials,” Combustion, Explosion, and Shock Waves, Vol. 43, No. 1, 2007, pp. 62-72.
doi: 10.1007/s10573-007-0010-9

[12] Anflo, K., Gronland, T., and Wingborg, N., "Development and Testing of ADN-based Monopropellants in Small Rocket Engines," AIAA-2000-3162, 17-19 July 2000.
doi: 10.2514/6.2000-3162

[13] Thormahlen, P., and Anflo, K., International Patent Application for a “Low-Temperature Operational and Storable Ammonium Dinitramide Based Liquid Monopropellant Blends,” No. PCT/SE2012/050589, filed 1 June 2012.

[14] Anflo, K., and Crowe, B., "In-Space Demonstration of High Performance Green Propulsion and its Impact on Small Satellites," SSC11-IX-2, 2011.

[15] Persson, M., Anflo, K., Dinardi, A., and Bahu, J. M., "A Family of Thrusters for ADN-Based Monopropellant LMP-103S," AIAA 2012-3815, 30 July - 1 August 2012.
doi: 10.2514/6.2012-3815

[16] Wingborg, N., Johansson, M., and Bodin, L., "Initial Development of a Laboratory Rocket Thruster for ADN-Based Liquid Monopropellants," FOI, Swedish Defence Research Agency Technical Report, No. FOI-R-2123-SE, December 2006.

[17] Negri, M., and Grund, L., “Replacement of Hydrazine: Overview and First Results of the H2020 Project Rheform,” 6th European Conference for Aeronautics and Space Sciences (EUCASS), 2015.

[18] Negri, M., Wilhelm, M., Hendrich, C., Wingborg, N., Gediminas, L., Adelöw, L., Maleix, C., Chabernaud, P., Brahmi, R., Beauchet, R., Batonneau, Y., Kappenstein, C., Koopmans, R. J., Schuh, S., Bartok, T., Scharlemann, C., Anflo, K., Persson, M., Dingertz, W., Gotzig, U., and Schwentenwein, M., “Technology development for ADN-based green monopropellant thrusters – an overview of the Rheform project,” 7th European Conference for Aeronautics and Space Sciences (EUCASS), 2017.
doi: 10.13009/EUCASS2017-319

[19] Kounalakis, M. E., and Faeth, G. M., “Combustion of HAN-Based Liquid Monopropellants Near the Thermodynamic Critical Point,” Combustion and Flame, published online 7 August 2003; Vol. 74, 1988, pp. 179-192.
doi: 10.1016/0010-2180(88)90016-8

[20] Ismail, M. K., and Hawkins, T. W., “Adiabatic Compression Sensitivity of Liquid Fuels and Monopropellants,” AFRL-PR-ED-TP-1999-0255, 1999.

[21] Babcock, J. R., and Wright, M. J., U.S. Patent Application for a “Self-Adjusting Catalyst for Propellant Decomposition,” No. 11/283, 575, filed Nov. 17, 2005.

[22] Spores, R. A., Masse, R., Kimbrel, S., and McLean, C., "GPIM AF-M315E Propulsion System," AIAA 2013-3849, 15-17 July 2013.
doi: 10.2514/6.2013-3849

[23] Masse, R. K., Allen, M., Driscoll, E., and Spores, R. A., "AF-M315E Propulsion System Advances & Improvements," AIAA 2016-4577, 25-27 July 2016.
doi: 10.2514/6.2016-4577

[24] Brand, A. J., and Drake, G. W., U.S. Patent Application for a "Energetic Hydrazinium Salts," No. 09/356, 227, filed Jul. 16, 1999.

[25] Deininger, W. D., Atteberry, J., Bygott, K., Gilmore, C. P., Marotta, B., McLean, C. H., Moler, V. D., Osborne, R., Riesco, M., Sexton, A., Shields, R., and Zeller, C. M., "Implementation of the Green Propellant Infusion Mission (GPIM) on a Ball Aerospace BCP-100 Spacecraft Bus," AIAA 2013-3848, 14-17 July 2013.
doi: 10.2514/6.2013-3848

[26] Tsay, M., Feng, C., Paritsky, L., Zwahlen, J., Lafko, D., and Robin, M., "Complete EM System Development for Busek's 1U CubeSat Green Propulsion Module," AIAA 2016-4905, 25-27 July 2016.
doi: 10.2514/6.2016-4905

[27] Togo, S., Hori, K., and Shibamoto, H., "Improvement of HAB-Based Liquid Monopropellant Combustion Characteristics," HEMs, 2004.

[28] Katsumi, T., Kodama, H., Matsuo, T., Ogawa, H., Tsuboi, N., and Hori, K., "Combustion Characteristics of a Hydroxylaamonium Nitrate Based Liquid Propellant. Combustion Mechanism and Application to Thrusters," Combustion, Explosion, and Shock Waves, Vol. 45, No. 4, 2009, pp. 442-453.
doi: 10.1007/s10573-009-0077-6

[29] Thrasher, J., Williams, S., Takashi, P., and Sousa, J., "Pulsed Plasma Thruster Development Using A Novel HAN-Based Green Electric Monopropellant," AIAA 2016-4846, 25-27 July 2016.
doi: 10.2514/6.2016-4846

[30] Hawkins, T. W., Brand, A. J., McKay, M. B., and Tinnirello, M., "Reduced Toxicity, High Performance Monopropellant at the U.S. Air Force Research Laboratory," 4th International Association for the Advancement of Space Safety Conference, AFRL-RZ-ED-TP-2010-219, 2010.

[31] Quach, P., Warmouth, G., and Brand, A., "Adiabatic Compression Sensitivity of AF-M315E," AIAA 2015-3752, 2015.
doi: 10.2514/6.2015-3752

[32] Anflo, K., Thormahlen, P., and Persson, M., "Hot-Firing Tests Using a Low Temperature Derivative of LMP-103S," 5th European Conference for Aeronautics and Space Sciences (EUCASS), 2017.

[33] Hosoya Company, "Safety Data Sheet of SHP163," No. SDS-0121, 2017.

[34] Kappenstein, C., Batonneau, Y., Perianu, E.-A., and Wingborg, N., “Non Toxic Ionic Liquids as Hydrazine Substitutes. Comparison of Physico-Chemical Properties and Evaluation of ADN and HAN,” Proceedings of the 2nd International Conference on Green Propellants for Space Propulsion, ESA SP-557, 7-8 June, 2004.

[35] Gordon, S., and McBride, B. J., “Computer Program for Calculation of Complex Chemical Equilibrium Compositions and Applications,” NASA Reference Publication 1311, 1994.

[36] Polaha, J., U.S. Patent Application for an “Internal Resistive Heating of Catalyst Bed for Monopropellant Catalyst,” No. 12/948, 558, filed Nov. 17, 2010.

[37] Masse, R. K., Overly, J. A., Allen, M. Y., and Spores, R. A., “A New State-of-The-Art in AF-M315E Thruster Technologies,” AIAA 2012-4335, 30 July – 01 August 2012.
doi: 10.2514/6.2012-4335

[38] Lani, B. P., “Microwave Ignition of Green Monopropellants,” Master Thesis at the Pennsylvania State University, 2014.

[39] Alfano, A. J., Mills, J. D., and Vaghjiani, G. L., “Resonant Laser Ignition Study on HAN-HEHN Propellant Mixture,” Combustion Science and Technology, published online 27 May 2009; Vol. 181, No. 6, 2009, pp. 902-913.
doi: 10.1080/00102200902901670

[40] Wu, M. –H., Yetter, R., and Yang. V., "Development and Characterization of Ceramic Micro Chemical Propulsion and Combustion Systems," AIAA 2008-966, 2008.
doi: 10.2514/6.2008-966

[41] Kakami, A., Yamamoto, N., Ideta, K., and Tachibana, T., “Design and Experiments of a HAN-Based Monopropellant Thruster Using Arc-Discharge Assisted Combustion,” Transactions of The Japan Society for Aeronautical and Sciences, Aerospace Technology Japan, Vol. 10, No. ists28, 2012, p.Pa_13–Pa_17.
doi: 10.2322/tastj.10.Pa_13

[42] Idea, Y., Takahashi, T., Iwai, K., Nozoe, K., Habu, H., and Tokudome, S., “Potential of ADN-Based Ionic Liquid Propellant for Spacecraft Propulsion,” Procedia Engineering, Vol. 99, 2015, pp. 332-337.
doi: 10.1016/j.proeng.2014.12.543

[43] Katsumi, T., and Furusawa, M., “Feasibility Study on Ignition of Green Monopropellant using a Pulse Laser,” JAXA Research and Development Report, 2017. (In Japanese)
doi: 10.20637/JAXA-RR-16-006/0003

[44] Itouyama, N., and Habu, H., “Study for Ignition of ADN-Based Solvent-Free Ionic Liquid with Pulse Laser,” Research and Development Report, 2017. (In Japanese)
doi: 10.20637/JAXA-RR-16-006/0004

[45] Wilson, M. J., “Demonstration Testing of a Long-Life 5-Lbf (22-N) MR-106L Monopropellant Hydrazine Rocket Engine Assembly,” AIAA 2005-3954, July 2005.

doi: 10.2514/6.2005-3954

[46] Iizuka, T., Wada, A., Shindo, T., Kawabata, S., Aoyagi, J., Watanabe, H., and Takegahara, H., “Basic Characteristics of Propellant Ignition by Discharge Plasma Ignition System for Green Propellants and its Effects of Gas Type,” Applied Plasma Science: Journal of IAPS, Vol. 22, No. 1, 2014, pp. 15-21. (In Japanese)

[47] Shindo, T., Wada, A., Maeda, H., Watanabe, H., and Takegahara, H., “Performance of a Green Propellant Thruster with Discharge Plasma,” Acta Astronautica, Vol. 131, 2017, pp. 92-95.
doi: 10.1016/j.actaastro.2016.11.022

Chapter 2

Discharge Plasma System for Green Monopropellants

2.1. Chemical Reaction by Plasma Ignition

The ignition of propellant using the discharge and plasma has been continuously researched for various engines (e.g. scramjet engine, gasoline engine, and arcjet thruster) [1-3]. Figure 2-1 shows the schematic of major pathways of combustion by discharge plasma ignition (using examples from [4] Yiguang Ju, and Wenting Sun, 2015). At the thermal pathway, it is expected to increase the temperature of chamber, and to accelerate chemical reaction of propellant by the Arrhenius equation. At the kinetic pathway, since the high energy of ions and electrons were produced further by discharge plasma, it is expected to produce the active radicals (e.g. NO, O, H, and OH) and excited molecules. At the transport pathway, it is expected that the ionic wind (as is well known in the corona discharge), the flow field and the fuel fragments are produced by changing process of combustion. Thus, the ignition system using discharge plasma is expected to enhance combustion reaction of the green monopropellant through these reactions.

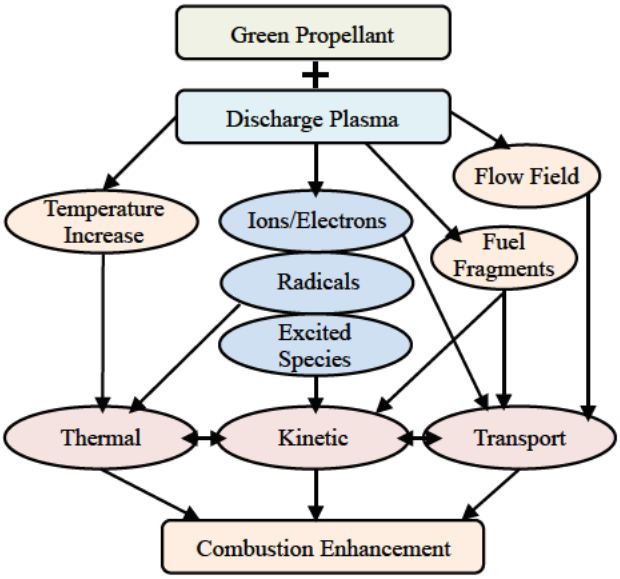

Fig. 2-1 Schematic of major enhancement pathways of combustion by discharge plasma ignition.

2.2. Concept of Discharge Plasma System

In this study, the discharge plasma system has been proposed for ignition of green-monopropellant of space propulsion system, and it can be expected to use green-bipropellant (e.g. N_2O/C_2H_5OH, and N_2O/DME) for the propulsion of lager thrust-level in the future. Additionally, this system is expected to enhance combustion reaction of the propellant through ion-molecule and radical-molecule reactions from the discharge plasma and to operate with a dual-mode, either in a high-specific-impulse-mode (at high-current and low-voltage, such as the arcjet thruster) or a high-thrust-mode. Figure 2-2 presents the process of reaction using discharge plasma system. The system consists of a cathode, insulator, and anode, and the electrodes have the hollow cylindrical geometry. First, the gas valve is opened, allowing gas to flow into the electrodes through the gas injector. Next, the DC power supply is turned on. An intense electric field forms between the cathode and anode, and a discharge plasma is then generated from ionized gas. Finally, the monopropellant ignites by joule heating and thermal decomposition when it comes into contact with the discharge plasma. Although the standard arcjet thruster have been operated at the high current (>10 A) and the low voltage (<100 V), this system is operated using that the discharge plasma is generated at the high voltage from 100 V to 1000 V and the low current below 1.0 A because the enhancement of ignition (the operation of high response and high thrust) for monopropellant is expected by the glow-discharge plasma (i.e. non-equilibrium plasma). Additionally, compared with other ignition systems, such as a spark plug, a plasma torch and a laser-ignition, this system has the potential for an increase in reactivity of propellant by the input of spatial energy using discharge plasma.

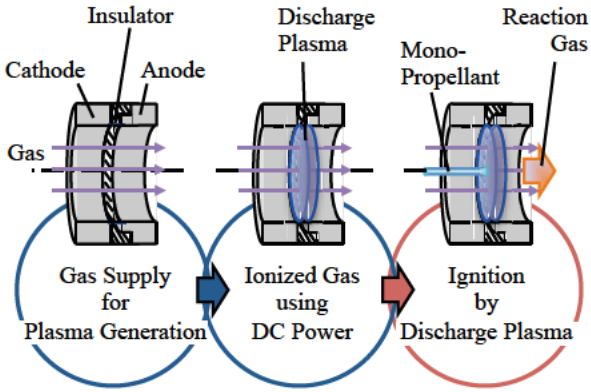

Fig. 2-2 Schematic of ignition process using discharge plasma system.

In this system, the gas species for plasma generation must be considered. Table 2-1 shows the characteristics properties of gas. The helium, xenon, and nitrogen were proven the space flight to use the propellant feed gas (i.e. helium, and nitrogen) and propellant (xenon, and nitrogen) for cold gas thruster, ion thruster, and hall thruster. Although the krypton and xenon have the lower ionization energy, and higher density, these gasses have expensive. On the other hand, one of noble gas, an argon gas, has beneficial effect on plasma generation, and lower cost. Additionally, since the consumed amounts of gas must be considered for long-term

operation of thruster, in this thesis, argon gas was selected for plasma generation.

Table 2-1 Characteristic properties of gas.

Gas Species	Helium		Argon		Krypton		Xenon		Nitrogen		
Compositions	He		Ar		Kr		Xe		N_2		
Meta-Stable State	2^3S_1	2^1S_0	3^3S_2	3^3S_0	3^3S_2	3^3S_0	3^3S_2	3^3S_0	$A^3\Sigma^+_u$	$B^3\Pi_g$	$C^3\Pi_u$
Excited Energy, eV	19.8 [5]	20.6 [5]	11.6 [5]	11.7 [5]	9.92 [5]	10.6 [5]	8.32 [5]	9.45 [5]	6.17 [6]	7.35 [6]	11.0 [6]
Ionization Energy, eV	24.59 [7]		15.76 [7]		14.00 [7]		12.13 [7]		15.58 [7]		
Density at 0 °C, kg/m^3	0.178		1.78		3.73		5.89		1.25		
Molecular Mass, kg/kmol	4.00		39.95		84.80		131.3		28.01		
Cost	Low		Low		High		High		Low		
Fight-Proven	Propellant Pressuriza-tion [8]		N/A (Flight-Qualified)		N/A (Flight-Qualified)		Propellant for Ion/Hall Thruster [9, 10]		Propellant Pressurization / Cold Gas [10]		

2.4. Reference in Chapter 2

[1] Takita, K., Uemoto, T., Sato, T., Ju, Y., and Masuya, G., "Ignition Characteristics of Plasma Torch for Hydrogen Jet in an Airstream," Journal of Propulsion and Power, Vol. 16, No. 2, 2000, pp. 227-233. doi: 10.2514/2.5587

[2] Shiraishi, T., Urushihara, T., and Gundersen, M., "A Trial of Ignition Innovation of Gasoline Engine by Nanosecond Pulsed Low Temperature Plasma Ignition," Journal of Physics D: Applied Physics, Vol. 42, No. 13, 2009, 135208. doi: 10.1088/0022-3727/42/13/135208

[3] Zube, D., Lichon, P., Cohen, D., Lichtin, D., Bailey, J., and Chilleli, N., "Initial On-Orbit Performance of Hydrazine Arcjets on A2100^{TM} Satellites," AIAA 99-2272, 20-24 June 1999. doi: 10.2514/6.1999-2272

[4] Yiguang, J., and Wenting, S., "Plasma Assisted Combustion: Dynamics and Chemistry," Progress in Energy and Combustion Science, Vol. 48, 2015, pp. 21-83. doi: 10.1016/j.pecs.2014.12.002

[5] Radzig, A.A., and Smirnov, B. M., "Reference Data on Atoms, Molecules, and Ions," Springer Series in Chemical Physics, 1985. doi: 10.1007/978-3-642-82048-9

[6] Itikawa, Y., Hayashi, M., Ichimura, A., Onda, K., Sakimoto, K., Takayanagi, K., Nakamura, M., Nishimura, H., and Takayanagi, T., "Cross Sections for Collisions of Electrons and Photons with Nitrogen Molecules," Journal of Physical and Chemical Reference Data, Vol. 15, No. 3, 1986. doi: 10.1063/1.555762

[7] National Institute of Standards and Technology (NIST) Atomic Spectra Database Ionization Energies Form, https://physics.nist.gov/PhysRefData/ASD/ionEnergy html.

[8] Byers, D. C., Woodcok, G., Benfield, M. P. J., "In-Space Chemical Propulsion System Model," 2004.

[9] Cassady, R.J., deGrys, K., Hoskins, W.A., King, D.Q., Morgan, O., Myers, R.M., and Wilson, F., "30 Years of Electric Propulsion Flight Experience at Aerojet Rocketdyne," IEPC-2013-439, 6-10 October 2013.

[10] Carpenter, C. B., Schmuland, D., Overly, J., and Masse, R., "CubeSat Modular Propulsion Systems Product Line Development Status and Mission Applications," AIAA-RS-2013-4001, 14-17 October 2013.

Chapter 3

Experimental Apparatus and Measurements

This chapter presents the apparatus for firing tests of thruster under sea level and vacuum condition, and the specifications of each measurement.

3.1. Vacuum Chamber

All of experiments were conducted inside vacuum chamber to ensure safety. Figure 3-1 shows the configuration of vacuum chamber. The cylindrically shaped chamber of length and diameter are 1000 mm, and 600 mm, respectively. In the case of firing tests under vacuum condition, all of experiments were conducted at ambient pressure below 1.5 kPa using a mechanical booster pump (Shimadzu Emit GDH-1302, MBP) and rotary pump (Shimadzu Emit MB-600F, RP), and the ambient pressure inside the vacuum chamber was measured using a vacuum gauge (Pfeiffer Vacuum TPR 280). To prevent the inflow of exhaust plume into the pump at vacuum firing test, the chamber was closed using the gate valve (VAT DN63-400), and the pump power was turned off before firing tests.

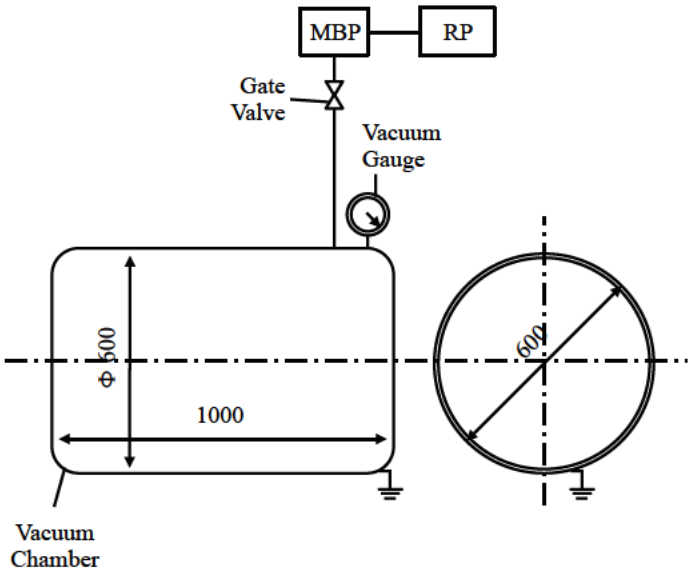

Fig. 3-1 Schematic of vacuum chamber.

3.2. Power Supply

The direct current (DC) power supply (NISTAC HV-2K10) was attached outside the vacuum chamber, as shown Fig. 3-2. Table 3-1 shows the specifications of power supply. In addition, to reduce the inrush current after the DC power supply was turned on, a stabilizing cement-resistance of 380 Ω was inserted. The discharge voltage and current waveforms were measured using a high-voltage probe (Tektronix P6015A) and a current probe (Tektronix TCP312A), respectively.

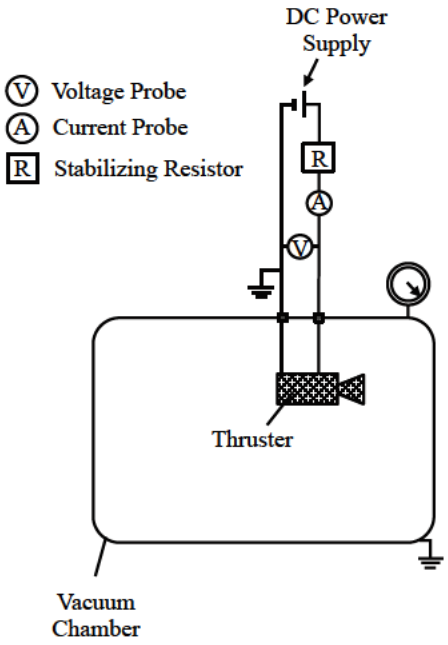

Fig. 3-2 Schematic of DC power supply.

Table 3-1 Specifications of DC power supply.

Model	NISTAC HV-2K10
Voltage Range	0 to 2.0 kV
Current Range	0 to 1.0 A

3.3. Feed System of Propellant and Gas

The gas feed system consists of an argon gas tank, solenoid valve (CKD AB31-02-2), mass flow meter (KEYENCE FD-A10), and needle valve (KEYENCE FD-C1), as shown in Fig. 3-3. The mass flow rate of argon gas is controlled by the pressure of upstream from the argon gas tank. The pressure of upstream was set before firing test, and the argon mass flow rate was measured using the mass flow meter at firing test.

The propellant feed system is a pressure-fed system. The propellant feed system consists of a nitrogen gas tank, propellant tank, propellant valve (CKD USB3-6-1), coriolis mass flow meter (KEYENCE FD-SS02A),

and a propellant injector. The propellant mass flow rate is adjusted using the pressure of the pressurant gas (i.e., nitrogen gas) before firing test, and the pressure of upstream was fixed at firing test.

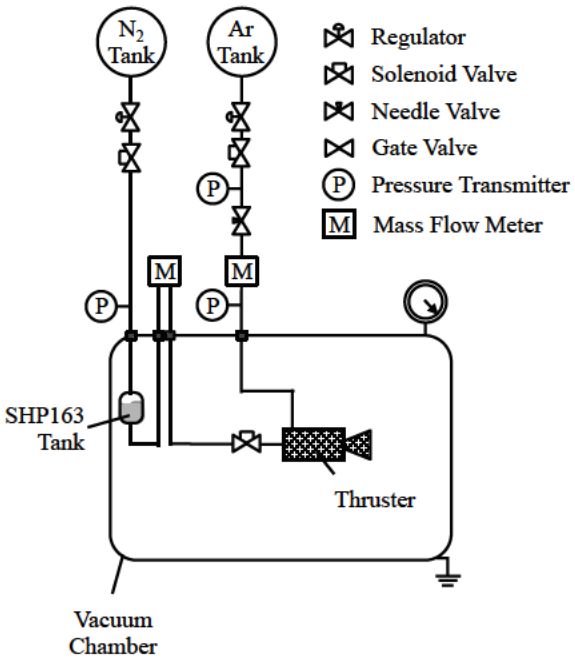

Fig. 3-3 Schematic of feed system.

3.4. Measurements

3.4.1. Discharge Voltage and Current Measurement

The discharge current and voltage were measured using each probe. Table 3-2 shows the specifications of each probe. The waveforms of current and voltage were recorded using data logger of KEYENCE NR-HA08.

Table 3-2 Specifications of probe.

Model	Tektronix TCP312A	Tektronix P6015A
Bandwidth	DC to100 MHz	DC to 75 MHz
Rise Time	< 3.5 ns	4.0 ns
Maximum Rating	1 A/V (Low-current Sensitivity)	1000X (1/1000)
Maximum Input	5 A (Low-current Sensitivity)	20 kV DC

3.4.2. Thrust Measurement

The thrust stand system consists of a load cell (KYOWA LTS-200GA), pulley, spring plate (made of aluminium), and calibration weight, as shown in Fig. 3-4. Table 3-3 shows the specifications of the load cell. The voltage-output of load cell (i.e. thrust) is calibrated using calibration weight. The calibrations of thrust stand at each time of firing tests for six times were conducted before firing tests. Figure 3-5 shows the result of calibration, and then the coefficient of load cell output was 1.599 mV/N. Thus, the thrust at firing tests was calculated by the load cell output using the calibration-coefficient of 0.625 N/mV. Additionally, the normal mode frequency of the thrust stand with a thruster and feed line was 29 Hz before firing test.

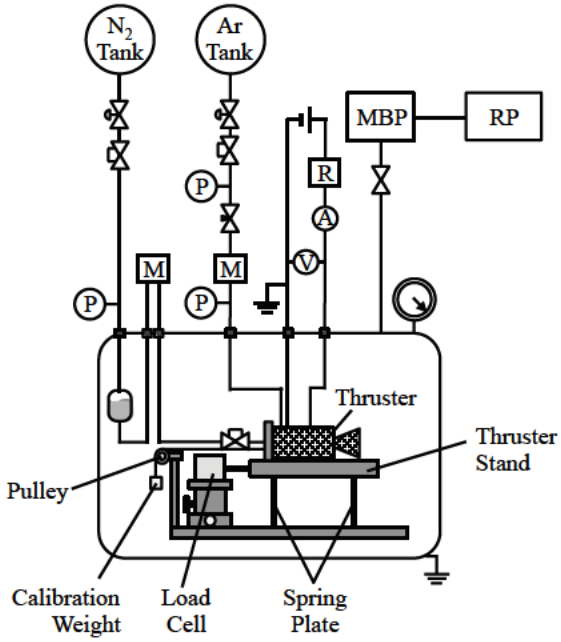

Fig. 3-4 Schematic of thrust stand system.

Table 3-3 Specifications of load cell.

Model	KYOWA LTS-200GA M2
Rated Output	1.5 mV/V (3000×10^{-6} strain)
Rated Capacity	0 to 2 N
Bridge Resistance	120 Ω ±10%
Bridge Voltage	±1V

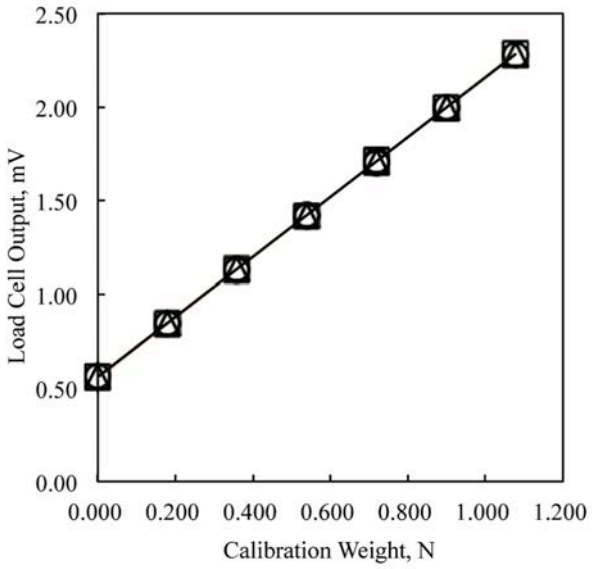

Fig. 3-5 Results of calibration for six times.

3.4.3. Pressure and Mass Flow Rate Measurement

The feed pressure and pressure of internal thruster were measured using the pressure transducers. Table 3-4 shows the specifications of pressure transducer.

The mass flow rate of propellant and gas at firing tests were measured using the mass flow meters. Table 3-5 shows the specifications of mass flow meter. The SHP163 mass flow rate below 0.2 g/s was unmeasurable using the mass flow meter. In that case, since the mass flow rate is proportional to the square root of the difference in pressure between the propellant tank and the orifice of the injector, the mass flow rate at firing test was calculated using that the predicted curve of mass flow rate was obtained from the measured mass flow rate at seal-level condition.

Table 3-4 Specifications of pressure transducer.

Model	NAGANO KEIKI KH-15	KEYENCE AP-13S	Gems 3500B250PA	Pfeiffer Vacuum TPR 280
Datum	Gauge	Gauge	Absolute	Absolute
Range	0 to 3.5 MPa	0 to 1 MPa	0 to 250 psi	$5 \cdot 10^{-4}$ to $1 \cdot 10^{3}$ mbar
Output	0 to 5 V	4 to 20 mA	4 to 20 mA	2.2 to 8.5 V
Response Time	< 1 ms	5 ms	1 ms	80 ms
Accuracy	±0.25% F.S.	±0.5% F.S.	0.25% F.S.	±15%

Table 3-5 Specifications of mass flow meter.

Model	KEYENCE FD-A10	KEYENCE FD-SS02A
Range	0.3 to 10 L/min	0 to 200 mL/min @ 1.00 g/cm^3 0 to 284 mL/min @ 1.41 g/cm^3
Pressure Drop	N/A	< 0.03 MPa @ 1 cSt < 0.3 MPa @ 30 cSt
Output	4 to 20 mA	4 to 20 mA
Response	5 ms	50 ms
Sampling Frequency	30 ms	50 ms
Resolution	0.01 L	0.1 mL/min
Accuracy	±0.5% F.S.	±3% F.S.

3.4.4. Data Logger

The waveforms of current, voltage, pressure, mass flow rate, and thrust were recorded using the data logger of KEYENCE NR-HA08 and NR-ST04. Table 3-6 shows the specifications of data logger.

Table 3-6 Specifications of data logger.

Model	KEYENCE NR-HA08	KEYENCE NR-ST04
Setting Range	±5 V 0 to 20 mA	±5 mV
Input Impedance	1 MΩ ±1% (Voltage) 250 Ω ±1% (Current)	> 1 MΩ
Setting Sampling Frequency	1 ms	1 ms
Bandwidth	250 kHz	DC to 5 kHz
A/D Resolution	14 bit	16 bit
Accuracy	±0.1% F.S.	±0.2% F.S.
Resistance for Strain Gauge	N/A	120 Ω @4 wire strain gauge

3.4.5. Spectrometer System

The emission spectroscopy system consists of a spectrometer (JASCO MK-300J), high-speed spectroscopy CCD camera (ANDOR iDus DU420A-0E) with 1024×255 pixels, optical fiber (OFT-10S, length: 1m), and condenser lens, as shown in Fig. 3-6. Table 3-7 shows the specifications of spectrometer. The resolution performance of the measurements was set with a exposure time of 1 ms, acquisition period of 49 Hz (20 ms), entrance slit of 10 μ m, center-wavelength of 600 nm, and diffraction grating of 120 lines per millimeter. The profiles of the exhaust plume were recoded at 200 mm from the exit of conical nozzle and then the profiles width was set at 20 mm.

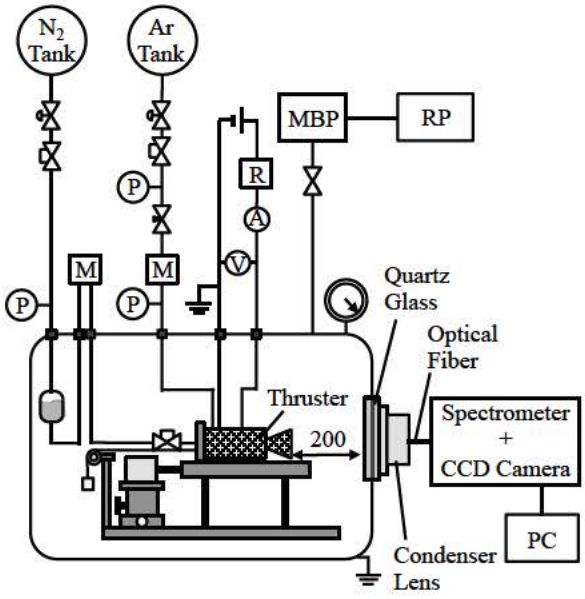

(a) Overview of experimental apparatus

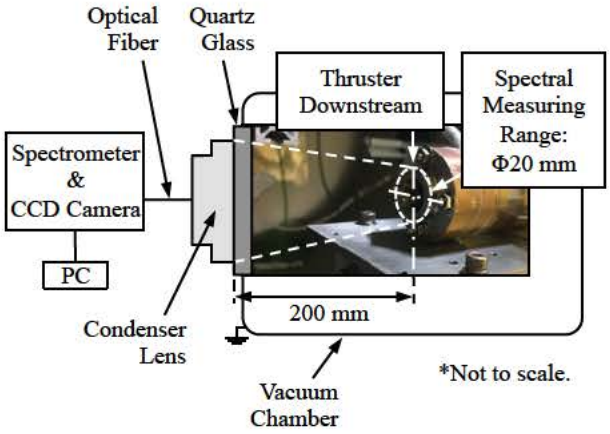

(b) Spectral measuring range.

Fig. 3-6 Schematic of spectrometer system.

To synchronize the operating time with the other waveforms (e.g. waveforms of thrust and pressure), the CCD was triggered using the opened propellant valve signal. The calibrations of wavelength at each time of experiments for three times were conducted using Hg pen-ray lamp (UVP, LLC).

Table 3-7 Specifications of spectrometer.

Model	JASCO MK-300J
Diffraction Grating	120 lines/mm (50 mm × 50 mm × 6)
Wavelength Resolution	0.2 nm @120 lines/mm
Wavelength Range	200 to 1000 nm (223 to 978 nm @ center-wavelength of 600 nm)
Measurement Time	20 s (from propellant valve open signal) @exposure time: 1 ms, acquisition period: 49 Hz
Blaze Wavelength	330 nm @120 lines/mm

Chapter 4

Ignition Characteristics of Discharge Plasma System

In this chapter, the basic propellant ignition characteristics are discussed in terms of the conditions that induce successful propellant ignition and the associated propellant ignition probability (also known as multiple propellant ignition), power consumption, and ignition delay time (also known as ignition delay time). The effects of the geometric swirl number (swirl strength) and argon gas flow rate on these basic ignition characteristics are experimentally evaluated under atmospheric conditions.

4.1. Experimental Conditions and Apparatus

Figure 4-1 shows a cross-sectional view of a laboratory model of the discharge plasma system with a swirl injector supplying the argon gas. A liquid propellant injector is located upstream of the swirl injector. The system also comprises outer housings both upstream and downstream, insulators, and electrodes (cathode and anode). The outer housings and swirl injector are made of polycarbonate material, the electrodes of stainless steel (SUS303), and the insulators of alumina ceramic.

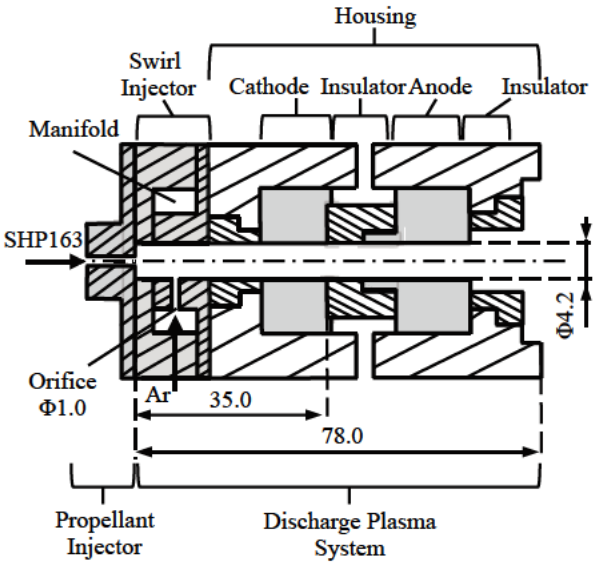

Fig. 4-1 Overview of a discharge plasma system with the swirl injector.

The schematics of the swirl injector for the various geometric swirl numbers are shown in Fig. 4-2. The swirl injectors are characterized by the geometric swirl number S_g. The geometric swirl number determines the angular momentum ratios of the argon gas using the geometry of the swirl injector, such as the orifice and central hole dimensions. Neglecting the viscous force of the argon gas, the geometric swirl number can be defined using only geometrical parameters [1]:

$$S_g \equiv \frac{P_\phi}{P_c R_c} = \frac{(R_c - R_o) A_c}{n R_c A_o} \tag{4-1}$$

where $P\phi$ is the angular momentum in the tangential direction and P_c is the momentum of the central hole. R_c and R_o are the radii of the central hole and orifice, A_c and A_o are the areas of the central hole and orifice, and n is the orifice number. In this study, the swirl strength of argon gas was varied using the geometric swirl number of the

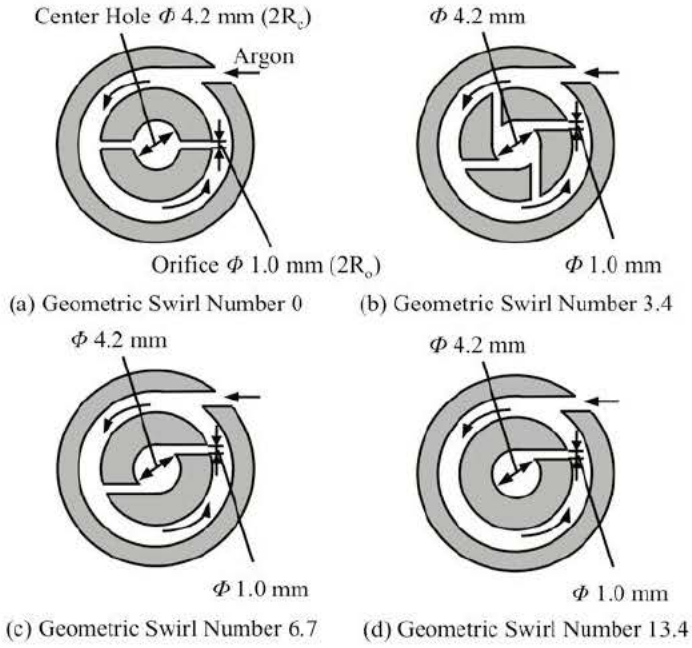

Fig. 4-2 Schematics of the swirl injector with geometric swirl numbers of (a) 0, (b) 3.4, (c) 6.7, and (d) 13.4 – top-down view.

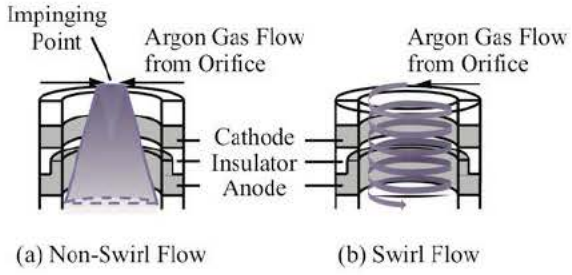

Fig. 4-3 Conceptual views of (a) swirled flow and (b) non-swirled flow.

swirl injector. Four swirl injectors were prepared to evaluate the effect of the geometric swirl number, for values of 0, 3.4, 6.7, and 13.4. A geometric swirl number of 0 has a non-swirled flow field and the other geometric swirl numbers have a swirled flow field, as shown in Fig. 4-3. The manifold is filled with argon gas, and the gas is supplied through an orifice to the discharge zone, a central hole with a diameter of 4.2 mm. The orifice has a diameter of 1.0 mm.

An experimental apparatus used for static firing tests is shown in Fig. 4-4. The experimental apparatus consists of the discharge plasma system, a gas supply system, a propellant supply system, and a DC power supply. All of the static firing tests were conducted inside a vacuum chamber to ensure safety under atmospheric conditions. The gas supply system consists of an argon gas tank and a solenoid valve (CKD AB41-02-3/AB31-02-2). The argon gas mass flow rate is controlled by the upstream pressure from the argon gas tank. The propellant supply system is a pressure-fed system. The supply system consists of a nitrogen gas tank, a propellant tank, a non-atomized propellant injector (LEE: INZA4710975H), and a propellant valve (LEE: INKX0514300A-A). The propellant mass flow rate is adjusted using the pressure of the pressurant gas (nitrogen gas). The input power supply was set with the following conditions: a maximum voltage of 2.0 kV and a current limit of 0.8 A. The discharge voltage and current waveforms were measured with a high-voltage probe (Tektronix: P6015A) and a current probe (HIOKI: 9274), respectively. To evaluate the exhaust flame, the static firing tests were recorded by video camera through the window of the vacuum chamber. In a different experiment, the discharge plasma distribution inside the discharge zone was observed downstream of the

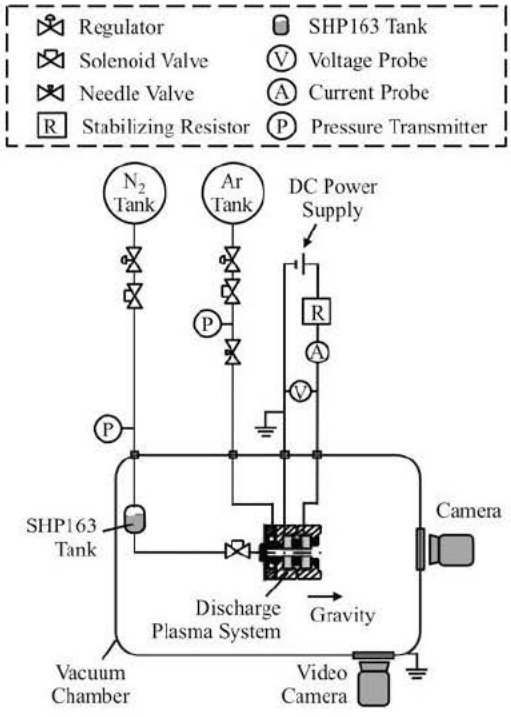

Fig. 4-4 Overview of the experimental apparatus.

discharge plasma system using a camera.

Figure 4-5 shows an illustration of the propellant ignition process. In Phase 1, the argon gas valve, as shown in Fig. 3, is opened, allowing argon gas to flow into the discharge zone through the swirl injector. In Phase 2, the DC power supply is turned on. An intense electric filed is formed between the cathode and anode, and then a discharge plasma is generated from ionized argon gas. In Phase 3, the propellant valve is opened. The propellant is ignited when it comes into contact with the discharge plasma.

Figure 4-6 shows a photograph of three ignition-categories, stable, unstable, and failed ignition. Stable ignition is defined as the continuity of the exhaust flame. Unstable ignition indicates discontinuity of the exhaust flame. Failed ignition indicates no exhaust plume, and the emission of unreacted propellant.

In this experiment, the mass flow rate of SHP163 is fixed at 0.3 g/s (± 0.03 g/s), and the mass flow rate

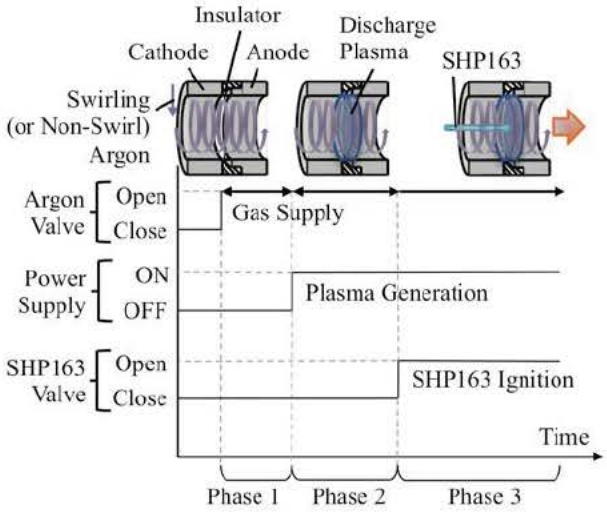

Fig. 4-5 Propellant ignition phase.

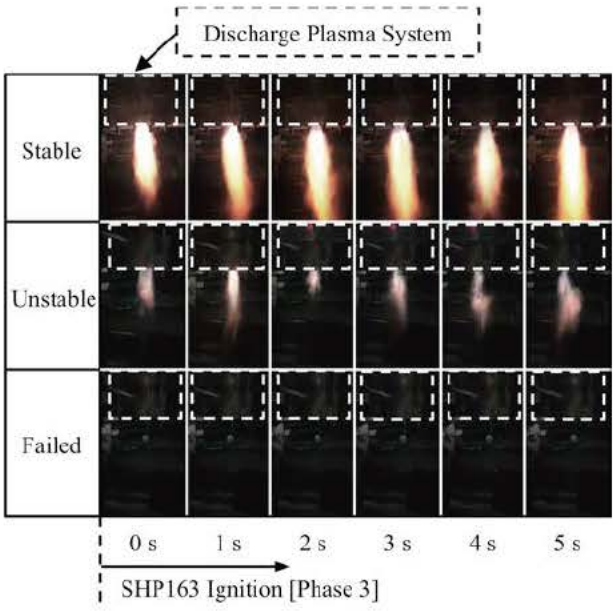

Fig. 4-6 Images of the three categories of ignition.

of argon gas is varied from 0.125 to 0.175 g/s because stable ignition was observed at this condition in previous experiments, as shown in Fig. 4-7 [2].

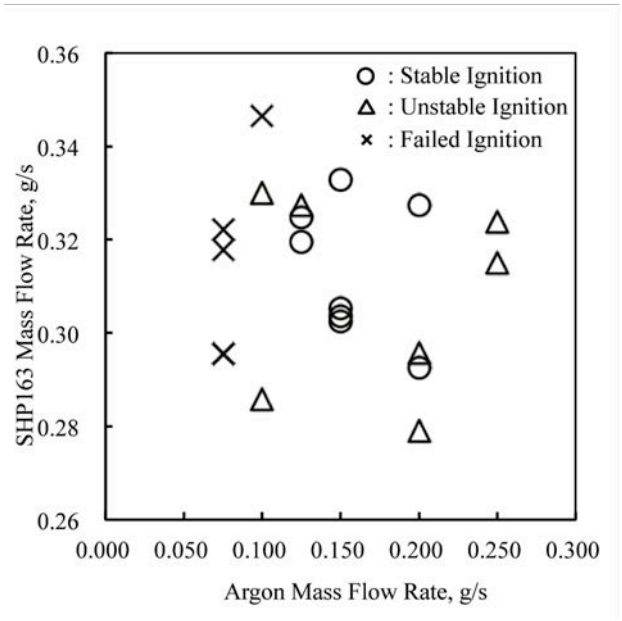

Fig. 4-7 Result of ignition tests of a discharge plasma system with geometric swirl number of 6.7.

4.2. Ignition Tests

4.2.1. Propellant Ignition Probability

First, SHP163 was successfully reacted without any failed ignitions under these experimental conditions with geometric swirl numbers 0, 6.7, and 13.4. However, for a geometric swirl number of 3.4, some failed cases were observed, seemingly because of the weak swirl strength. After the ignition of the propellant, some cases (e.g., with a swirl number of 0 at an argon mass flow rate of 0.150 g/s) resulted in discontinuity of the exhaust flame. In the unstable ignition cases, it seems that the propellant ignition may be periodic during Phase 3.

Figure 4-8 shows the effect of the geometric swirl number on the ratio of continuous propellant ignition and power consumption at Phase 3. The static firing tests were conducted ten times for each argon gas mass flow rate and geometric swirl number. Here, the errors represent the standard deviation for ten times from each trial. In all cases under our conditions, with swirl numbers 0, 6.7, and 13.4 and for all argon mass flow rates, there were no failed ignition. In the case of a geometric swirl number of 3.4, the propellant ignition became more unstable and ignition failed. Thus, it seems that the lower swirl strength induces a flame instability at the discharge zone in the case of swirling argon gas.

The power consumption was varied approximately from 260 W to 300 W with successful ignition under our experimental conditions, and it was confirmed that the power consumption is not significantly affected by the swirl strength.

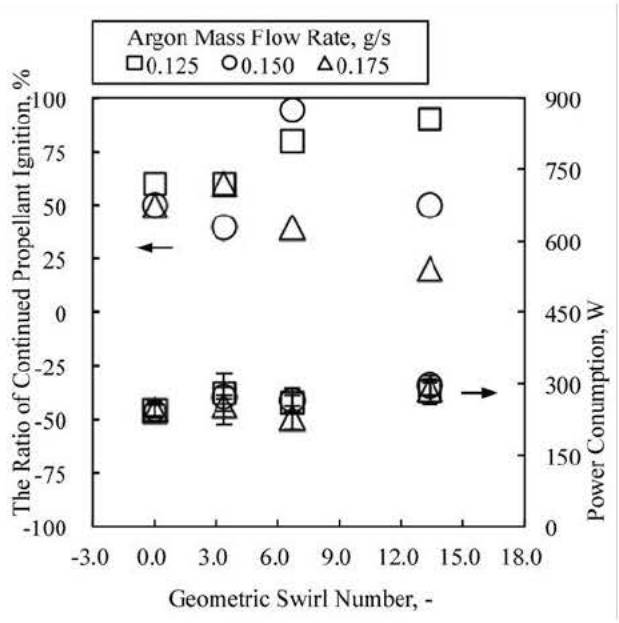

Fig. 4-8 Ratio of continued propellant ignition to the effects of geometric swirl number on the power consumption at Phase 3.

4.2.2. Discharge Plasma Distribution

In the previous section, the relation between the propellant ignition and geometric swirl number was discussed. In this section, the discharge plasma conditions, such as the distribution inside the discharge zone prior to supplying the propellant (Phase 2), are evaluated for the different experiments. The photographs shown in Fig. 4-9 were taken from downstream of the discharge plasma system during Phase 2, and optimally taken from a single experiment. In addition, the plasma distribution randomly changed as a function of time, as shown in Fig. 4-10, and so were taken downstream of the discharge plasma system during Phase 2 using a high-speed

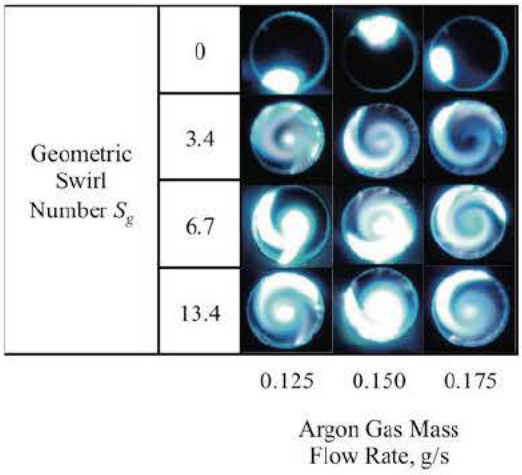

Fig. 4-9 Effects of the argon gas mass flow rate and geometric swirl number on the plasma distribution. These photographs were taken from downstream of the discharge plasma system. (ISO: 800, exposure time: 2.5 ms, f: 20).

digital CCD camera (KATOKOKEN, K-II). It seems that the fullness of the discharge plasma increases as a function of geometric swirl number. At a geometric swirl number of 0, the plasma is less distributed in the discharge zone, and changes location as a function of time. The lack of plasma distribution makes it difficult for the propellant to make contact with the plasma. However, in the case of a geometric swirl number of 0, the propellant ignition is more stable than with a geometric swirl number of 3.4. It seems that the impingement of argon gas atomizes the propellant at the center hole of the swirl injector with a geometric swirl number of 0, while the propellant at the geometric swirl number of 3.4 is less affected by the swirling argon gas. In addition, stable ignition has a non-negligible effect on the plasma distribution before propellant ignition. Thus, it seems that the propellant ignition is stabilized by the atomized propellant.

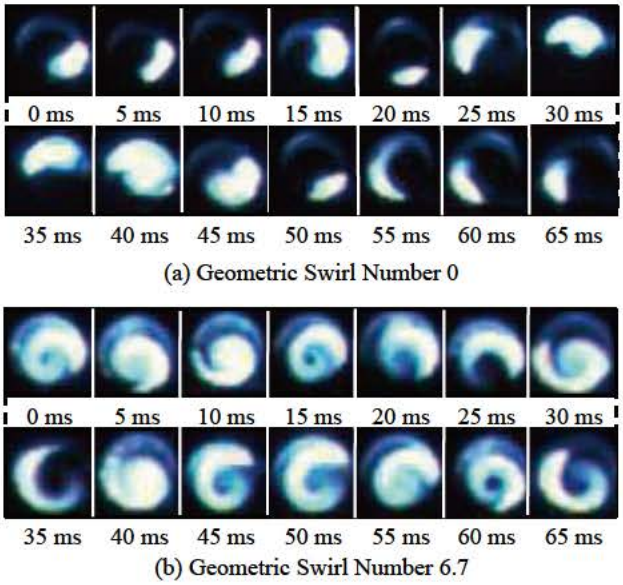

Fig. 4-10 Plasma distribution with geometric swirl number (a) 0 and (b) 6.7 at an argon gas mass flow rate of 0.150 g/s. These photographs were taken from downstream of the discharge plasma system using a high-speed digital CCD camera (fps: 200, exposure time: 1 ms).

4.2.3. Ignition Delay Time

In this thesis, a ignition delay time is defined as the time from the opening of the propellant valve to the start of the chemical reaction, as shown in Fig. 4-11. In this discharge plasma system, when the propellant makes contact with the discharge plasma, the discharge voltage becomes higher. The discharge voltage fluctuates with changes in the electric resistance because the resistance of the mixture of the discharge plasma, the unreacted propellant, and the intermediate and combustion products is higher than the resistance of the discharge plasma. Thus, when the discharge voltage starts fluctuating, the propellant reaction has also started.

The measured delay times are shown in Fig. 4-12. It was confirmed that the delay time is less affected by the argon gas mass flow rate at each geometric swirl number. At a geometric swirl number of 0, the delay time tends to be longer, e.g., more than 100 ms. In contrast, at the highest geometric swirl number, the delay times are

less than 100 ms. It seems therefore that the plasma conditions inside the discharge zone have a non-negligible effect on the delay time.

The relation between the geometric swirl number and the averaged ignition delay time is shown in Fig. 4-13. Here, the errors represent the standard deviation for ten times from each trial. The averaged delay time tends to be shorter at higher geometric swirl numbers. With the lack of plasma distribution at the lowest

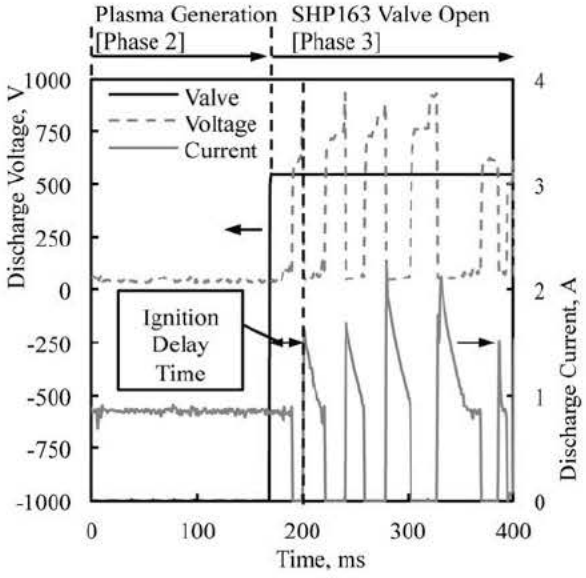

Fig. 4-11 Evaluation of ignition delay time. The discharge plasma system with a geometric swirl number of 6.7 at a propellant mass flow rate of 0.3 g/s, and an argon gas mass flow rate of 0.125 g/s.

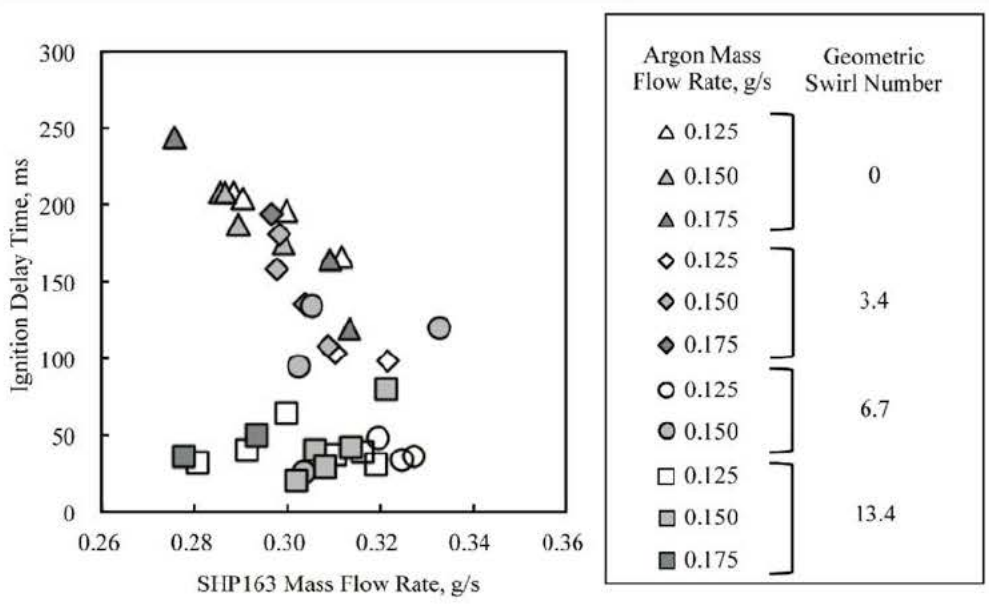

Fig. 4-12 Comparison between ignition delay times of each geometric swirl number.

geometric swirl number, propellant has less contact with the discharge plasma; thus, the delay time may become longer.

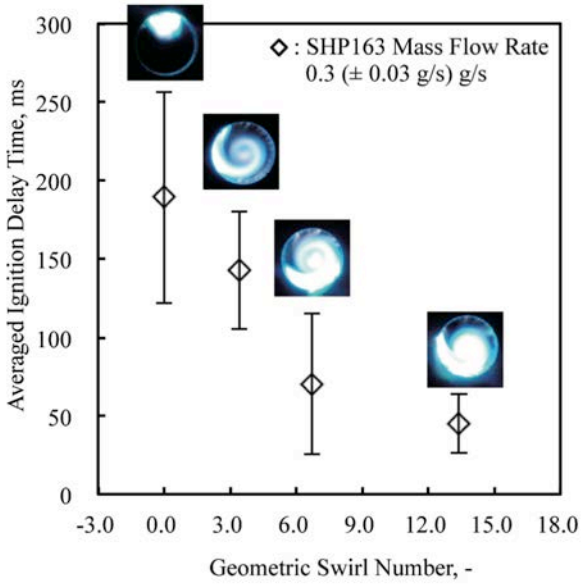

Fig. 4-13 Effect of the plasma distribution for each geometric swirl number on the averaged ignition delay time. These photographs of the plasma distribution were taken downstream of the discharge plasma system for an argon gas mass flow rate of 0.150 g/s. (ISO: 800, exposure time: 2.5 ms, f: 20).

4.3. Summary

In the chapter 4, to understand the propellant ignition characteristics of discharge plasma system, the effects of geometric swirl number on the ignition characteristics were evaluated under atmospheric conditions. It is concluded that the geometric swirl number has strong effects on the plasma distribution, the propellant ignition probability, and the ignition delay time. The continuity of the combustion flame was confirmed at an argon gas mass flow rate from 0.125 to 0.175 g/s and SHP163 mass flow rate of 0.3 g/s. In addition, the effect of the geometric swirl number on the ignition delay time was confirmed, with higher geometric swirl numbers reducing the delay time.

4.4. Reference in Chapter 4

[1] Beer, J. M. and Chigier, N. A., “Combustion Aerodynamics,” (1972), pp100-146.

[2] Wada, A., “Study on Discharge Plasma Catalyzer for Space Propulsion with Green Monopropellant,” Master’s Thesis, 2014.

Chapter 5

Design and Build of HAN-Based Monopropellant Thruster with Discharge Plasma System

The experiments in previous chapter evaluated the effects of the geometric swirl number of the swirl gas injector and noble gas (argon gas) mass flow rate on ignition characteristics. At an argon mass flow rate of 0.15 g/s and SHP163 mass flow rate of 0.3 g/s, the continuity of the exhaust flame from downstream of the discharge plasma system with a geometric swirl number of 6.7 was confirmed at sea level. However, performances of a thruster—such as the thrust, combustion chamber pressure, characteristic exhaust velocity efficiency and power consumption—with a discharge plasma system under a vacuum condition have not been well evaluated. Additionally, in the case of this HAN-based monopropellant, previous experimental data of the thruster do not exist to guide the design of the combustion chamber.

In this chapter, static firing tests of a 1-N-class thruster with a discharge plasma system are conducted under a vacuum condition. The combustion characteristics are discussed considering the characteristic exhaust velocity efficiency and power consumption of SHP163 ignition. The effects of the characteristic length of the combustion chamber (L^*, L-star) and SHP163 injection methods on combustion characteristics are experimentally evaluated at an argon mass flow rate of 0.15 g/s and nozzle expansion ratio of 1. The L-star of the combustion chamber is varied by varying the combustion chamber length and the design combustion chamber pressure is set at 0.4 MPa.

5.1. Experimental Conditions and Apparatus

A cross-sectional view of a laboratory model of the thruster with a discharge plasma system is shown in Fig. 5-1. A propellant injector for SHP163 is located upstream of the swirl gas injector. A swirl injector with a geometric swirl number of 6.7 is prepared because the continuity of the combustion flame was confirmed for this injector under a sea-level condition. The system also has outer housing both upstream and downstream, insulators, electrodes (i.e., a cathode and anode) and a convergent nozzle (i.e., a throat nozzle). The outer housing is made of polycarbonate materials, the electrodes and convergent nozzle of stainless steel (i.e., SUS303) and the insulators of alumina ceramic. The central hole of the thruster (i.e., the combustion chamber diameter) is 4.2 mm and the electrode gap is 3.5 mm.

To evaluate combustion characteristics of the combustion chamber, a nozzle with an expansion ratio of 1 was prepared. The combustion chamber of the monopropellant RCS thruster is generally designed at about 1.0 MPa [1]. Additionally, SHP163 has a high burning rate under the pressure above 1.0 MPa [2, 3]. However, the effect of the combustion chamber pressure on the combustion characteristics of SHP163 with discharge plasma is not well understood. Thus, in this experiment, to evaluate the operation of the thruster at low combustion chamber pressure, the chamber pressure was designed to be 0.4 MPa. The configuration of the thruster is given in Table 5-1.

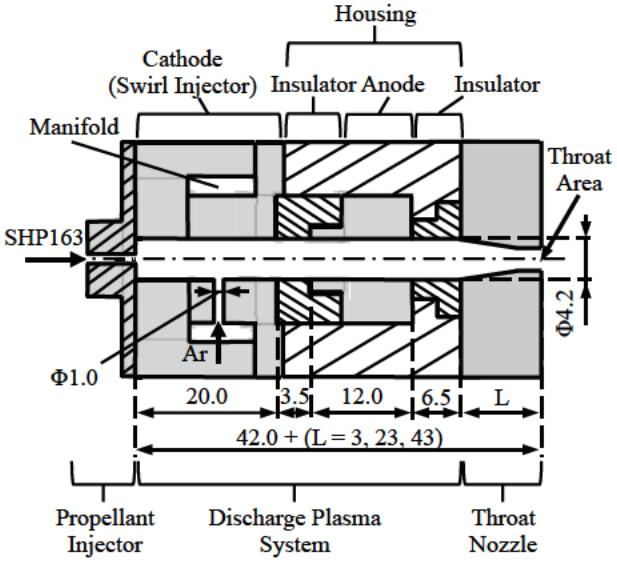

Fig. 5-1 Overview of the thruster with a discharge plasma system.

Table 5-1 Configuration of the designed thruster.

Target thrust, N	0.17 to 0.68
SHP163 feed pressure, kPa, gauge	200 to 800
Target SHP163 mass flow rate, g/s	0.10 to 0.40
Target Argon mass flow rate, g/s	0.15
Designed combustion chamber pressure, MPa	0.40
Combustion chamber characteristics length, mm	508, 734, 960
Nozzle throat area, mm^2	1.2
Nozzle expansion ratio, -	1
Discharge current limit, A	0.8

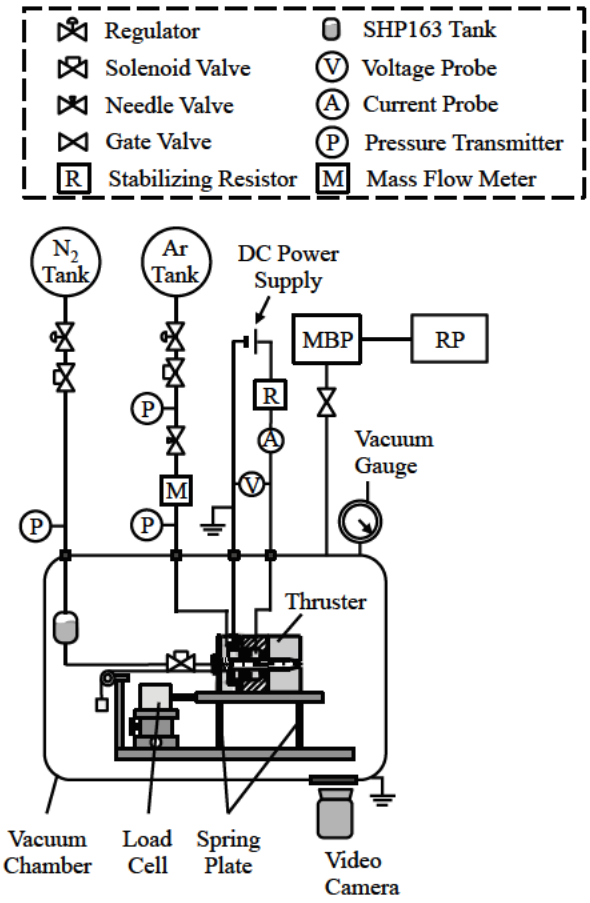

Fig. 5-2 Overview of the experimental apparatus.

The experimental apparatus for vacuum firing tests is shown in Fig. 5-2. The experimental apparatus consists of the thruster with a discharge plasma system, gas feed system, propellant feed system, thrust stand system and DC power supply for discharge plasma generation. All of experiments were conducted under ambient pressure of 1.2 kPa using a mechanical booster pump (MBP) and rotary pump (RP). In addition, the ambient pressure in the vacuum chamber was measured using a vacuum gauge (Phiffer Vacuum TPR 280). The gas feed system consists of an argon gas tank, solenoid valve (CKD AB31-02-2), mass flow meter (Keyence FD-A10) and needle valve (Keyence FD-C1). The argon gas mass flow rate is controlled by the pressure upstream of the argon gas tank. In static firing tests, the argon mass flow rate was measured using the mass flow meter. The propellant feed system is a pressure-fed system. The propellant feed system consists of a nitrogen gas tank, propellant tank, propellant valve (CKD USB3-6-1), and laboratory model of a like-impinging doublet injector. The propellant mass flow rate is adjusted using the pressure of the pressurant gas (i.e., nitrogen gas). The HAN-based monopropellant (SHP163) mass flow rate of a 1-N-class RCS thruster is about 0.4 g/s. In this experiment, the SHP163 mass flow rate is varied from 0.17 to 0.68 g/s and the mass flow rate of argon gas is fixed at 0.15 g/s. Figure 5-3 illustrates the atomized condition of the doublet injector at feed pressure of 600 kPa. The orifice diameter and angle of impinging streams are 0.11 mm and 62 degrees, respectively. The measured

mass flow rate of SHP163 with the doublet injector under a sea-level condition is shown in Fig. 5-4. The mass flow rate is proportional to the square root of the difference in pressure between the propellant tank and the orifice of the doublet injector [4]. Thus, in static firing tests, the mass flow rate of SHP163 is calculated from the difference in pressure between the propellant feed and the orifice exit of the propellant injector. The propellant feed pressure and the pressure of the internal thruster (i.e., argon gas tube) were measured using Keyence AP-13S and Nagano KH-15 pressure transmitters, respectively. The thrust stand system consists of a load cell (Kyowa LTS-200GA), pulley, spring plate (made of aluminum) and calibration weight. The thrust is calibrated using the calibration weight. The DC power supply (NISTAC HV-2K10) was connected outside the vacuum chamber. The input power supply was set with a maximum voltage of 2.0 kV and a current limit of 0.8 A. In addition, to reduce the inrush current after the DC power supply was turned on, stabilizing resistance of 380 Ω was inserted. The discharge voltage and current were measured using a high-voltage probe (Tektronix P6015A) and current probe (Tektronix TCP312), respectively.

Figure 5-5 is an illustration of the propellant ignition process using the discharge plasma system. In Phase 1, the argon gas valve is opened, allowing argon gas to flow into the combustion chamber through the swirl gas injector. In Phase 2, the DC power supply is turned on. An intense electric field forms between the cathode and anode, and a discharge plasma is then generated from ionized argon gas. In Phase 3, the propellant valve is opened. The propellant ignites when it comes into contact with the discharge plasma.

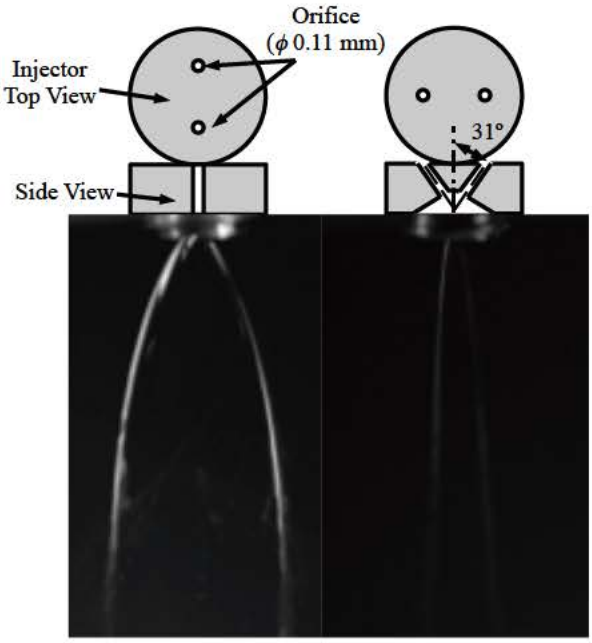

Fig. 5-3 Side view of the atomized condition with the like-impinging doublet injector. (exposure time: 1.25 ms, f: 4).

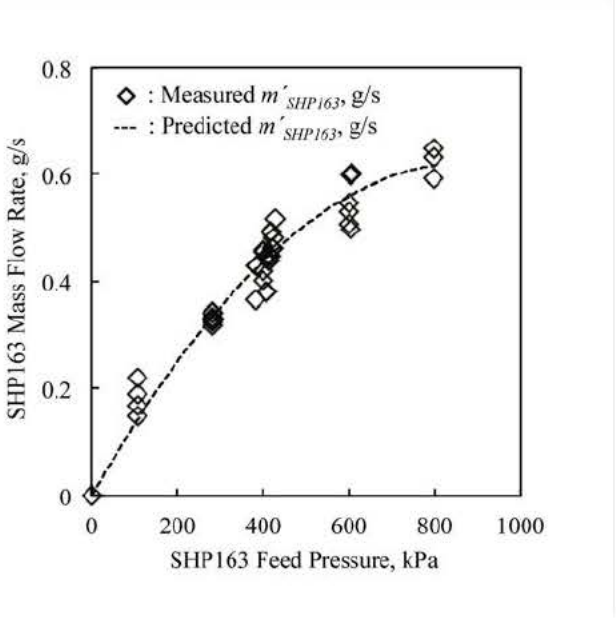

Fig. 5-4 Measured mass flow rate of SHP163 at various feed pressures.

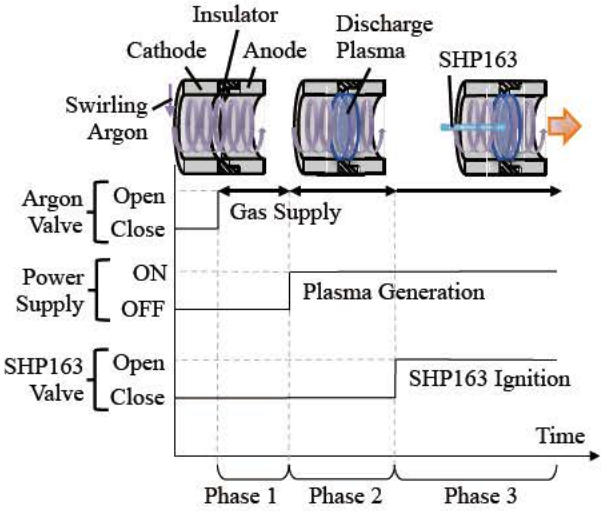

Fig. 5-5 Propellant ignition sequence.

5.2. Evaluation of Combustion Characteristics

5.2.1. Firing Tests in Vacuum Condition

In this section, the doublet injector for SHP163 supply was prepared because it was confirmed that ignition performances (i.e. ignition probability, and power consumption) at sea-level were almost same in comparison with single-hole injector. In firing tests performed under a vacuum, the effects of the feed pressure of SHP163 on ignition characteristics were confirmed. Figure 5-6 shows waveforms of successful ignition and failed ignition. Stable operation was confirmed at SHP163 feed pressure of 400 kPa, and steady thrust of 0.31 N and internal argon tube-pressure of 0.38 MPa were then observed at an argon mass flow rate of 0.15 g/s and

SHP163 mass flow rate of 0.24 g/s. Here, the steady thrust and pressure were evaluated for 5 s before the SHP163 valve was closed. The thrust and pressure increased at approximately the same time after the propellant valve was opened. The waveform of thrust after the ignition of SHP163 depended on the normal mode frequency of the thrust stand because the output from thrust stand included oscillation at 29 Hz. In addition, the discharge voltage instantaneously increased in Phase 3. The thruster was operated in constant current mode in Phase 2 when the power supply was turned on. The discharge voltage and current fluctuated with changes in the electric resistance because the resistance and pressure between the electrodes was increased by reaction products and unreacted propellant. Although the constant-current mode operated in Phase 2, it seems that the constant-voltage mode and constant-current mode operated with changes in Phase 3. The increased power consumption in Phase 3 was therefore affected by the reaction of SHP163 utilizing discharge plasma.

In contrast with the case for feed pressure of 400 kPa, some failed cases were observed at a feed pressure above 600 kPa. The SHP163 ignited for a few seconds after the propellant valve opened as shown in Fig. 5-6 (b). However, the thrust and pressure decreased after the SHP163 ignited. In cases of failed ignition, power consumption of approximately 58 W was observed in Phase 3. It seems that the discharge plasma of argon could

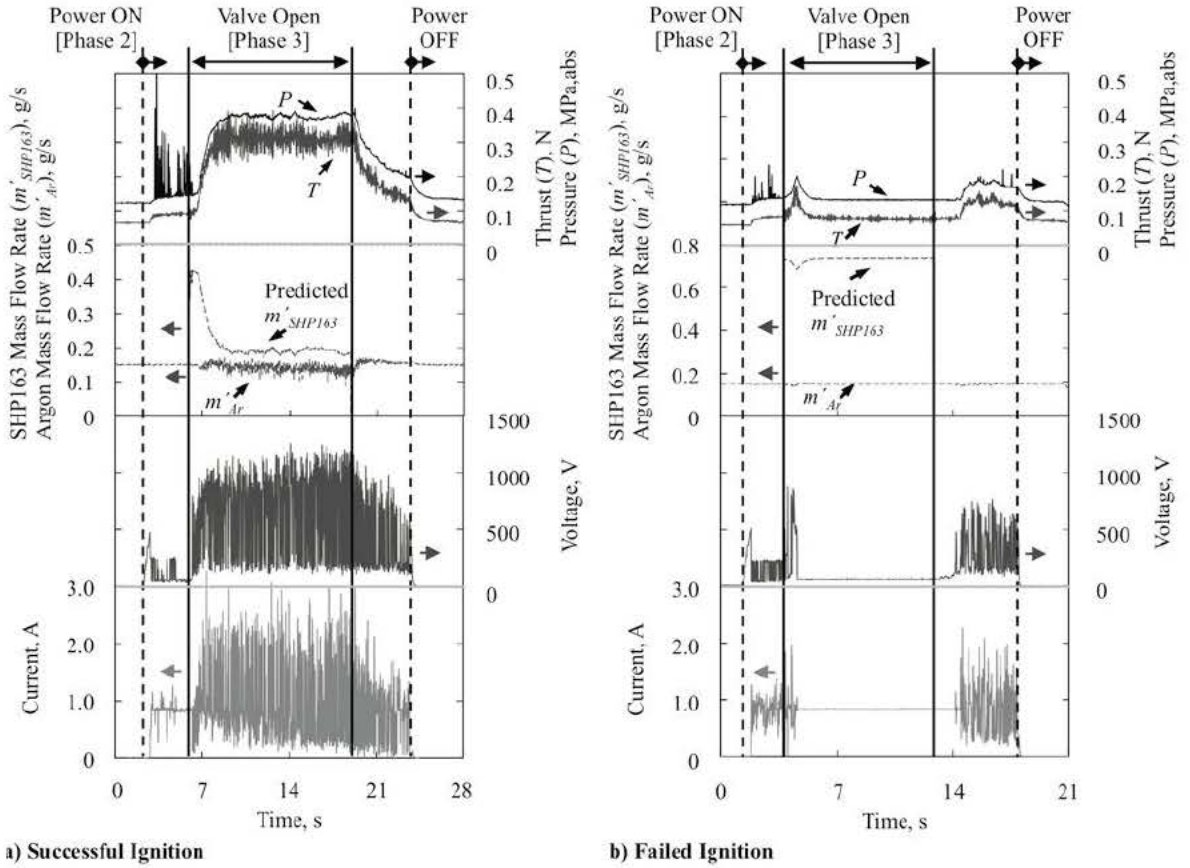

Fig. 5-6 a) Waveform of successful ignition at SHP163 feed pressure of 400 kPa and b) that of failed ignition at SHP163 feed pressure of 800 kPa.

not be generated between the electrodes because the discharge zone was filled with unreacted propellant and electric current then conducted through propellant between the cathode and anode.

At successful ignition, the Mach disk in underexpanded flow was observed from downstream of the thruster as shown in Fig. 5-7. In addition, no plume of argon plasma in Phase 2 was observed. This result suggests that the flow of reacted gas was choked in the throat nozzle. In addition, it seems that the observed emissions of the plume from the throat nozzle were affected by reaction products (e.g., N_2 NO, N_2O, NO_2, CO and CO_2) of SHP163. It is likely that some of the products of SHP163 were ionized and dissociated in the combustion chamber in Phase 3. The following equation (i.e., an experimental equation of H. Ashkenas and F. S. Sherman) [5] gives the relation between the combustion chamber pressure P_c and the length from the throat part to the location of the Mach disk X_M.

$$\frac{X_M}{D_t} = 0.67 \left(\frac{P_c}{P_a}\right)^{0.5} \tag{5-1}$$

This equation is independent of gas properties at $15 < P_c / P_a < 17{,}000$. The relation between the pressure ratio (P_c / P_a) and X_M / D_t is shown in Fig. 5-8. The error bars represent the standard deviation for testing of three times. Although the ambient pressure in the vacuum chamber was 100 Pa before the firing test, the ambient pressure after the firing test varied from 1.0 to 1.2 kPa owing to the effect of the argon gas and reaction products. It was confirmed that the prediction line of Eq. (5-1) and measurements were almost the same. It was thus observed that the measured pressure of the internal argon gas tube approximates the combustion chamber pressure.

a) Downstream views of a thruster.

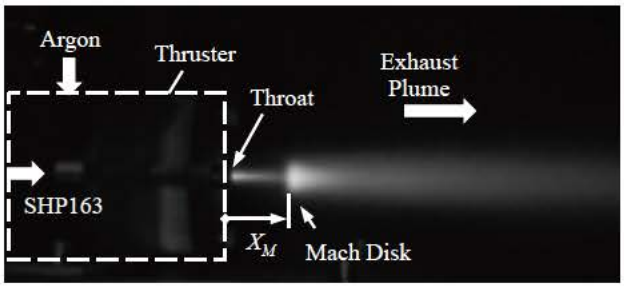

b) Side-view of a thruster.

Fig. 5-7 Hot-fire testing of the thruster with the discharge plasma system under vacuum conditions.

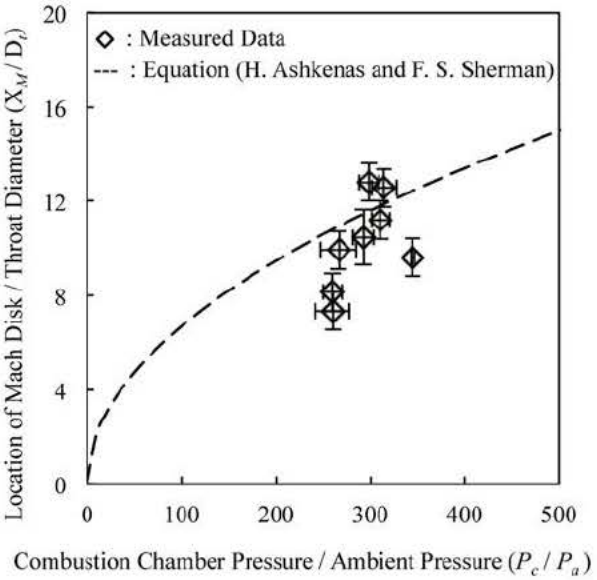

Fig. 5-8 Relation between the pressure ratio (combustion chamber pressure/ambient pressure) and the location of the Mach disk.

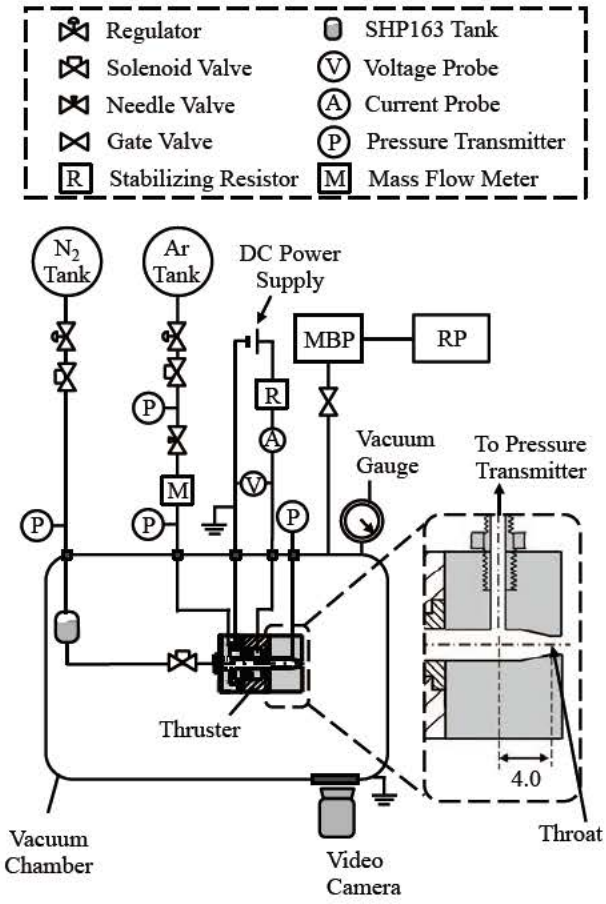

Fig. 5-9 Overview of the experimental apparatus for the pressure evaluation.

5.2.2. Evaluation of Combustion Chamber Pressure

To evaluate internal pressure of thruster, the pressure of upstream (internal pressure of argon-tube) and downstream (combustion chamber pressure) of thruster were measured using Keyence AP-13S and Nagano KH-15 pressure transmitters, as shown in Fig. 5-9. The combustion chamber characteristics length is 1365 mm because the port of pressure transmitter was attached to combustion chamber. The port of pressure transmitter was installed at 4 mm away from throat nozzle. Additionally, The Keyence AP-13S pressure transmitter was attached outside the vacuum chamber using the stainless tube that has a length of 415 mm. Hence the sum of

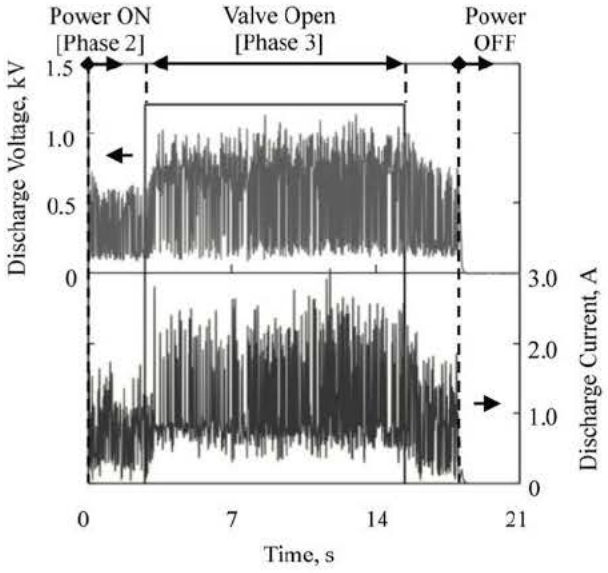

a) Waveforms of discharge voltage and current.

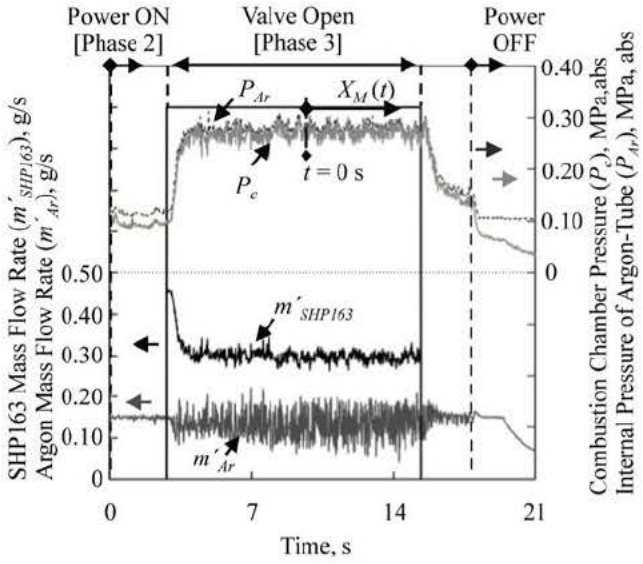

b) Waveforms of pressure and mass flow rate.

Fig. 5-10 Waveforms at firing tests.

internal volume of argon tube (from needle valve to the port of swirl injector manifold) and the tube for pressure measurement is occupied 87% of the volume in the thruster. The feed pressure of SHP163 and the feed pressure of argon gas were set 0.42 MPa and 0.55 MPa, respectively.

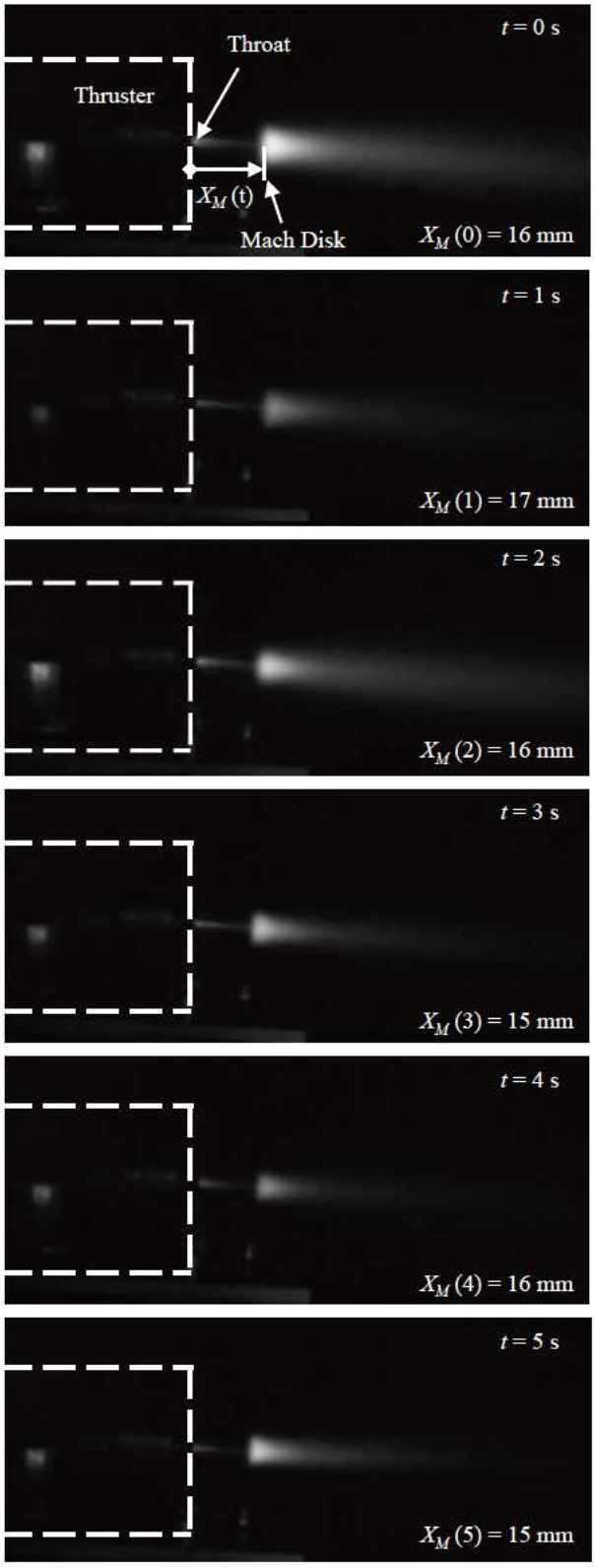

Fig. 5-11 Side-views of the thruster at firing test.

Figure 5-10 shows the result of pressure measurement of argon tube and combustion chamber. At the operation time of 0 s, the argon plasma was generated in discharge zone. Next, it was confirmed that the internal pressure of argon tube and combustion chamber pressure increased immediately after the SHP163 was injected, as shown in Fig. 5-10 b). The averaged internal pressure of argon tube and the averaged combustion chamber pressure at Phase 3 were 0.28 MPa and 0.27 MPa, respectively, and the averaged SHP163 mass flow rate and the averaged argon mass flow rate were then 0.31 g/s and 0.13 g/s, respectively. Figure 5-11 shows the photographs from side view of the thruster for 6 s before propellant valve was closed. At X_M (t = 0) = 16 mm and P_a = 800 Pa, the predicted combustion chamber pressure was 0.29 MPa by Eq. (5-1). Additionally, the length from the throat part to the location of the Mach disk in a range of operation time t from 0 s to 5 s was from 15 mm to 17 mm, and the predicted combustion chamber pressure was then from 0.26 MPa to 0.33 MPa. It was thus observed that the measured combustion chamber pressure approximates the predicted pressure by the length from the throat part to the location of the Mach disk. In addition, it was confirmed that pressure drop between the upstream of thruster (i.e. argon tube) and combustion chamber at steady operation was 0.01 MPa.

The response of the 1N-class RCS thruster is generally required at about 50 ms for pulse operation in orbit [6, 7]. The ignition delay time and the rise time of pressure were evaluated by the discharge waveforms and measured combustion chamber pressure. In this thesis, the ignition delay time and rise time of combustion chamber pressure were defined as follows.

- “Ignition Delay Time” is the time from the opening of the propellant valve to the start of chemical reaction (i.e. the start of reaction of SHP163).
- “Rise Time of combustion chamber pressure” is the time from the start of increased pressure to 90% steady combustion chamber pressure (90% P_c).

Figure 5-12 shows the waveforms in a range of operation from the open signal of the propellant valve to the steady operation of thruster (for 1 s of the operation time). At the operation time of 0 s, the open signal of propellant valve was acquired from the data logger. As a result, ignition delay time was 458 ms when the discharge voltage starts fluctuating. In the case of doublet injector, the ignition delay time was longer than with a single-hole injector, as shown in the results of chapter 4. It thus seems that it takes propellant a while to stabilize the atomization conditions (i.e. the distribution and particle diameter of the droplet) and the mass flow rate.

Next, the rise time of combustion chamber pressure (from the start time of increased pressure 270 ms to 90% P_c) was 597 ms. In addition, the time required for combustion chamber pressure to approximate the internal pressure of argon tube from the start of increased pressure was 150 ms. Thus, it seems that the rise time of the pressure is able to decrease by design of the smaller volume about the tube (i.e. tube for measurement system and gas feed system) and the combustion chamber because the response depends on the internal volume of thruster. Additionally, since the propellant was supplied in the swirling gas, it seems that the propellant makes

contact with the electrode and the wall of combustion chamber before propellant feeding in the discharge zone, and is fed along the wall.

Therefore, it seems that the response of the thruster is depended on the swirl strength of argon gas and atomization conditions of SHP163 because the response of the thruster was strongly affected by plasma distribution before propellant ignition by the result of chapter 4.

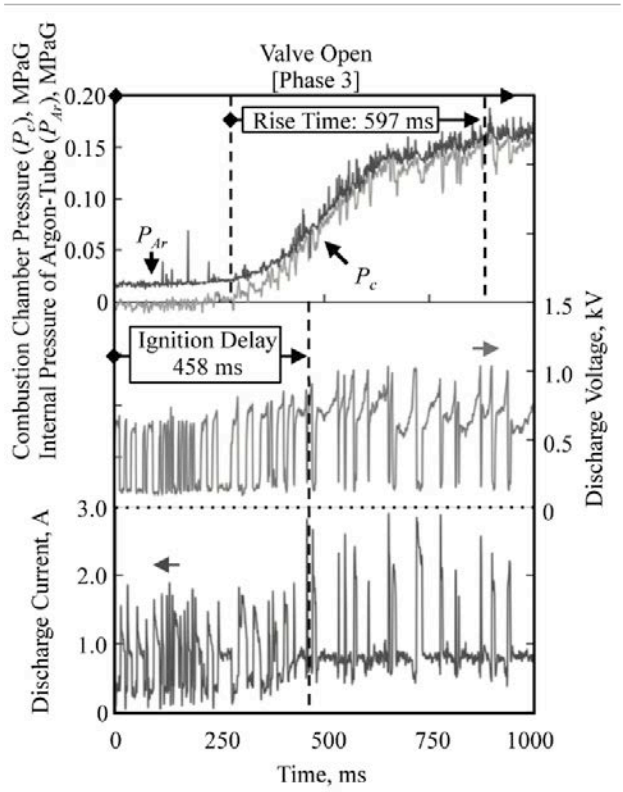

Fig. 5-12 Ignition delay time and rise time of combustion chamber pressure.

5.2.3. Effects of L-star on Combustion Characteristics

In this section, the feed pressure of the SHP163 is fixed at 400 kPa because some failed cases were observed at feed pressures above 600 kPa as described in the previous section. Here, from this section, all of firing tests were conducted at the configuration of Fig. 5-2. Figure 5-13 shows the effects of the combustion chamber characteristic length (L-star) on thrust and power consumption. The errors represent the standard deviation for testing of three times. The average thrust was varied from 0.27 to 0.29 N at each L-star. It was confirmed that power consumption of the argon plasma (in Phase 2) and thrust are less affected by L-star. The average power consumption in Phase 2 was 142 W. In addition, power consumption in Phase 3 varied from 393 to 516 W.

To evaluate the combustion characteristics, the efficiency of the characteristic exhaust velocity (C^*, C-star) is defined as the ratio of measured and theoretical values of C-star. In this experiment, the experimental C-star is evaluated using the pressure of the internal argon gas tube P_c because the difference in pressure between

the internal argon gas tube and combustion chamber was small, such as in the results of the previous section. The combustion chamber pressure is evaluated by the measured pressure of the internal argon gas tube (upstream of the thruster) under steady operation. The following equation is used to calculate the C-star efficiency η_{C^*} [4].

$$\eta_{C^*} = \frac{C^*_{Exp.}}{C^*_{Theory}} = \frac{\left(\frac{P_c A_t}{m'_{SHP163}}\right)}{C^*_{SHP163}} \tag{5-2}$$

Here, m'_{SHP163} is the predicted mass flow rate of SHP163 when the combustion chamber pressure increases. Assuming equable pressure produced in combustion chamber, the theoretical characteristic exhaust velocity of SHP163 C^*_{SHP163} is calculated using NASA-CEA code [8] at a combustion chamber pressure of 0.4 MPa and a nozzle expansion ratio of 1 under the condition of frozen flow. C^*_{CEA} is a function of combustion conditions (the properties of the product gas) at the exit of the combustion chamber (throat nozzle).

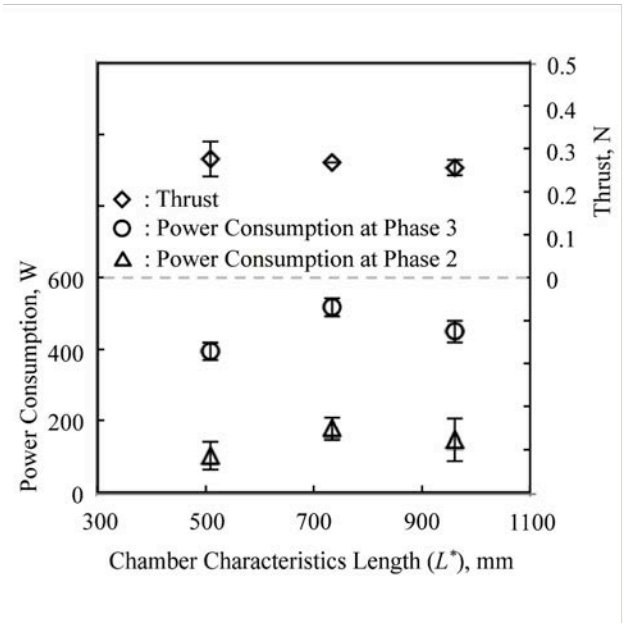

Fig. 5-13 Thrust and power consumption at each chamber characteristic length.

The C-star efficiency at each L-star is shown in Fig. 5-14. The errors represent the standard deviation. It is seen that a shorter L-star increased the C-star efficiency. At a shorter L-star, the C-star efficiency exceeded 100% according to Eq. (5-2) because this equation neglects the enthalpy of argon plasma. In this thruster system, C-star reflects the effective energy of SHP163, argon gas, the quality of combustion chamber and injectors. Thus, in this thruster, to evaluate the combustion characteristics of SHP163, the following equation is used to calculate the C-star efficiency without the argon plasma η'_{C^*}.

$$\eta'_{C^*} = \frac{C^*_{Exp.}}{C^*_{Theory}} = \frac{\left\{\frac{(P_3 - P_2)A_t}{m'_{SHP163}}\right\}}{C^*_{SHP163}} \tag{5-3}$$

Here, P_2 is the pressure of generated argon plasma at Phase 2, and P_3 is the pressure in combustion chamber at Phase 3. Neglecting the ionization and dissociation of some reaction product of SHP163, and assuming that the argon plasma is generated at Phase 3 in the same reaction as Phase 2, it is assumed that the increased pressure (the difference in pressure between the pressure of Phase 2 and Phase 3) indicates the reacting SHP163 by argon plasma.

At an L-star of 508 mm, a C-star efficiency of 88% is obtained using Eq. (5-3). In addition, it is observed that a shorter L-star increases the C-star efficiency of Eq. (5-3). However, in all experiments, unreacted propellant was observed from the throat nozzle. It thus seems that the input energy of argon plasma is insufficient for a reaction with a propellant under these experimental conditions. In addition, it seems that the performance of the thrust and C-star efficiency is strongly affected by the thermal and friction loss at the combustion chamber wall at a longer combustion chamber length (from the orifice of the injector to the throat nozzle).

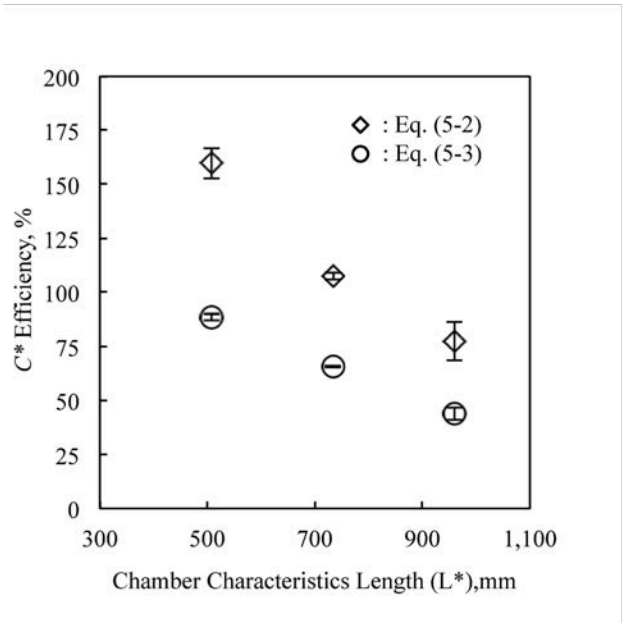

Fig. 5-14 C-star efficiency at each chamber characteristic length.

5.2.4. Improvement in Ignition Performance

Sections 5.2.1 to 5.2.3 reported experimental results of a thruster with a like-impinging doublet injector. However, some failed cases at an SHP163 feed pressure exceeding 600 kPa were observed for the doublet injector. To improve ignition performance in terms of ignition probability at a feed pressure above 600 kPa, firing tests under a vacuum condition with a single-hole (non-atomized) injector (LEE INZA4710975H) were conducted five times for each SHP163 feed pressure. The measured mass flow rate of SHP163 with the single-hole injector under a sea-level condition is shown in Fig. 5-15.

The L-star of the combustion chamber was fixed at 508 mm because the high C-star efficiency under this condition was confirmed with the doublet injector. Figure 5-16 shows ignition characteristics of the doublet and

single-hole injectors at various SHP163 feed pressures. In addition, before vacuum firing tests were conducted, the measured mass flow rate of SHP163 under a sea-level condition is shown in Fig. 5-16. In the case of the doublet injector, failed ignition cases, such as that corresponding to the waveform in Fig. 5-6 (b), were observed. Conversely, for the single-hole injector, there was no failed ignition case at any SHP163 feed pressure. This result suggests that the stable ignition of SHP163 is strongly affected by the propellant injection method. It seems that the propellant reaction is stabilized because the non-atomized propellant (with the single-hole injector) is less affected by the swirling argon gas in comparison with the atomized propellant (with the doublet injector).

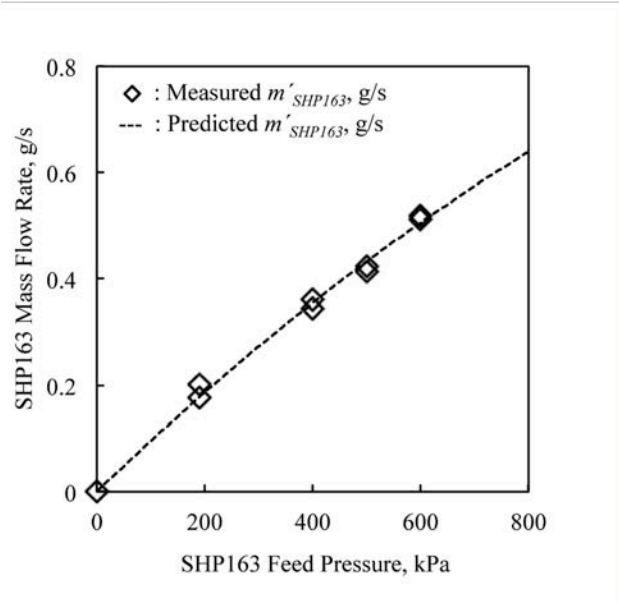

Fig. 5-15 SHP163 mass flow rate of the single-hole injector at various feed pressures.

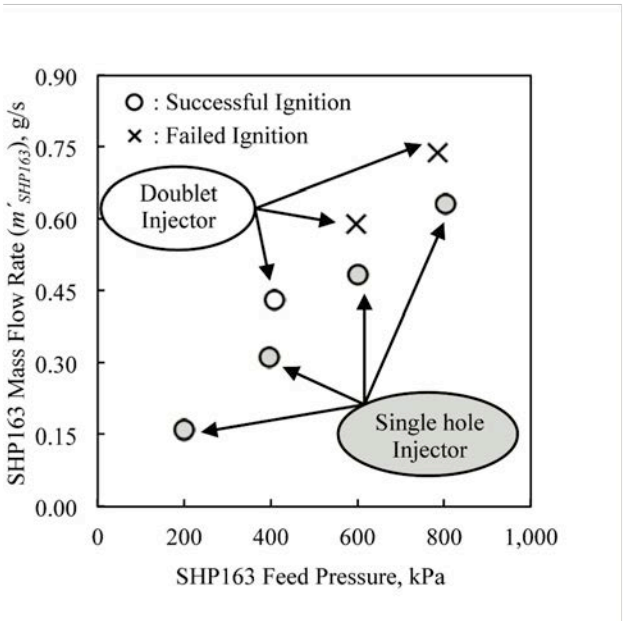

Fig. 5-16 Effect of the propellant injection method on ignition performance.

Figure 5-17 shows the thruster performance with each injector, power consumption and measured thrust. In addition, Fig. 5-18 shows the effect of the ratio of mass flow rate (m'_{SHP163} / m'_{total}) on C-star efficiency. Here, the total mass flow rate m'_{total} indicates the sum of SHP163 mass flow rate and argon mass flow rate. The errors represent the standard deviation for five times from each trial. It is seen that the measured thrust and power consumption are less affected by the injection method at an SHP163 feed pressure of 400 kPa. In contrast, a C-star efficiency of the single-hole injector higher than that of the doublet injector is confirmed at an SHP163 feed pressure of 400 kPa. For the single-hole injector, power consumption in Phase 3 tends to increase; e.g., it exceeds 200 W at an SHP163 feed pressure of 200 kPa. The power consumption in Phase 2 was varied approximately from 62 to 103 W, and it was reproducibly observed that argon plasma in Phase 2 is generated for each feed pressure. It thus seems that power consumption in Phase 3 is strongly affected by the mass flow rate of SHP163.

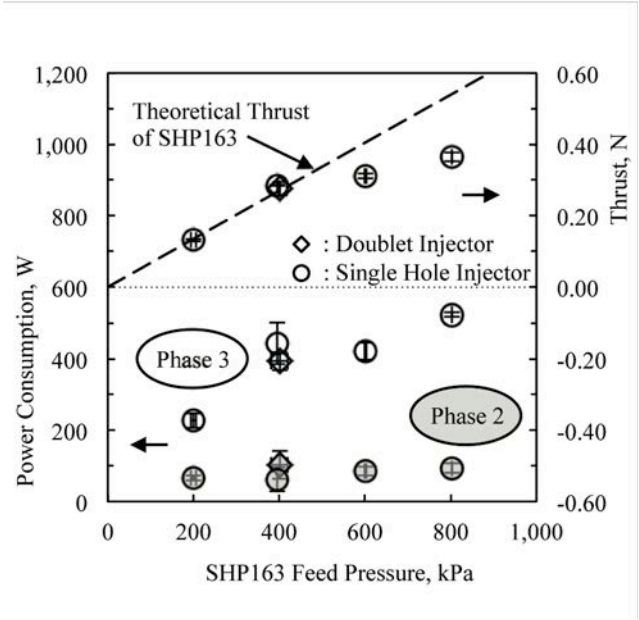

Fig. 5-17 Effects of SHP163 feed pressure on the performance of the thruster.

The following equation is used to calculate the theoretical thrust of SHP163. In this equation, C-star and the thrust coefficient are assumed to be 1417 m/s and 1.24 at efficiency of 100%, respectively. C-star of SHP163 is calculated using NASA-CEA code at a combustion chamber pressure of 0.4 MPa and a nozzle expansion ratio of 1 under the condition of frozen flow.

$$F = m'_{SHP163} C^*_{SHP163} C_F \tag{5-4}$$

Here, m'_{SHP163} is the predicted mass flow rate of SHP163 and is defined as follows.

$$m'_{SHP163} = -1.53 + \sqrt{\frac{P_F - P_c}{330.34} - 1.53^2} \tag{5-5}$$

In Eq. (5-5), P_F and P_c are the SHP163 feed pressure and measured combustion chamber pressure, respectively. The mass flow rate is proportional to the square root of the difference in pressure between the propellant tank and the orifice of the single-hole injector [4]. Equation (5-5) thus gives the predicted SHP163 mass flow rate of Fig. 11. The measured thrust in a range of feed pressure from 200 to 400 kPa is broadly consistent with the theoretical thrust. In comparison with the theoretical thrust of SHP163, the measured thrust was low at feed pressure exceeding 600 kPa. In addition, it was confirmed that the C-star efficiency tends to be lower at higher SHP163 feed pressure (higher ratio of mass flow rate). In the case of the single-hole injector, a maximum thrust of 0.37 N was achieved with power consumption of 527 W and an SHP163 mass flow rate of 0.34 g/s, in conjunction with C-star efficiency of 98%. In contrast, at an SHP163 feed pressure of 200 kPa (mass flow rate-ratio of 0.22), a maximum C-star efficiency of exceeding 200% was achieved with power consumption of 213 W and an SHP163 mass flow rate of 0.04 g/s, in conjunction with thrust of 0.13 N. Here, the C-star efficiency is calculated using Eq. (5-3). This result indicates that this thruster was operated with exceeding input energy of argon plasma at lower mass flow rate-ratio. In addition, this result indicates that the propellant reaction is insufficient at the higher SHP163 mass flow rate and suggests that the reaction amount of SHP163 is limited by the discharge plasma of argon under this experimental condition. In addition, it was confirmed that the reactivity of propellant is strongly affected by the effect of the propellant injection method and the ratio of mass flow rate.

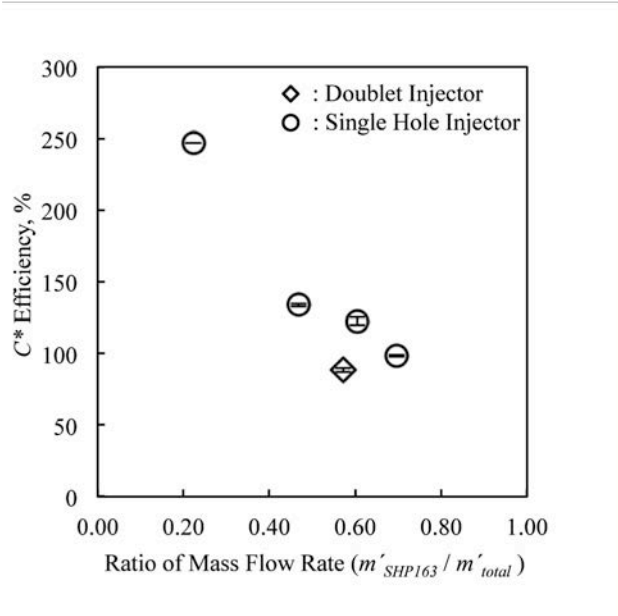

Fig. 5-18 Effect of the ratio of mass flow rate (SHP163 mass flow rate/total mass flow rate) on C-star efficiency.

The pre-heating energy requirement of 0.5 N class HAN-based thruster with catalyst is approximately 1.3 W-Hr (20 W for 240 s) [9]. In contrast with our system, energy consumption is approximately 2.2 W-Hr (527 W for 15 s). Assuming the operation of thruster for 1 s, the energy consumption for SHP163 ignition will be

approximately 0.15 W-Hr (527 W for 1 s), and the operation for 1 s at approximately ten times will be possible with the same energy requirement because of a thruster with a discharge plasma system can be cold started (without preheating). However, to improve the reactivity and the input energy efficiency, it seems necessary to consider the effects of input energy and plasma generation method on the performances.

Figure 5-19 shows the histories of measured thrust and combustion chamber pressure at various feed pressures of SHP163 for the single-hole injector. Here, the firing test time is 13 s at feed pressures of 400 and 600 kPa and 18 s at feed pressures of 200 and 800 kPa. In this thesis, the response of the thrust and pressure is defined as the time from the start of propellant ignition (i.e., rising thrust or combustion chamber pressure) to 90% steady thrust (or 90% steady combustion chamber pressure). It was confirmed that the thrust and pressure response tends to be higher at higher SHP163 feed pressure. However, at feed pressure of 800 kPa, the response tends to be longer because the flow velocity of the propellant increases. The response is thus strongly affected by the feed pressure. To improve the response of this thruster system, it seems necessary to extend the stay time of propellant at the generated discharge plasma.

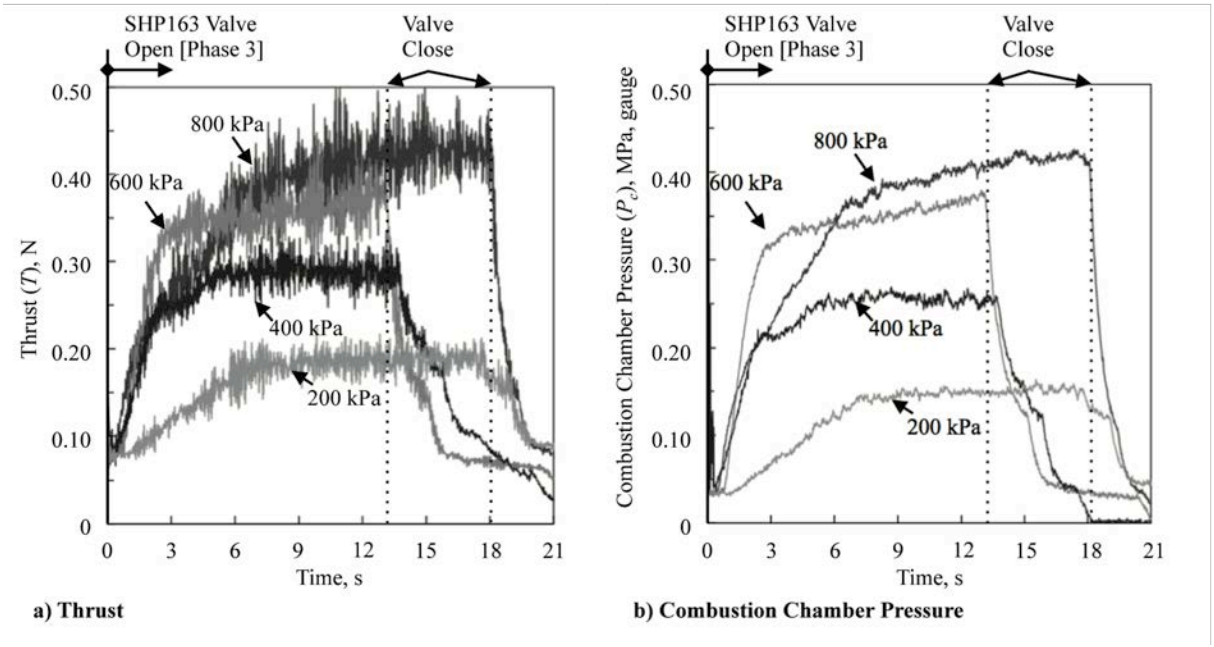

Fig. 5-19 a) Thrust and b) pressure histories at various SHP163 feed pressures.

5.3. Summary

Firing tests of a 1-N-class laboratory model thruster with a discharge plasma system using a hydroxylammonnium-nitrate based monopropellant (SHP163) were conducted under a vacuum condition. The experiments evaluated the effects of the HAN based monopropellant mass flow rate and combustion chamber characteristic length (L-star) on combustion characteristics by measuring thrust and pressure under ambient pressure of 1.2 kPa. The L-star was varied by varying the combustion chamber length, and the designed

combustion chamber pressure (in the throat area) was fixed. With a laboratory model of a like-impinging doublet injector, stable operation at feed pressure of 400 kPa was confirmed without any failed ignition, and average thrust of 0.28 N, combustion chamber pressure of 0.38 MPa and power consumption of 393 W were then observed at an argon mass flow rate of 0.15 g/s, HAN-based monopropellant mass flow rate of 0.24 g/s, L-star of 508 mm and nozzle expansion ratio of 1. However, some failed cases were observed at feed pressures above 600 kPa. In addition, it was observed that a shorter L-star increased the characteristic exhaust velocity efficiency. At L-star of 508 mm, C-star efficiency of 88% was obtained with argon plasma. To improve the ignition performance in terms of the ignition probability at feed pressures above 600 kPa, firing tests under a vacuum condition with a single-hole (non-atomized) injector were conducted. As a result, for all SHP163 feed pressures, there were no failed ignition cases with a single-hole injector. With a single-hole injector, at SHP163 feed pressure of 800 kPa, maximum thrust of 0.37 N was achieved with power consumption of 527 W and an SHP163 mass flow rate of 0.34 g/s, in conjunction with C-star efficiency of 98%. In this fundamental study of HAN-based thruster with discharge plasma system, it was obtained the consumed power at combustion of SHP163 for 15 s was similar to preheating energy of catalyst, and the hot firing tests of the thruster was demonstrated the operation successfully under vacuum condition.

5.4. Reference in Chapter 5

[1] Jankovsky, R. S., "HAN-Based Monopropellant Assessment for Spacecraft," AIAA-96-2863, July 1996. doi: 10.2514/6.1996-2863

[2] Amrousse, R., Katsumi, T., Itouyama, N., Azuma, N., Kagawa, H., Hatai, K., Ikeda, H., and Hori, K., "New HAN-based Mixtures for Reaction Control System and Low Toxic Spacecraft Propulsion Subsystem: Thermal Decomposition and Possible Thruster Applications," *Combustion and Flame*, published online 17 April 2015; Vol. 162, No. 6, 2015, pp. 2686–2692. doi: 10.1016/j.combustflame.2015.03.026

[3] Katsumi, T., Inoue, T., Nakatsuka, J., Hasegawa, K., Kobayashi, K., Sawai, Sh., and Hori, K. H., "HAN-Based Green Propellant, Application, and its Combustion Mechanism," *Combustion, Explosion, and Shock Waves*, Vol. 48, No. 5, 2012, pp. 536–543. doi: 10.1134/S001050821205005X

[4] Huzel, D. K., and Huang, D. H., "Design of Thrust Chambers and Other Combustion Devices," *Modern Engineering for Design of Liquid-Propellant Rocket Engines*, Progress in Astronautics and Aeronautics, AIAA, Washington DC, 1992, pp. 67-133.

[5] Ashkenas, H., and Sherman, F. S., "The Structure and Utilization of Supersonic Free Jets in Low Density Wind Tunnels," *Proceedings of the 4th International Symposium, Rarefied Gas Dynamics*, Vol. 2, 1965, pp. 84–105.

[6] Neff, K., King, P., Anflo, K. and Mollerberg, R.: High Performance Green Propellant for Satellite Applications, 45th AIAA/ASME/SAE/ASEE Joint Propulsion Conference & Exhibit, AIAA-2009-4878, 2009. doi: 10.2514/6.2009-4878

[7] Valencia-Bel, F. and Smith, M.: Replacement of Conventional Spacecraft Propellants with Green Propellants, Space Propulsion Conference, 2009.

[8] Gordon, S., and McBride, B. J., "Computer Program for Calculation of Complex Chemical Equilibrium Compositions and Applications," NASA Reference Publication 1311, 1994.

[9] Tsay, M., Feng, C., Paritsky, L., Zwahlen, J., Lafko, D., and Robin, M., "Complete EM System Development for Busek's 1U CubeSat Green Propulsion Module," AIAA 2016-4905, July 2016. doi: 10.2514/6.2016-4905

Chapter 6

Performance Evaluation of a HAN-Based Monopropellant Thruster with Discharge Plasma System

In this chapter, the feasibility of HAN-based monopropellant thruster with the discharge plasma system has been evaluated. The vacuum firing tests of a laboratory model thruster with the discharge plasma system have been conducted. The performance characteristics of the thruster are discussed in terms of conditions that specific impulse, characteristic exhaust velocity (C^*, C-star) efficiency, thrust efficiency, and power consumption of SHP163 ignition. The effects of SHP163 mass flow rate on performance characteristics are experimentally evaluated at a nozzle expansion ratio of 100. Furthermore, to evaluate the reactivity and reaction products of SHP163 by argon plasma, the emission spectra from conical nozzle have been evaluated by spectroscopy. Additionally, lifetime of thruster are evaluated by the measurement of the electrodes degradation.

6.1. Experimental Conditions and Apparatus

A cross-sectional view of a laboratory model thruster with a discharge plasma system is shown in Fig. 6-1. A propellant injector for SHP163 is located upstream of the swirl gas injector. A swirl gas injector with a geometric swirl number of 6.7 is prepared because the continuity of the combustion flame was observed for this gas injector under sea-level condition in our previous study.[13] The system also comprises outer housing both upstream and downstream, insulators, electrodes (i.e., a cathode and anode), and divergent nozzle (conical nozzle). The outer housings is made of polycarbonate materials, the electrodes and conical nozzle of stainless steel (i.e., SUS303), and the insulators of alumina (Al_2O_3) ceramic. The central hole of combustion chamber (from a orifice of propellant injector to a throat nozzle) is 4.2 mm and the electrode gap is 3.5 mm.

The combustion chamber of monopropellant thruster is generally designed at about 1.0 MPa [1]. Additionally, SHP163 has a high burning rate at above 1.0 MPa [2]. However, the effect of combustion chamber pressure on combustion characteristics of SHP163 with discharge plasma is not well understood. Thus, in this study, to evaluate a operation of thruster at low combustion chamber pressure, the chamber pressure was designed to operate at 0.4 MPa.

The experimental apparatus at vacuum firing tests is shown in Fig. 6-2. The experimental apparatus consists of the thruster with discharge plasma system, gas feed system, propellant feed system, thrust stand system, DC power supply for discharge plasma generation, and emission spectroscopy system. All of

experiments were conducted under ambient pressure of 0.10 kPa for using mechanical booster pump (MBP) and rotary pump (RP). In addition, ambient pressure in vacuum chamber was measured for using vacuum gauge (Phiffer Vacuum TPR 280).

The gas feed system consists of an argon gas tank, solenoid valve (CKD AB31-02-2), mass flow meter (Keyence FD-A10), and needle valve (Keyence FD-C1). The mass flow rate of argon gas is controlled by the pressure of upstream from the argon gas tank. At static firing tests, the argon mass flow rate was measured using the mass flow meter. The propellant feed system is a pressure-fed system. The propellant feed system consists of a nitrogen gas tank, propellant tank, propellant valve (CKD USB3-6-1), coriolis mass flow meter (Keyence FD-SS02A), and single-hole injector (LEE INZA4710975H). The propellant mass flow rate is adjusted using the pressure of the pressurant gas (i.e., nitrogen gas). The HAN-based monopropellant (SHP163) mass flow rate of a 1 N-class thruster is about 0.4 g/s. In this study, the SHP163 mass flow rate is varied from 0.10 g/s to 0.50 g/s and the mass flow rate of argon gas is fixed at 0.15 g/s.

The propellant feed pressure and the internal pressure of thruster (i.e., argon gas tube) were measured using Keyence AP-13S and Nagano KH-15 pressure transmitter, respectively. In our previous study, the internal pressure of the thruster (from needle valve of downstream to throat area) was evaluated by the measurements of the differential pressure and the relation between the pressure ratio and the location of Mach disk. It was observed that the measured internal pressure of the argon gas tube approximates the combustion chamber pressure, and then the difference in pressure between the combustion chamber and the argon gas tube was 10 kPa. Thus, the combustion chamber pressure is evaluated by the measured internal pressure of the argon gas tube (upstream of the thruster) under steady operation. In this study, the experimental value (e.g. characteristic exhaust velocity) is evaluated using the internal pressure of argon gas tube.

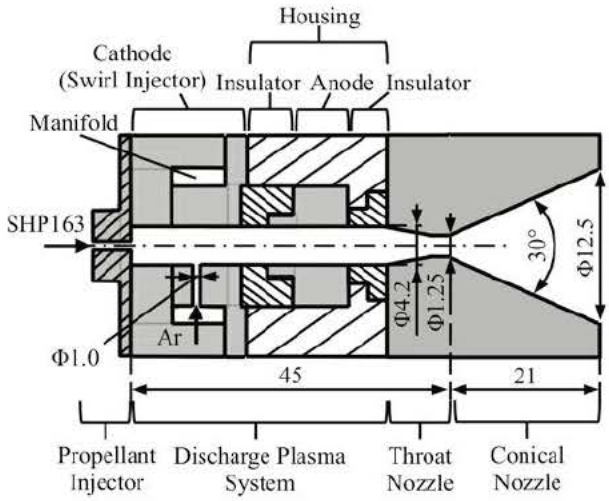

Fig. 6-1 Overview of a laboratory model HAN-based monopropellant thruster with a discharge plasma system.

The thrust stand system consists of a load cell (Kyowa LTS-200GA), pulley, spring plate (made of aluminium), and calibration weight. The thrust is calibrated using calibration weight. The normal mode-frequency of the thrust stand is 29 Hz. The DC power supply (NISTAC HV-2K10) was attached outside the vacuum chamber. The input power supply was set with following conditions: a maximum voltage of 2.0 kV and a current limit of 0.8 A. The discharge voltage and current waveforms were measured a high-voltage probe (Tektronix P6015A) and a current probe (Tektronix TCP312), respectively.

The emission spectroscopy system consists of a spectrometer (JASCO MK-300J), high speed spectroscopy CCD camera (ANDOR iDus DU420A-0E) with 1024 × 255 pixels, optical fiber, and condenser lens. The resolution performance of the measurements was set with a exposure time of 1 ms, acquisition period of 49 Hz (20 ms), entrance slit of 10 μm, and diffraction grating of 120 lines per millimeter. The profiles of the exhaust plume were recoded at 200 mm from the exit of conical nozzle. The profiles width was set at 20 mm. The CCD was triggered using the opened valve signal. The configuration of the designed thruster is given in Table 6-1.

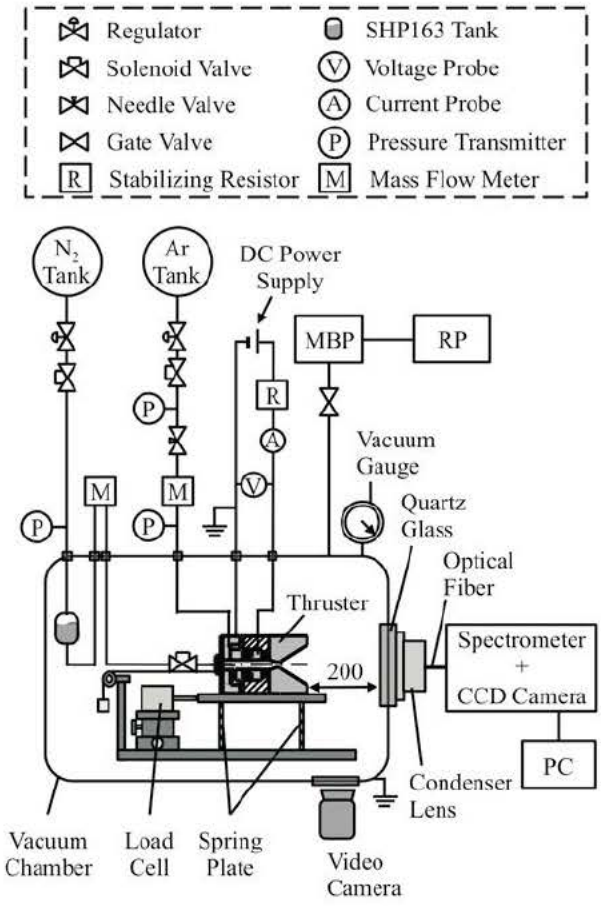

Fig. 6-2 Overview of experimental apparatus.

Table 6-1 Configurations of the designed thruster with discharge plasma system.

Target Thrust, N	0.2 to 1.0
Target SHP163 Mass Flow Rate, g/s	0.1 to 0.4
Target Argon Mass Flow Rate, g/s	0.15
Designed Combustion Chamber Pressure, MPa	0.40
Combustion Chamber Characteristic Length, mm	508
Nozzle Expansion Ratio, -	100
Half Angle of Conical Nozzle, deg.	15
Electrode Gap, mm	3.5
Discharge Current Limit, A	0.8

6.2. Performance Evaluation

6.2.1. Basic Performance

Figure 6-3 is the photograph of hot-fire testing of a laboratory model thruster with discharge plasma system under vacuum condition. At successful ignition of SHP163, the emission of plume from downstream of thruster was observed. In our previous study, the mach disk in under-expanded flow was observed from downstream of thruster with convergent nozzle as shown in Fig. 6-3 a). In addition, no plume of argon plasma in Phase 2 was observed. This result suggests that the flow of reacted gas was choked in the throat nozzle. Furthermore, it seems that the observed emission of the plume from the throat nozzle were affected by the intermediate and the reaction products (e.g. N_2, NO, N_2O, NO_2, CO, and CO_2) of SHP163. In contrast with the case for a thruster with divergent nozzle, no Mach disk was observed from nozzle exit in Phase 3 as shown in Fig. 6-3 b). In addition, the observed emission intensity of the plume from downstream of divergent nozzle was lower than the case of a thruster with convergent nozzle. This result suggests that the emission of plume in Phase 3 is strongly affected by the geometry of nozzle. Thus, it seems that the energy losses (e.g. thermal and frozen flow loss) reduced by the recombination reactions at divergent nozzle.

The waveforms at firing test of Fig. 6-3 b) is shown in Fig. 6-4. The stable operations under vacuum condition were confirmed at SHP163 feed pressure of 0.6 MPa, and steady thrust of 0.50 N and combustion chamber pressure of 0.38 MPa were then observed at an argon mass flow rate of 0.15 g/s and SHP163 mass flow rate of 0.31 g/s. Here, to evaluate the performance characteristic of the thruster, the steady thrust, combustion chamber pressure, and each mass flow rate were evaluated for 5 s before the SHP163 valve was closed. Although the ambient pressure in vacuum chamber was set at 0.10 kPa for using the pump before the hot-fire

testing was conducted, the ambient pressure was varied from 0.10 kPa to 1.2 kPa. It is likely that increased ambient pressure is affected by the reaction products and argon gas.

The instantaneous discharge voltage and current at steady operation were measured using the probe. The following equation is used to calculate the power consumption E of each phase.

$$\mathrm{E} = \frac{1}{t_f - t_i} \sum_{t_i}^{t_f} V(t) I(t) \Delta t \tag{6-1}$$

Here, Δt is the data sampling rate of 1 ms. In Phase 2, the discharge current and voltage were 0.8 A and 226 V, respectively, and then the power consumption was 181 W. Conversely, in Phase 3, the discharge current and voltage were 0.8 A and 705 V, respectively, and then the power consumption was 564 W. In addition, the energy consumption of SHP163 ignition was approximately 2.4 W-Hr (564 W for 15 s).

The thrust and pressure increased at approximately the same time after the propellant valve was opened as shown in Fig. 6-4 a). It seems that a slow rise of thrust-waveform is affected by the heat soak around throat nozzle. The waveform of thrust after the ignition of SHP163 depended on the normal mode-frequency of the thrust stand because the oscillation of thrust-waveform at 29 Hz was confirmed by frequency spectrum analysis, as shown in Fig. 6-5. Additionally, in comparison with discharge waveform of Phase 2, the discharge voltage

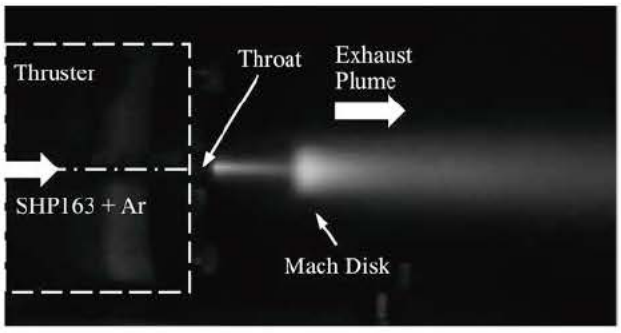

a) Thruster with convergent nozzle (expansion ratio of 1).

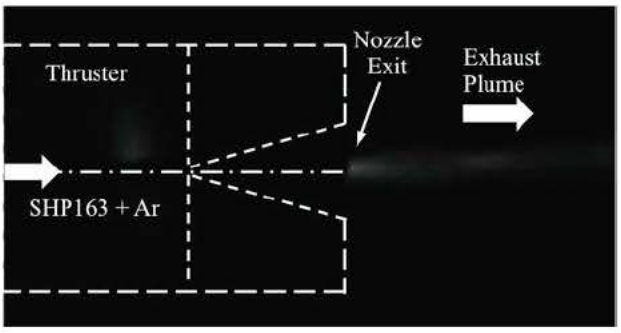

b) Thruster with divergent nozzle (expansion ratio of 100).

Fig. 6-3 Hot-fire testing of the thruster under vacuum condition.

instantaneously increased in Phase 3 as shown in Fig. 6-4 b). The thruster was operated in constant current mode at Phase 2 when the power supply was turned on. The discharge voltage and current fluctuated with changes in the electric resistance between the electrodes because the resistance and pressure in combustion chamber was increased by reaction products, intermediate products, and unreacted propellant. Although the constant-current mode operated in Phase 2 (argon plasma generation), it seems that the constant-voltage mode and constant-current mode operated with changes in Phase 3. The increased power consumption in Phase 3 was therefore affected by the ignition of SHP163 utilizing discharge plasma. Figure 6-6 shows the zoomed waveforms of discharge voltage and current. It seems that the monopropellant was ignited by discharge plasma

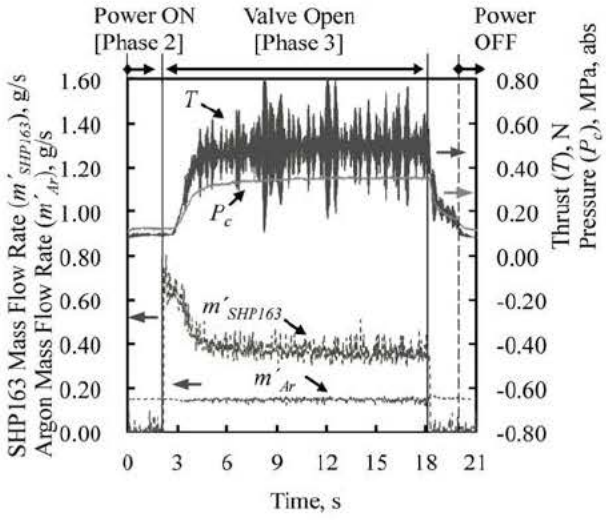

a) Thrust, pressure and each mass flow rate.

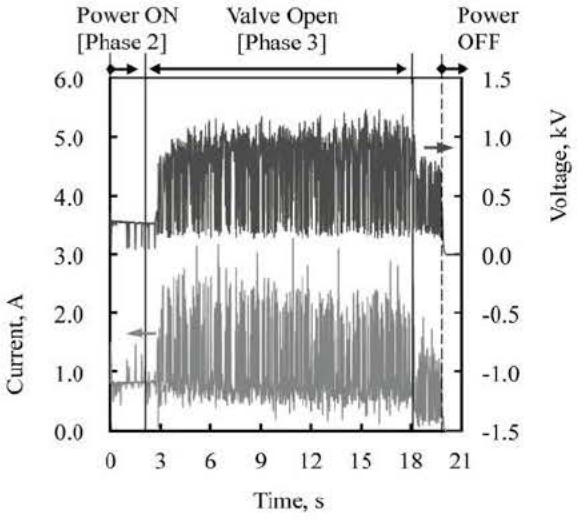

b) Discharge voltage and current.

Fig. 6-4 Waveform at hot-fire testing of the thruster with divergent nozzle.

as the following process. The reaction pathway at steady operation is presented as the sequence of events leading from (2) to (4).

(1) At constant current mode, the discharge plasma was generated from ionized argon gas because an intense electric field formed between the cathode and anode.

(2) The reacted gas of monopropellant was generated by joule heating and thermal decomposition when

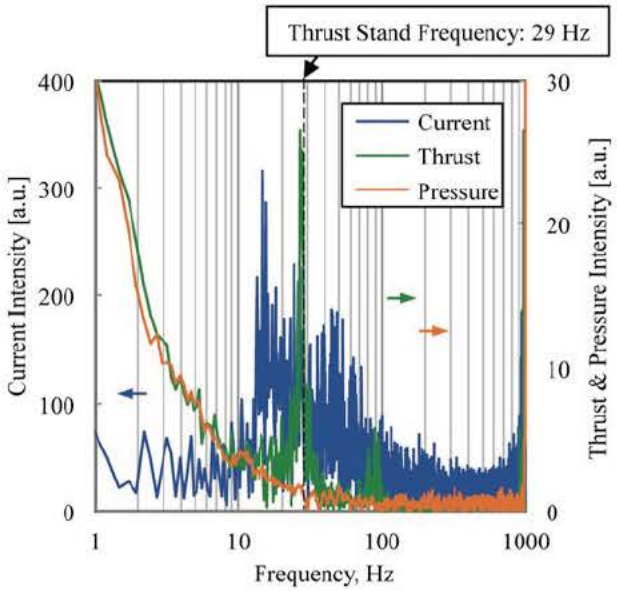

Fig. 6-5 Frequency spectrum analysis for the waveforms.

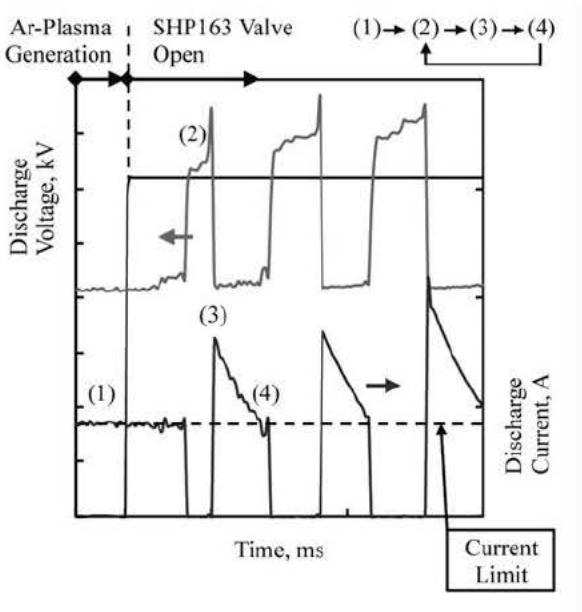

Fig. 6-6 Relationship with monopropellant ignition and discharge waveform.

it comes into contact with thermal source (i.e. discharge plasma). As a result, the keeping discharge voltage was increased by the increased pressure and resistance between the electrodes.

(3) Allowing an inrush current to flow the gas of high conductivity, at the breakdown voltage, the discharge plasma was generated by argon gas and reacted gas, and then discharge voltage was decreased.

(4) The discharge current was decreased to current limit value (at constant current mode).

Next, the effects of SHP163 feed pressure on performance characteristics have been evaluated as shown in Fig. 6-7. The performance characteristics of the thruster are discussed considering the thrust, specific impulse, characteristic exhaust velocity (C^*, C-star) efficiency, thrust efficiency and power consumption. The firing tests were conducted three times at each SHP163 feed pressure. To evaluate the performance characteristics in combustion chamber, the efficiency of the C-star is defined as the ratio of measured C-star to theoretical value of C-star. In this study, the experimental value of C-star is evaluated using the internal pressure of the argon gas tube P_c because the difference in pressure between the argon gas tube and combustion chamber was small. In addition, a value of consumed mass flow rate of SHP163 is evaluated using the mass flow meter. The following equation is used to calculate the C-star efficiency η_{C^*} [3].

$$\eta_{C^*} = \frac{C^*_{Exp.}}{C^*_{Theory}} = \frac{\left(\frac{P_c A_t}{\dot{m}_{SHP163}}\right)}{C^*_{SHP163}} \tag{6-2}$$

Here, the theoretical characteristic exhaust velocity C^*_{CEA} is calculated using NASA-CEA code [4] at a combustion chamber pressure of 0.4 MPa and a nozzle expansion ratio of 100 under the condition of frozen flow. This equation postulated the constant-pressure field in combustion chamber. C^*_{CEA} is a function of combustion conditions (the properties of the product gas) at the exit of the combustion chamber (i.e., at throat nozzle-inlet). The C-star efficiency exceeded 100% according to Eq. (6-2) because this equation neglects the enthalpy of argon plasma. In this thruster system, C-star reflects the effective energy of SHP163 and plasma, and the quality of combustion chamber and injectors. Thus, in this study, to evaluate the combustion characteristics of SHP163 utilizing argon plasma in combustion chamber, the following equation is used to calculate the C-star efficiency with the argon plasma η'_{C^*}.

$$\eta_{C^*} = \frac{C^*_{Exp.}}{C^*_{Theory}} = \frac{C^*_{Exp.}}{C^*_{SHP163}+C^*_{Ar}} = \frac{\left(\frac{P_c A_t}{\dot{m}_{SHP163}+\dot{m}_{Ar}}\right)}{C^*_{CEA}+\sqrt{2E_2/m_{Ar}}/C_F} \tag{6-3}$$

Here, neglecting the ionization and disassociation of some reaction products of SHP163, it is assumed that the power consumption of argon plasma in Phase 3 is the same as that in Phase 2. In Eq. (6-3), the thrust coefficient (C_F) is assumed to be 1.7 at a thrust coefficient efficiency of 100%. For the argon plasma of the

theoretical C-star, it is assumed that the consumed power is used for electric energy and the energy is converted to kinetic energy without energy loss (e.g. frozen flow loss, thermal loss and friction loss). The theoretical value of C-star of argon plasma for Eq. (6-3) is obtained from the conservation equation of energy that is used to calculate the relation between the kinetic energy (i.e., exhaust velocity) and thermal energy (i.e., enthalpy) at a combustion chamber and nozzle exit. Additionally, theoretical value of C-star is calculated using the sum of C-star of argon plasma and SHP163 because the argon is a noble gas. At the power consumption of 195 W and mass flow rate of 0.15 g/s, the theoretical value of C-star of argon plasma is approximately 948 m/s. To evaluate the performance characteristics of a thruster, the specific impulse *Isp* is defined as follows.

$$I_{SP} = \frac{T}{(m_{SHP163} + m_{Ar})} \tag{6-4}$$

Figure 6-7 a) shows the power consumption and SHP163 mass flow rate in Phase 3. It was observed that the power consumption for SHP163 ignition tends to be higher at higher mass flow rate of SHP163. Here, power consumption in Phase 2 was varied from 171 W to 214 W. Thus, this result demonstrates that power consumption in Phase 3 is affected by the mass flow rate of SHP163.

The measured thrust and specific impulse is shown in Fig. 6-7 b). The measured thrust in a range of feed pressure from 0.2 to 0.4 MPa was broadly consistent with the theoretical thrust. In comparison with the theoretical thrust of SHP163, the measured thrust was low at feed pressure exceeding 0.6 MPa. The thrust was varied from 0.25 to 0.50 N in a range of mass flow rate from 0.09 g/s to 0.31 g/s. Here, thrust coefficient was approximately 1.1 with a conical nozzle, and then the efficiency of thrust coefficient was 60%. It seems that the thrust coefficient was decreased owing to the effect of ionization and disassociation of the products. The specific impulse in a range of feed pressure from 0.2 MPa to 0.6 MPa was varied from 100 s to 114 s. Conversely, the specific impulse at the feed pressure of 0.8 MPa was 77 s. It was confirmed that the specific impulse tends to be lower at higher SHP163 feed pressure as shown in Fig. 6-7 b). Here, argon mass flow rate in Phase 3 was 0.15 g/s at all of experiments.

The C-star efficiency of Eq. (6-2), Eq. (5-3), and Eq. (6-3) is shown in Fig. 6-7 c). At the feed pressure ranging from 0.2 MPa to 0.6 MPa, the C-star efficiency of SHP163 exceeded 100% according to Eq. (6-2). At the feed pressure of 0.2 MPa, maximum C-star efficiency of SHP163 with argon plasma was 48% according to Eq. (6-3). In addition, it was confirmed that the C-star efficiency tends to be lower at higher SHP163 feed pressure. It is likely that stay time of the propellant between the electrodes was decreased because the velocity of the propellant increased at higher feed pressure. At the feed pressure of 0.6 MPa, maximum thrust of 0.50 N was achieved with power consumption of 564 W and an SHP163 mass flow rate of 0.31 g/s, in conjunction with specific impulse of 109 s and C-star efficiency of 41%. These results indicate that the propellant reaction is insufficient at the higher SHP163 mass flow rate and suggests that the reaction amount of SHP163 are limited by the discharge plasma of argon under this experimental condition.

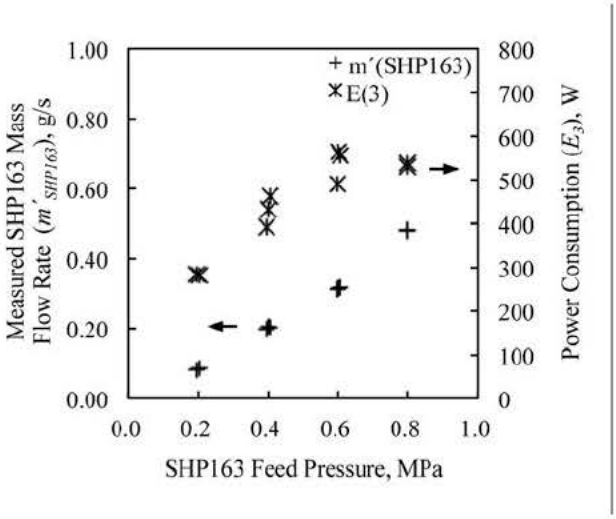

a) SHP163 mass flow rate and power consumption.

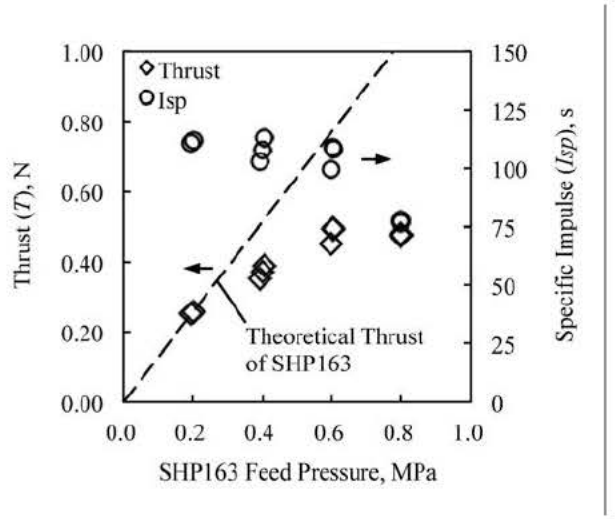

b) Thrust and specific impulse.

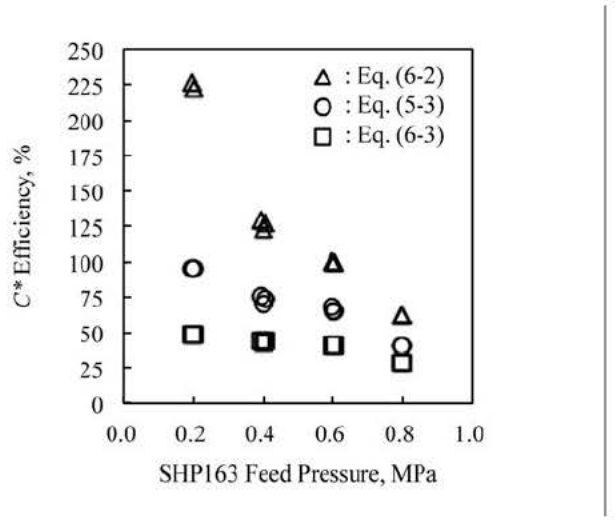

c) C-star efficiency.

Fig. 6-7 Performance characteristics of the thruster at various feed pressure.

To evaluate the performance characteristics for a thruster with discharge plasma system, the thrust efficiency by the input power is defined as follows.

$$\eta_{thrust} = \frac{T^2}{2E_3(m_{SHP163} + m_{Ar})} \tag{6-5}$$

The effects of specific power on the efficiency of C-star and thrust are depicted in Fig. 6-8. Here, specific power is the ratio of power consumption E_3 to the sum of mass flow rate of argon and SHP163. The thrust efficiency was varied from 45% to 50% in a range of specific power from 1.1 MJ/kg to 1.3 MJ/kg, and the C-star efficiency with argon plasma was then varied from 41% to 48%. It was confirmed that the efficiency increased with increasing specific power. It thus seem that the efficiencies are affected by the specific power of SHP163 because the mass flow rate of argon was fixed.

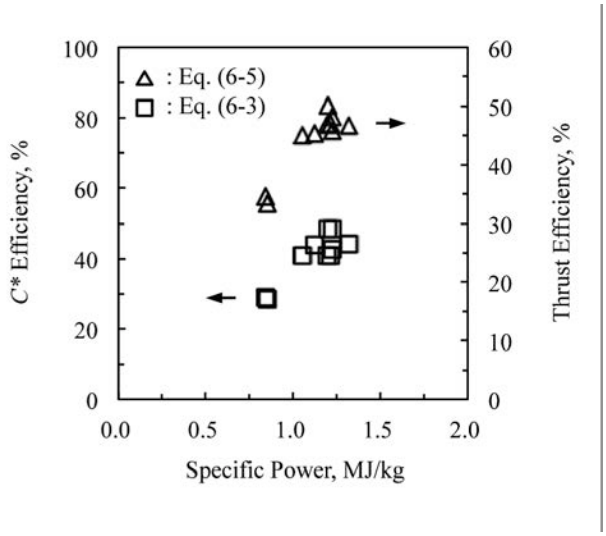

Fig. 6-8 Effects on thrust efficiency and C-star efficiency of specific power.

6.2.2. Emission Spectra

In this section, to evaluate the reactivity and reaction products of SHP163 by argon plasma, the emission spectra from conical nozzle have been evaluated by spectroscopy. Here, all of measurements were conducted at conditions of chapter 3-3.4.5.

After adiabatic combustion, predicting combustion products of SHP163 are mainly composed of water vapor (H_2O) / nitrogen (N_2) / carbon dioxide (CO_2) / molecular hydrogen (H_2) / carbon monoxide (CO) / molecular oxygen (O_2) in a ratio of 68/18/11/1/1/1 by weight percentages. For one composition of SHP163, a solid HAN is unstable and potentially explosive in a dry form [5], thus a HAN is typically mixed with water, and stored. To ensure safety for the storage and handling of HAN and understand the decomposition mechanism, on the experimental observations, the thermal decomposition pathways of HAN were proposed by Oxley and Brower [6].

$$HONH_3^+NO_3^- \rightarrow NH_2OH+HNO_3$$

$$NH_2OH+2HNO_3 \rightarrow 3HNO_3+H_2O$$

$$NH_2OH+HNO_3 \rightarrow N_2O+2H_2O$$

$$NH_2OH+HNO_3 \rightarrow NOH+HNO_2+H_2O$$

$$NH_2OH+HNO \rightarrow N_2+2H_2O$$

$$HNO+HNO_3 \rightarrow 2HNO_2$$

Additionally, the decomposition mechanisms of pure HAN and aqueous HAN have been proposed and evaluated in order to optimize the design of catalysts and thrusters with HAN-based monopropellant [7-9]. However, due to the different to form ion and radical in each ignition methods (e.g. direct heating, solid catalyst, and discharge plasma), the decomposition mechanism of HAN-based monopropellant is different. In this study, for comparison between Phase 2 (argon plasma) and Phase 3 (SHP163 ignition), the spectra of exhaust plume is evaluated from

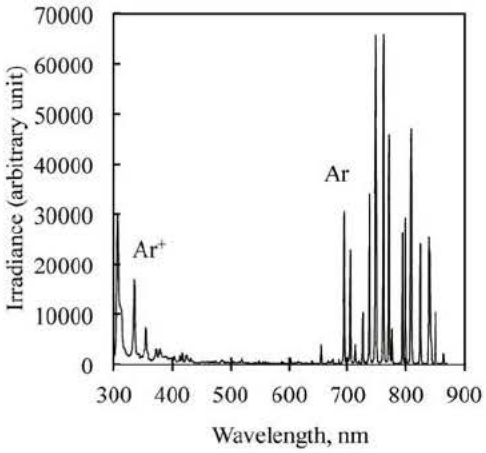

a) Argon plasma in Phase 2.

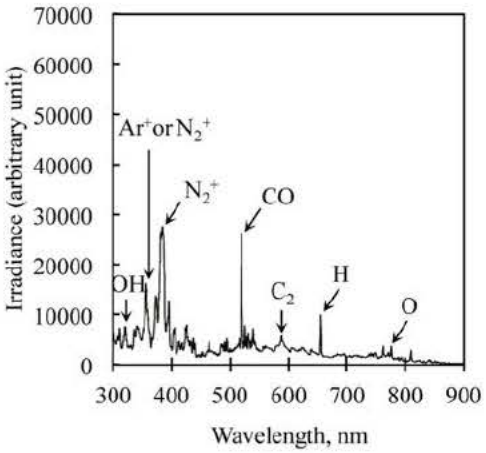

b) SHP163 ignition in Phase 3.

Fig. 6-9 Emission spectra at hot-fire testing of the thruster.

the exit of conical nozzle because no plume of argon plasma in Phase 2 was observed, such as in the results of the previous section. The emission spectra at the steady operation have been evaluated using the spectra-database [10, 11].

Figure 6-9 shows the emission spectra of argon plasma in Phase 2 and the propellant ignition in Phase 3 at the waveforms of Fig. 6-4. The univalent ion of argon and excited argon (in a range of wavelength from 690 nm to 900 nm) were observed at Phase 2 as shown in Fig. 8 a). The emission spectra of SHP163 ignition are shown in Fig. 6-9 b). In terms of the combustion products of SHP163, the carbon monoxide (CO, 519 nm), swan band (C_2, 589 nm), hydroxyl radical (OH, 309 nm), hydrogen atom (H, 656 nm), and oxygen atom (O, 777 nm) were mainly observed. In addition, NO and NO_2 (in a range of wavelength from 500 nm to 800 nm) were observed. It is likely that the visible plume-emission at the firing tests is affected by NO and NO_2 as shown in Fig. 6-3. It seems that the monopropellant was reacted by the excited argon because no excited argon in Phase 3 was observed. Thus, the generated discharge plasma is the glow discharge, and it is likely that the energy to electron by electric field is lager than the thermal energy of argon gas in Phase 3 because the ignition is strongly affected by the excitation and electron collision. The strong univalent ion of nitrogen (second positive system, 380 nm) was can be seen to appear at Phase 3. It thus seems that the ionized nitrogen (i.e., nitrogen plasma) was generated by the penning effect of argon because the difference in energy between the metastable state of argon and the ionization of nitrogen was small. Here, the metastable energy of argon and ionizing energy of nitrogen are 11.6 eV and 10.8 eV, respectively.

The effects on spectral intensity of SHP163 feed pressure were evaluated because it was confirmed that the C-star efficiency tends to be lower at higher SHP163 feed pressure as described in the previous section. Figure 6-10 shows the emission spectra at SHP163 feed pressure from 0.2 MPa to 0.8 MPa. The ratio of irradiance (i.e., emission intensity) of spectra from water vapor (e.g. hydroxyl radical, hydrogen atom, and oxygen atom) to other spectrums was evaluated because the amount of water vapor is predicted to account for

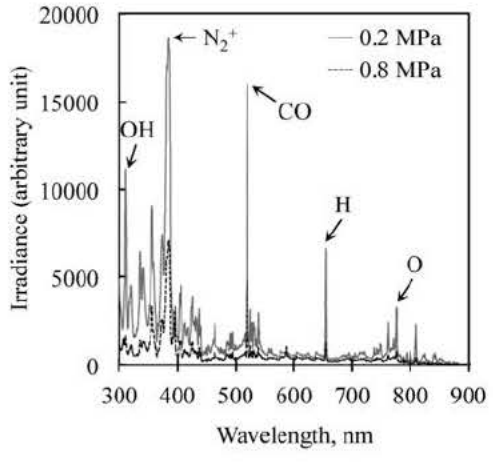

Fig. 6-10 Emission spectra at each SHP163 feed pressure.

about 68 % of reaction products at complete combustion of SHP163. Additionally, it is assumed that hydroxyl radical was generated by the oxidation reaction of carbon monoxide, and the generation and decomposition process of NO_x. Table 6-2 shows the ratio of spectral intensity at the feed pressure. At the feed pressure of 0.8 MPa, the ratio of emission intensity of hydroxyl radical (I-OH) to the nitrogen-univalent ion ($I\text{-}N_2^+$) was 0.24 ($I\text{-}OH / I\text{-}N_2^+$), and then the ratio of emission intensity of I-OH to the carbon monoxide (I-CO) was 0.26 (I-OH / I-CO), in conjunction with C-star efficiency of 28%. In contrast, at the feed pressure of 0.2 MPa, $I\text{-}OH / I\text{-}N_2^+$ and I-OH / I-CO were 0.72 and 0.65, respectively, in conjunction with C-star efficiency of 48%. These results suggest that the ratio of spectral intensity from water vapor tends to be higher at higher C-star efficiency. Additionally, in terms of the intensity of other spectrum (hydrogen and oxygen atom), the same tendency of the case of hydroxyl radical was observed. It thus indicates that the ratio of spectral intensity of water vapor is strongly affected by the reactivity (i.e., C-star efficiency) of SHP163. Fig. 6-11 shows the relationship with C-star efficiency and ratio of spectral intensity at each ratio of mass flow rate. Here, the C-star efficiency was evaluated to consider the reaction of argon plasma by Eq. (6-3), and the total mass flow rate $\dot{m}_{total}$ indicates the sum of SHP163 mass flow rate and argon mass flow rate. In comparison with the feed pressure of 0.4 MPa, the each ratio of spectral intensity at the feed pressure of 0.2 MPa was decreased. It seems that water vapor was generated by the deactivation of hydroxyl radical at higher combustion pressure. In addition, due to the difference in the ratio of mass flow rate at each SHP163 feed pressure, it is likely that the mole fraction of products is different at reactivity.

Table 6-2 Ratio of spectral intensity at the feed pressure.

		SHP163 Feed Pressure, MPa			
		0.2	0.4	0.6	0.8
The Ratio of Spectral Intensity	$I\text{-}OH / I\text{-}N_2^+$	0.72	1.01	0.81	0.24
	$I\text{-}H / I\text{-}N_2^+$	0.80	1.00	1.40	0.30
	$I\text{-}O / I\text{-}N_2^+$	0.50	1.02	0.72	0.15
	I-OH / I-CO	0.65	1.28	1.60	0.26
	I-H / I-CO	0.72	1.26	2.70	0.32
	I-O / I-CO	0.45	1.29	1.38	0.16

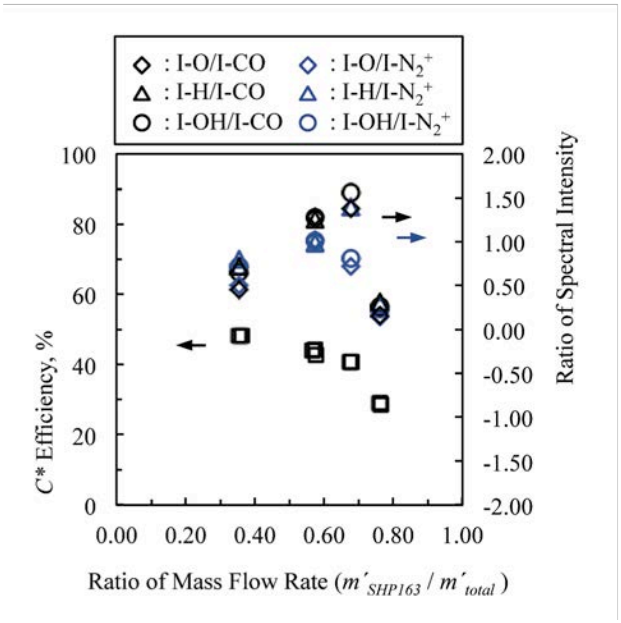

Fig. 6-11 Relationship with C* efficiency and ratio of spectral intensity.

6.2.3. Evaluation of The Thruster Lifetime

In this study, to evaluate the effect of electrodes degradation on the thruster performances, the electrodes are made of stainless steel (SUS303) that has lower the resistance characteristics of oxidizing combustion and melting point in comparison with Inconel Alloys and Tungsten-Copper (WCu). Figure 6-12 shows the surface degradation of electrodes versus accumulated firing time. In this paper, the degradation condition of electrodes in the firing tests is discussed in terms of the mass and diameter of an electrode. The diameter of the electrode was 4.2 mm before firing tests (i.e., at an accumulated time of 0 s). In firing tests for the sea-level condition, the masses of the cathode and anode decreased with increasing accumulated firing time; the cathode and anode had lost 0.009 and 0.008 g, respectively, at an accumulated time of 1169 s. The diameters of the cathode and anode at that time were 4.3 mm (D_C (1169 s)) and 4.5 mm (D_A (1169 s)), respectively. In contrast, in firing tests under the vacuum condition, the cathode and anode had lost 0.025 and 0.047 g, respectively, at an accumulated firing time of 477 s, and the diameters of the cathode and anode were 4.5 mm (D_C (1646 s)) and 5.0 mm (D_A (1646 s)), respectively. It is thus confirmed that the wear rate of electrodes is affected by atmospheric pressure. It seems that the degradation condition of electrodes is strongly affected by the generated plasma and combustion products. However, at accumulated times ranging from 1169 to 1646 s, no effect of the surface degradation of electrodes on performances of the thruster was observed at feed pressure of 400 kPa. Assuming accumulated vacuum firing tests of 24 hours (corresponding to the end of life, EOL) conducted for an RCS thruster [12, 13], the linearly decreasing masses of cathode and anode will reach 2.596 and 6.9129 g, respectively, and it seems that the performance of thruster will decrease at the EOL owing to the effects of electrode degradation.

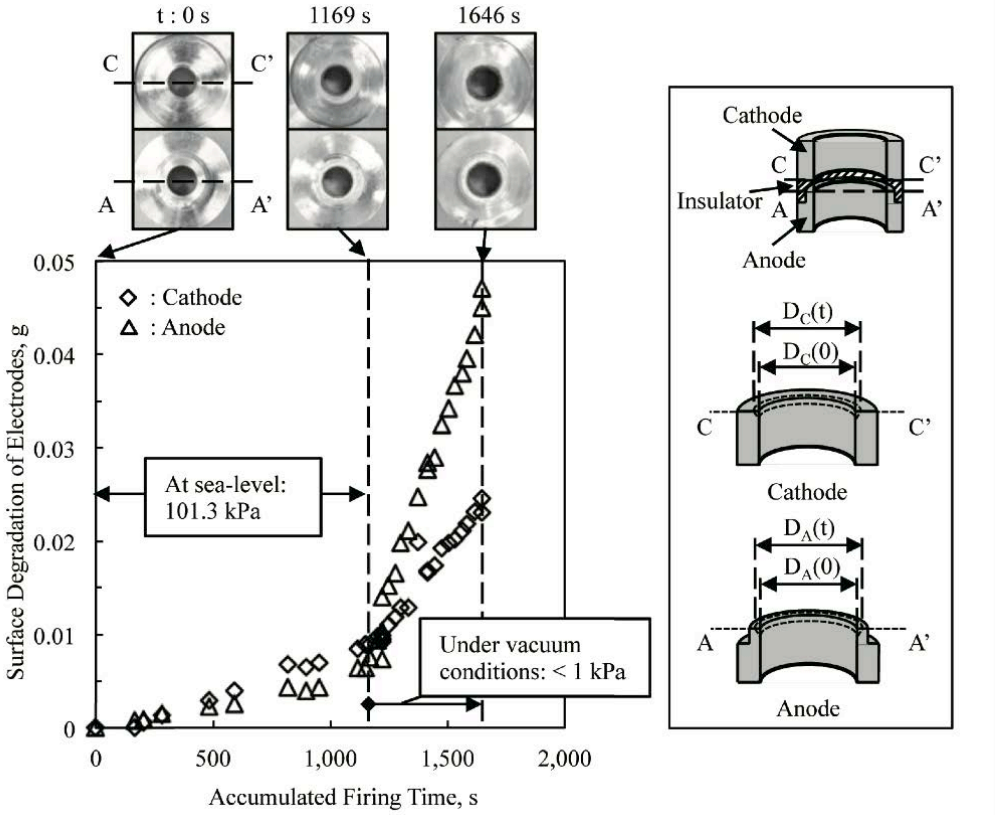

Fig. 6-12 Effects of the accumulated firing time on electrode degradation.

6.3. Summary

To evaluate the performance characteristics of the thruster by measuring thrust, pressure and spectra of exhaust plume, the vacuum firing tests of a laboratory model thruster with discharge plasma system using hydroxylammonium-nitrate based monopropellant (SHP163) have been conducted. As a result, the hot-fire tests of the thruster have demonstrated the operation successfully under vacuum. At the feed pressure of 0.6 MPa, maximum thrust of 0.50 N was achieved with power consumption of 564 W and SHP163 mass flow rate of 0.31 g/s, in conjunction with specific impulse of 109 s, C-star efficiency with argon plasma of 41%, and thrust efficiency of 47%. In addition, it was confirmed that measured thrust was varied from 0.25 N to 0.50 N in a range of SHP163 mass flow rate from 0.09 g/s to 0.31 g/s. Here, the mass flow rate of argon gas is fixed at 0.15 g/s for plasma generation. To evaluate the reactivity and reaction products of SHP163 by argon plasma, the emission spectra from conical nozzle evaluated by spectroscopy. For the intermediate products of SHP163, NO and NO_2 were observed. Additionally, in terms of the combustion products of SHP163, the emission spectrums of carbon monoxide, swan band, hydroxyl radical, hydrogen atom, and oxygen atom were observed at hot-fire tests. It was confirmed that the characteristic exhaust velocity efficiency tends to be higher at higher spectral intensity (e.g. OH). However, the spectral intensity of reaction products from water vapor was lower than the other products (e.g. CO_2 and N_2). Thus, these results indicate that the propellant reaction is insufficient at the higher SHP163 mass flow rate and suggests that the reaction amount of SHP163 is limited by the discharge

plasma of argon under this experimental condition. Moreover, as a result of thruster lifetime-evaluation, at an accumulated firing time of 1646 s, no effect of electrode degradation on the performance of the thruster was observed. Although the higher power (>500 W) at current operation of this system is required in comparison with catalyst-heater level (<20 W), it seems that this system has possibilities to reduce energy consumption (is expressed as a product of power consumption and operation time) in comparison with the catalyst because the temperature of catalysts must be kept at heater temperature above 350 °C using power from 10 to 20 W, and the pre-heating is unnecessary in this discharge plasma system.

Although the standard arcjet thrusters have been operated at the high current (>10 A) and the low voltage (<100 V), this system is operated using that the discharge plasma is generated at the high voltage from 100 V to 1000 V and the low current below 1.0 A because the enhancement of ignition (i.e. the operation of high response and high thrust) for monopropellant is expected by the glow-discharge plasma (non-equilibrium plasma). Additionally, in other operation mode at lower mass flow rate (<100 mg/s), this system is expected to operate with higher specific impulse (>500 s) by Joule-heating at the high current (>10 A) and the low voltage (<100 V). Thus, this system has possibilities to operate with a dual-mode using the same power, either in a high-specific-impulse-mode (at high-current and low-voltage, such as the standard arcjet thruster) or a high-thrust-mode (in the current operation mode).

6.4. Reference in Chapter 6

[1] Jankovsky, R. S., "HAN-Based Monopropellant Assessment for Spacecraft," AIAA-96-2863, July 1996. doi: 10.2514/6.1996-2863

[2] Amrousse, R., Katsumi, T., Itouyama, N., Azuma, N., Kagawa, H., Hatai, K., Ikeda, H., and Hori, K., "New HAN-based Mixtures for Reaction Control System and Low Toxic Spacecraft Propulsion Subsystem: Thermal Decomposition and Possible Thruster Applications," *Combustion and Flame*, published online 17 April 2015; Vol. 162, No. 6, 2015, pp. 2686–2692. doi: 10.1016/j.combustflame.2015.03.026

[3] Huzel, D. K., and Huang, D. H., "Design of Thrust Chambers and Other Combustion Devices," *Modern Engineering for Design of Liquid-Propellant Rocket Engines*, Progress in Astronautics and Aeronautics, AIAA, Washington DC, 1992, pp. 67-133.

[4] Gordon, S., and McBride, B. J., "Computer Program for Calculation of Complex Chemical Equilibrium Compositions and Applications," NASA Reference Publication 1311, 1994.

[5] Harlow, D. G., Felt, R. E., Agnew, S., Barney, G. S., McKibben, J. M., Garber, R., and Lewis, M., "Technical Report on Hydroxylamine Nitrate, " U. S. Department of Energy, DOE/EH-0555, February 1998.

[6] Oxley, J. C., and Brower, K. R., "Thermal Decomposition of Hydroxylamine Nitrate," *Proc. SPIE*, Vol. 0872, Propulsion, 1988, pp.63-70. doi: 10.1117/12.943754

[7] Lee, H., and Litzinger, T. A., "Chemical Kinetic Study of HAN Decomposition," *Combustion and Flame*, Vol. 135, 2003, pp. 151-169. doi: 10.1016/S0010-2180(03)00157-3

[8] Amrousse, R., Katsumi, T., Azuma, N., and Hori, K., "Hydroxylammonium Nitrate (HAN)-based Green Propellant as Alternative Energy Resource for Potential Hydrazine Substitution: From Lab Scale to Pilot Plant Scale-Up," Combustion and Flame, published online 8 December 2016; Vol. 176, 2017, pp. 334-348. doi: 10.1016/j.combustflame.2016.11.011

[9] Brill, T. B., Spohn, P. D., and Cronin, J. T., "Thermal Decomposition of Energetic Materials 32. On the Instantaneous Molecular Nature of Aqueous Liquid Gun Propellants at High Temperature and Pressure Before Thermal Decomposition," *Journal of Energetic Materials*, Vol. 8, 1990, pp. 75-84. doi: 10.1080/07370659008017246

[10] National Institute of Standards and Technology Physical Measurement Laboratory, "NIST Atomic Spectra Database," URL: http://physics nist.gov/PhysRefData/ASD/lines_form html

[11] Pearse, R. W. B., and Gaydon, A. G., *The Identification of Molecular Spectra*, 4th ed., Chapman and Hall, 1976.

[12] Persson, M., Anflo, K., and Dinardi, A., “A Family of Thrusters For AND-Based Monopropellant LMP-103S,” AIAA-2012-3815, July 2012.
doi: 10.2514/6.2012-3815

[13] Anflo, K., and Möllerberg, R., “Fight Demonstration of New Thruster and Green Propellant Technology on the PRISMA Satellite,” *Acta Astronautica*, published online 2009; Vol. 65 2009, pp. 1238–1249.
doi: 10.1016/j.actaastro.2009.03.056

Chapter 7
Conclusion

This chapter summarizes this thesis in terms of a one newton class green monopropellant propulsion with an alternative ignition system of solid catalyst that uses discharge plasma system for spacecraft.

7.1. Summary of Thesis

The objective of this thesis is to design and build the laboratory model thruster for HAN-based monopropellant, and to evaluate the performance characteristics of the thruster. In conclusion, the findings and contributions of this thesis are summarized the following.

- An ignition system that uses discharge plasma of noble gas, called discharge plasma system was proposed. The geometric swirl number for gas supply has strong effects on the plasma distribution, the propellant ignition probability, and the ignition delay time. At an argon mass flow rate of 0.15 g/s and SHP163 (HAN-based monopropellant) mass flow rate of 0.3 g/s, the continuity of the exhaust flame from downstream of the discharge plasma system with a geometric swirl number of 6.7 was confirmed under sea level condition.

- It was observed that a shorter L-star of the thruster increased the characteristic exhaust velocity efficiency.

- For all SHP163 feed pressure, there were no failed ignition cases with a single-hole injector, and the stability combustion was confirmed under vacuum condition. It was found from the result that a maximum thrust of 0.37 N at nozzle expansion ratio of one was achieved with power consumption of 527 W and an SHP163 mass flow rate of 0.34 g/s, in conjunction with C-star efficiency of 98%.

- It was obtained the consumed power 2.4 W-Hr (564 W for 15 s) at 0.5 N-steady thrust was similar to preheating energy of catalyst, and the hot firing tests of the thruster was demonstrated the operation successfully under vacuum condition. Additionally, the ignition repeatability of this thruster was demonstrated.
- At the feed pressure of 0.6 MPa, a maximum thrust of 0.50 N was achieved with power consumption of

564 W and SHP163 mass flow rate of 0.31 g/s, in conjunction with specific impulse of 109 s, C-star efficiency with argon plasma of 41%, and thrust efficiency of 47%. In addition, it was confirmed that measured thrust was varied from 0.25 N to 0.50 N in a range of SHP163 mass flow rate from 0.09 g/s to 0.31 g/s.

- In terms of the combustion products of SHP163, the emission spectrums of carbon monoxide, swan band, hydroxyl radical, hydrogen atom, and oxygen atom were observed under vacuum condition.

- It was observed that the ignition of monopropellant using discharge plasma is strongly affected by the excitation and electron collision from the results of emission spectra.

- It was confirmed that the characteristic exhaust velocity efficiency tends to be higher at higher spectral intensity (e.g. OH).

- In terms of thruster lifetime-evaluation, at an accumulated firing time of 1646 s, no effect of electrode degradation on the performance of the thruster was observed.

Since this study, the green monopropellant propulsion with discharge plasma system has been proposed, evaluated the performance, and demonstrated under vacuum condition.

Publications

Peer-Reviewed Journal Papers

[1] Asato Wada, Hiroki Watanabe, and Haruki Takegahara, "Combustion Characteristics of a Hydroxylammonium-Nitrate-Based Monopropellant Thruster with Discharge Plasma System," *Journal of Propulsion and Power*. (Accepted for Publication)
doi: 10.2514/1.B36762

[2] 和田明哲，前田洋志，進藤崇央，渡邊裕樹，竹ヶ原春貴, "低毒性一液式推進剤を用いた1N級放電プラズマスラスタの燃焼室圧力評価," 日本航空宇宙学会論文集, Vol. 65, No.3, 2017, pp.117-122. (In Japanese)
doi: 10.2322/jjsass.65.117

[3] Asato Wada, Toshiaki Iizuka, Takahiro Shindo, Hiroshi Maeda, Hiroki Watanabe, and Haruki Takegahara, "Effect of Geometric Swirl Number of Discharge Plasma Catalyzer on Green Monopropellant Reaction Characteristics," *Transactions of The Japan Society for Aeronautical and Space Sciences, Aerospace Technology Japan*, Vol. 14, No. ists30, 2016, Pa_139-Pa_144.
doi: 10.2322/tastj.14.Pa_139

International Conference Proceedings

[1] ○Asato Wada, Hiroki Watanabe, and Haruki Takegahara, "Performance Evaluation of a Hydroxylammonium-Nitrate-Based Monopropellant Thruster with Discharge Plasma System," AIAA Propulsion and Energy Forum, AIAA 2017-4757, Atlanta, Georgia, July 2017.
doi: 10.2514/6.2017-4757

[2] ○Asato Wada, Toshiaki Iizuka, Takahiro Shindo, Shunsuke Kawabata, Hiroshi Maeda, Hiroki Watanabe, and Haruki Takegahara, "Effect of Geometric Swirl Number of Discharge Plasma Catalyzer on Green Monopropellant Reaction Characteristics," 30th International Symposium on Space Technology and Science (ISTS), Kobe, Japan, 10 July, 2015.

Domestic Conference Proceedings

[1] ○和田明哲，前田洋志，渡邊裕樹，竹ヶ原春貴, “放電プラズマシステムを用いた1N級HAN系一液式スラスタの基本性能評価,” 平成28年度宇宙輸送シンポジウム, STCP-2016-007, 相模原，2017年1月. (In Japanese)

[2] ○和田明哲，前田洋志，進藤崇央，渡邊裕樹，竹ヶ原春貴, “低毒性一液式推進剤を用いた1N級放電プラズマ点火スラスタの燃焼室圧力評価,” 第60回宇宙科学技術連合講演会，2I09, 函館，2016年9月. (In Japanese)

[3] ○和田明哲，前田洋志, 進藤崇央, 渡邊裕樹，竹ヶ原春貴，“低毒性一液式推進剤を用いた1N級プラズマロケットエンジンの真空燃焼試験,” 平成27年度宇宙輸送シンポジウム, STCP-2015-019, 相模原，2016年 1月. (In Japanese)

[4] ○和田明哲，飯塚俊明, 進藤崇央，河端駿典，前田洋志，渡邊裕樹，竹ヶ原春貴，“旋回強度がプラズマと低毒性一液式推進剤の燃焼反応に与える影響評価,” 平成26年度宇宙輸送シンポジウム, STCP-2014-042，相模原，2015年 1月. (In Japanese)

[5] ○和田明哲，飯塚俊明, 進藤崇央, 河端駿典，渡邊裕樹，竹ヶ原春貴, “低毒性推進剤のための放電プラズマ点火機構ガス供給方法の点火性能に与える影響評価,” 第58回宇宙科学技術連合講演会，JSASS-2014-4245，長崎，2014年 11月. (In Japanese)

[6] ○和田明哲，飯塚俊明, 進藤崇央, 佐藤雄太, 河端駿典，青柳潤一郎，竹ヶ原春貴，“低毒性推進剤を用いたRCS スラスタ用放電プラズマ型点火機構の基本性能,” 平成25年度宇宙輸送シンポジウム, STCP-2013-063，相模原，2014年 1月. (In Japanese)

Award

[1] 平成27年度宇宙輸送シンポジウム, STCP-2015-019, 優秀学生賞.

Other Journal Papers and Conference Proceedings

[1] Takahiro Shindo, Asato Wada, Hiroshi Maeda, Hiroki Watanabe, and Haruki Takegahara “Performance of a Green Propellant Thruster with Discharge Plasma,” *Acta Astronautica*, 131 (2017), pp.92-95. doi: 10.1016/j.actaastro.2016.11.022

[2] Takahiro Shindo, Asato Wada, Hiroshi Maeda, Hiroki Watanabe and Haruki Takegahara “Influence of Design Factors on the Thrust Performance of a Green Monopropellant Reaction System with Plasma,” *Transactions of the Japan Society for Aeronautical and Space Sciences*, 60 (2017), No.2, pp.103-108. doi: 10.2322/tjsass.60.103

[3] ○進藤崇央，和田明哲，前田洋志，渡邊裕樹，竹ヶ原春貴, “パルス放電による低毒性推進剤スラスタの燃焼室圧力計測,” 第60回宇宙科学技術連合講演会, 2I10, 函館，2016年 9月. (In Japanese)

[4] ○進藤崇央，和田明哲，前田洋志，渡邊裕樹，竹ヶ原春貴,“プラズマを用いたHAN 系推進剤反応機構の形状および放電形態による影響評価,” 2015年度宇宙輸送シンポジウム, STCP-2015-021, 相模原，2016年 1月. (In Japanese)

[5] ○Takahiro Shindo, Asato Wada, Shunsuke Kawabata, Hiroshi Maeda, Toshiaki Iizuka, Hiroki Watanabe, and Haruki Takegahara, “Fundamental Study on In-liquid Plasma of HAN based Propellant,” 30th International Symposium on Space Technology and Science (ISTS), 2015-a-70, Kobe, Japan, 10 July, 2015.

[6] ○Shuka Takeda, Toshiaki Iizuka, Asato Wada, Takahiro Shindo, Hiroki Watanabe, and Haruki Takegahara “Spectroscopic Evaluation on Induction of Chemical Reaction in Green Propellant RCS with Discharge Plasma Catalyzer,” 30th International Symposium on Space Technology and Science (ISTS), 2015-a-74, Kobe, Japan, 10 July, 2015.

[7] ○武田柊花，飯塚俊明，和田明哲，進藤崇央，河端駿典，渡邊裕樹，竹ヶ原春貴 “プラズマ化学推進器の化学反応誘起のための放電プラズマ分光評価,” 日本航空宇宙学会第46期年会講演会, JSASS-2015-1052, 2015年 4月. (In Japanese)

[8] 進藤崇央，和田明哲，河端駿典，前田洋志，飯塚俊明，渡邊裕樹，竹ヶ原春貴, “低毒性一液式推進剤を直接プラズマ化させ反応を誘起する機構の基本特性,” *Journal of IAPS*, Vol.22-2, 2014. (In Japanese)

[9] ○進藤崇央，和田明哲，河端駿典，前田洋志，渡邊裕樹，飯塚俊明，竹ヶ原春貴, “高周波放電プラズマによるHAN 系推進剤SHP163 の反応性評価,” 第58回宇宙科学技術連合講演会, 1J08, 長崎, 2014年 11月. (In Japanese)

[10] ○Toshiaki Iizuka, Takahiro Shindo, Asato Wada, Shunsuke Kawabata Yuta Sato, Junichiro Aoyagi, Haruki Takegahara, and Taiichi Nagata “Basic Characteristics of Discharge Plasma Ignition System for 1NClass RCS Thruster with Green Monopropellant,” 50thAIAA/ASME/SAE/ASEE Joint Propulsion Conference, Propulsion and Energy Forum, AIAA 2014-3885, 2014.
doi: 10.2514/6.2014-3885

[11] 飯塚俊明, 和田明哲，進藤崇央，河端駿典，青柳潤一郎，渡邊裕樹，竹ヶ原春貴，“低毒性推進剤のための放電プラズマ点火システムの基本性能およびガス種が点火性能に与える影響,” プラズマ応用科学，Vol. 22，No. 1，2014. (In Japanese)

[12] ○Takahiro Shindo, Toshiaki Iizuka, Asato Wada, Shunsuke Kawabata, Yuta Sato, Junichiro Aoyagi, Haruki Takegahara, and Taiichi Nagata, “Study on Discharge Plasma Ignition System for Green Monopropellant,” Space Propulsion 2014, Cologne, Germany, May 2014.

Appendix

Appendix A: Thermochemical Calculations for HAN-Based Monopropellant: SHP163

```
******************************************************************************

       NASA-GLENN CHEMICAL EQUILIBRIUM PROGRAM CEA2, MAY 21, 2004
                BY  BONNIE MCBRIDE AND SANFORD GORDON
    REFS: NASA RP-1311, PART I, 1994 AND NASA RP-1311, PART II, 1996

******************************************************************************



problem
   rocket  frozen  nfz=1
  p,bar=4,8,12,20,
  sup,ae/at=50,100,
react
  oxid=H2O(L) wt=6.2  t,k=298.15
  fuel=CH3OH(L) wt=16.3  t,k=298.15
  oxid=NH4NO3(IV) wt=3.9  t,k=298.15
  oxid=HAN  wt=73.6  t,k=298.15
    h,kj/mol=-366.5  N 2 H 4 O 4
end

OPTIONS: TP=F  HP=F  SP=F  TV=F  UV=F  SV=F  DETN=F  SHOCK=F  REFL=F  INCD=F
RKT=T  FROZ=T  EQL=F  IONS=F  SIUNIT=T  DEBUGF=F  SHKDBG=F  DETDBG=F  TRNSPT=F

TRACE= 0.00E+00  S/R= 0.000000E+00  H/R= 0.000000E+00  U/R= 0.000000E+00

Pc,BAR =    4.000000    8.000000   12.000000   20.000000

Pc/P =

SUBSONIC AREA RATIOS =

SUPERSONIC AREA RATIOS =   50.0000   100.0000

NFZ=  1  Mdot/Ac= 0.000000E+00  Ac/At= 0.000000E+00

   REACTANT        WT.FRAC   (ENERGY/R),K   TEMP,K  DENSITY
      EXPLODED FORMULA
O: H2O(L)         0.074074  -0.343773E+05   298.15  0.0000
       H  2.00000  O  1.00000
F: CH3OH(L)       1.000000  -0.287341E+05   298.15  0.0000
       C  1.00000  H  4.00000  O  1.00000
O: NH4NO3(IV)      0.046595  -0.439713E+05   298.15  0.0000
       N  2.00000  H  4.00000  O  3.00000
O: HAN            0.879331  -0.440796E+05   298.15  0.0000
       N  2.00000  H  4.00000  O  4.00000

 SPECIES BEING CONSIDERED IN THIS SYSTEM
(CONDENSED PHASE MAY HAVE NAME LISTED SEVERAL TIMES)
```

```
 LAST thermo.inp UPDATE:   9/09/04

 g 7/97  *C             tpis79  *CH            g 4/02  CH2
 g 4/02  CH3            g11/00  CH2OH          g 7/00  CH3O
 g 8/99  CH4            g 7/00  CH3OH          srd 01  CH3OOH
 g 8/99  *CN            g12/99  CNN           tpis79  *CO
 g 9/99  *CO2           tpis91  COOH           tpis91  *C2
 g 6/01  C2H            g 1/91  C2H2,acetylene   g 5/01  C2H2,vinylidene
 g 4/02  CH2CO,ketene     g 3/02  O(CH)2O         srd 01  HO(CO)2OH
 g 7/01  C2H3,vinyl       g 9/00  CH3CN          g 6/96  CH3CO,acetyl
 g 1/00  C2H4           g 8/88  C2H4O,ethylen-o  g 8/88  CH3CHO,ethanal
 g 6/00  CH3COOH         srd 01  OHCH2COOH       g 7/00  C2H5
 g 7/00  C2H6           g 8/88  CH3N2CH3        g 8/88  C2H5OH
 g 7/00  CH3OCH3         srd 01  CH3O2CH3        g 7/00  CCN
 tpis91  CNC            srd 01  OCCN           tpis79  C2N2
 g 8/00  C2O            tpis79  *C3            n 4/98  C3H3,1-propynl
 n 4/98  C3H3,2-propynl   g 2/00  C3H4,allene      g 1/00  C3H4,propyne
 g 5/90  C3H4,cyclo-      g 3/01  C3H5,allyl       g 2/00  C3H6,propylene
 g 1/00  C3H6,cyclo-      g 6/01  C3H6O,propylox   g 6/97  C3H6O,acetone
 g 1/02  C3H6O,propanal   g 7/01  C3H7,n-propyl    g 9/85  C3H7,i-propyl
 g 2/00  C3H8           g 2/00  C3H8O,1propanol  g 2/00  C3H8O,2propanol
 srd 01  CNCOCN          g 7/88  C3O2            g tpis  *C4
 g 7/01  C4H2,butadiyne   g 8/00  C4H4,1,3-cyclo-  n10/92  C4H6,butadiene
 n10/93  C4H6,1butyne     n10/93  C4H6,2butyne     g 8/00  C4H6,cyclo-
 n 4/88  C4H8,1-butene    n 4/88  C4H8,cis2-buten  n 4/88  C4H8,tr2-butene
 n 4/88  C4H8,isobutene   g 8/00  C4H8,cyclo-      g10/00  (CH3COOH)2
 n10/84  C4H9,n-butyl     n10/84  C4H9,i-butyl     g 1/93  C4H9,s-butyl
 g 1/93  C4H9,t-butyl     g12/00  C4H10,n-butane   g 8/00  C4H10,isobutane
 g 6/01  C4N2           g 8/00  *C5            g 5/90  C5H6,1,3cyclo-
 g 1/93  C5H8,cyclo-      n 4/87  C5H10,1-pentene  g 2/01  C5H10,cyclo-
 n10/84  C5H11,pentyl     g 1/93  C5H11,t-pentyl   n10/85  C5H12,n-pentane
 n10/85  C5H12,i-pentane  n10/85  CH3C(CH3)2CH3    g 2/93  C6H2
 g11/00  C6H5,phenyl      g 8/00  C6H5O,phenoxy    g 8/00  C6H6
 g 8/00  C6H5OH,phenol    g 1/93  C6H10,cyclo-     n 4/87  C6H12,1-hexene
 g 6/90  C6H12,cyclo-     n10/83  C6H13,n-hexyl    g 6/01  C6H14,n-hexane
 g 7/01  C7H7,benzyl      g 1/93  C7H8           g12/00  C7H8O,cresol-mx
 n 4/87  C7H14,1-heptene  n10/83  C7H15,n-heptyl   n10/85  C7H16,n-heptane
 n10/85  C7H16,2-methylh  n 4/89  C8H8,styrene     n10/86  C8H10,ethylbenz
 n 4/87  C8H16,1-octene   n10/83  C8H17,n-octyl    n 4/85  C8H18,n-octane
 n 4/85  C8H18,isooctane  n10/83  C9H19,n-nonyl    g 3/01  C10H8,naphthale
 n10/83  C10H21,n-decyl   g 8/00  C12H9,o-bipheny  g 8/00  C12H10,biphenyl
 g 6/97  *H             g 6/01  HCN            g 1/01  HCO
 tpis89  HCCN           g 6/01  HCCO           g 6/01  HNC
 g 7/00  HNCO           g10/01  HNO            tpis89  HNO2
 g 5/99  HNO3           g 4/02  HO2            tpis78  *H2
 g 5/01  HCHO,formaldehy  g 6/01  HCOOH          g 8/89  H2O
 g 6/99  H2O2           g 6/01  (HCOOH)2        g 5/97  *N
 g 6/01  NCO            g 4/99  *NH            g 3/01  NH2
 tpis89  NH3            tpis89  NH2OH          tpis89  *NO
 g 4/99  NO2            j12/64  NO3            tpis78  *N2
 g 6/01  NCN            g 5/99  N2H2           tpis89  NH2NO2
 g 4/99  N2H4           g 4/99  N2O            g 4/99  N2O3
 tpis89  N2O4           g 4/99  N2O5           tpis89  N3
 g 4/99  N3H            g 5/97  *O            g 4/02  *OH
 tpis89  *O2            g 8/01  O3            n 4/83  C(gr)
 n 4/83  C(gr)          n 4/83  C(gr)          g11/99  H2O(cr)
 g 8/01  H2O(L)         g 8/01  H2O(L)

O/F =   5.134969

                    EFFECTIVE FUEL     EFFECTIVE OXIDANT       MIXTURE
ENTHALPY                 h(2)/R             h(1)/R             h0/R
(KG-MOL)(K)/KG      -0.89676769E+03    -0.57052262E+03    -0.62370057E+03

KG-FORM.WT./KG            bi(2)              bi(1)              b0i
 *H                0.12483670E+00     0.47174436E-01     0.59833385E-01
```

```
 *O                0.31209174E-01     0.42480578E-01     0.40643339E-01
 *C                0.31209174E-01     0.00000000E+00     0.50870954E-02
 *N                0.00000000E+00     0.19475482E-01     0.16300978E-01

POINT ITN     T          H          O          C          N

  1   23    2315.657    -11.738    -16.229    -21.332    -13.874
```

THEORETICAL ROCKET PERFORMANCE ASSUMING FROZEN COMPOSITION

Pin = 58.0 PSIA
CASE =

	REACTANT	WT FRACTION (SEE NOTE)	ENERGY KJ/KG-MOL	TEMP K
OXIDANT	H2O(L)	0.0740741	-285830.088	298.150
FUEL	CH3OH(L)	1.0000000	-238910.001	298.150
OXIDANT	NH4NO3(IV)	0.0465950	-365600.003	298.150
OXIDANT	HAN	0.8793309	-366500.000	298.150

O/F= 5.13497 %FUEL= 16.300000 R,EQ.RATIO= 0.986407 PHI,EQ.RATIO= 0.965065

	CHAMBER	THROAT	EXIT	EXIT
Pinf/P	1.0000	1.7722	767.73	1965.24
P, BAR	4.0000	2.2571	0.00521	0.00204
T, K	2315.66	2106.61	649.02	522.29
RHO, KG/CU M	4.7385-1	2.9391-1	2.2022-3	1.0690-3
H, KJ/KG	-5185.76	-5646.72	-8470.20	-8670.24
U, KJ/KG	-6029.92	-6414.68	-8706.80	-8860.64
G, KJ/KG	-32666.0	-30646.2	-16172.2	-14868.4
S, KJ/(KG)(K)	11.8672	11.8672	11.8672	11.8672
M, (1/n)	22.808	22.808	22.808	22.808
Cp, KJ/(KG)(K)	2.2262	2.1828	1.6108	1.5465
GAMMAs	1.1958	1.2005	1.2925	1.3084
SON VEL,M/SEC	1004.7	960.2	553.0	499.1
MACH NUMBER	0.000	1.000	4.635	5.289

PERFORMANCE PARAMETERS

Ae/At	1.0000	50.000	100.00
CSTAR, M/SEC	1417.4	1417.4	1417.4
CF	0.6774	1.8082	1.8625
Ivac, M/SEC	1760.0	2655.3	2712.0
Isp, M/SEC	960.2	2563.0	2639.9

MOLE FRACTIONS

*CO	0.00679	*CO2	0.10924	*H	0.00045
*H2	0.00738	H2O	0.67098	*NO	0.00176
*N2	0.18501	*O	0.00028	*OH	0.00750
*O2	0.01060				

* THERMODYNAMIC PROPERTIES FITTED TO 20000.K

PRODUCTS WHICH WERE CONSIDERED BUT WHOSE MOLE FRACTIONS
WERE LESS THAN 5.000000E-06 FOR ALL ASSIGNED CONDITIONS

NOTE. WEIGHT FRACTION OF FUEL IN TOTAL FUELS AND OF OXIDANT IN TOTAL OXIDANTS

POINT	ITN	T	H	O	C	N
1	3	2332.798	-11.503	-15.944	-21.089	-13.539

THEORETICAL ROCKET PERFORMANCE ASSUMING FROZEN COMPOSITION

Pin = 116.0 PSIA
CASE =

	REACTANT	WT FRACTION (SEE NOTE)	ENERGY KJ/KG-MOL	TEMP K
OXIDANT	H2O(L)	0.0740741	-285830.088	298.150
FUEL	CH3OH(L)	1.0000000	-238910.001	298.150
OXIDANT	NH4NO3(IV)	0.0465950	-365600.003	298.150
OXIDANT	HAN	0.8793309	-366500.000	298.150

O/F= 5.13497 %FUEL= 16.300000 R,EQ.RATIO= 0.986407 PHI,EQ.RATIO= 0.965065

	CHAMBER	THROAT	EXIT	EXIT
Pinf/P	1.0000	1.7717	763.61	1952.90
P, BAR	8.0000	4.5155	0.01048	0.00410
T, K	2332.80	2122.96	657.97	530.05
RHO, KG/CU M	9.4225-1	5.8441-1	4.3749-3	2.1235-3
H, KJ/KG	-5185.76	-5649.24	-8493.84	-8696.21
U, KJ/KG	-6034.80	-6421.90	-8733.31	-8889.13
G, KJ/KG	-32280.5	-30306.8	-16135.9	-14852.5
S, KJ/(KG)(K)	11.6147	11.6147	11.6147	11.6147
M, (1/n)	22.845	22.845	22.845	22.845
Cp, KJ/(KG)(K)	2.2296	2.1867	1.6148	1.5496
GAMMAs	1.1951	1.1997	1.2910	1.3070
SON VEL,M/SEC	1007.3	962.8	556.0	502.1
MACH NUMBER	0.000	1.000	4.626	5.277

PERFORMANCE PARAMETERS

Ae/At	1.0000	50.000	100.00
CSTAR, M/SEC	1421.8	1421.8	1421.8
CF	0.6771	1.8091	1.8636
Ivac, M/SEC	1765.3	2665.3	2722.5
Isp, M/SEC	962.8	2572.2	2649.7

MOLE FRACTIONS

*CO	0.00566	*CO2	0.11055	*H	0.00032
*H2	0.00605	H2O	0.67395	*NO	0.00174
*N2	0.18532	*O	0.00021	*OH	0.00656
*O2	0.00963				

* THERMODYNAMIC PROPERTIES FITTED TO 20000.K

PRODUCTS WHICH WERE CONSIDERED BUT WHOSE MOLE FRACTIONS
WERE LESS THAN 5.000000E-06 FOR ALL ASSIGNED CONDITIONS

NOTE. WEIGHT FRACTION OF FUEL IN TOTAL FUELS AND OF OXIDANT IN TOTAL OXIDANTS

POINT	ITN	T	H	O	C	N
1	3	2341.871	-11.368	-15.776	-20.957	-13.343

THEORETICAL ROCKET PERFORMANCE ASSUMING FROZEN COMPOSITION

Pin = 174.0 PSIA
CASE =

	REACTANT	WT FRACTION (SEE NOTE)	ENERGY KJ/KG-MOL	TEMP K
OXIDANT	H2O(L)	0.0740741	-285830.088	298.150
FUEL	CH3OH(L)	1.0000000	-238910.001	298.150
OXIDANT	NH4NO3(IV)	0.0465950	-365600.003	298.150
OXIDANT	HAN	0.8793309	-366500.000	298.150

O/F= 5.13497 %FUEL= 16.300000 R,EQ.RATIO= 0.986407 PHI,EQ.RATIO= 0.965065

	CHAMBER	THROAT	EXIT	EXIT
Pinf/P	1.0000	1.7714	761.44	1946.42
P, BAR	12.000	6.7742	0.01576	0.00617
T, K	2341.87	2131.62	662.73	534.18
RHO, KG/CU M	1.4091 0	8.7392-1	6.5393-3	3.1738-3
H, KJ/KG	-5185.76	-5650.57	-8506.33	-8709.95
U, KJ/KG	-6037.37	-6425.72	-8747.33	-8904.20
G, KJ/KG	-32040.4	-30094.2	-16105.9	-14835.5
S, KJ/(KG)(K)	11.4672	11.4672	11.4672	11.4672
M, (1/n)	22.864	22.864	22.864	22.864
Cp, KJ/(KG)(K)	2.2315	2.1887	1.6169	1.5512
GAMMAs	1.1947	1.1993	1.2902	1.3062
SON VEL,M/SEC	1008.7	964.2	557.6	503.7
MACH NUMBER	0.000	1.000	4.622	5.271

PERFORMANCE PARAMETERS

Ae/At	1.0000	50.000	100.00
CSTAR, M/SEC	1424.2	1424.2	1424.2
CF	0.6770	1.8095	1.8642
Ivac, M/SEC	1768.1	2670.6	2728.0
Isp, M/SEC	964.2	2577.0	2654.9

MOLE FRACTIONS

*CO	0.00505	*CO2	0.11126	*H	0.00025
*H2	0.00535	H2O	0.67552	*NO	0.00173
*N2	0.18549	*O	0.00017	*OH	0.00605
*O2	0.00912				

* THERMODYNAMIC PROPERTIES FITTED TO 20000.K

PRODUCTS WHICH WERE CONSIDERED BUT WHOSE MOLE FRACTIONS
WERE LESS THAN 5.000000E-06 FOR ALL ASSIGNED CONDITIONS

NOTE. WEIGHT FRACTION OF FUEL IN TOTAL FUELS AND OF OXIDANT IN TOTAL OXIDANTS

POINT	ITN	T	H	O	C	N
1	3	2352.307	-11.201	-15.562	-20.803	-13.095

THEORETICAL ROCKET PERFORMANCE ASSUMING FROZEN COMPOSITION

Pin = 290.1 PSIA
CASE =

	REACTANT	WT FRACTION (SEE NOTE)	ENERGY KJ/KG-MOL	TEMP K
OXIDANT	H2O(L)	0.0740741	-285830.088	298.150
FUEL	CH3OH(L)	1.0000000	-238910.001	298.150
OXIDANT	NH4NO3(IV)	0.0465950	-365600.003	298.150
OXIDANT	HAN	0.8793309	-366500.000	298.150

O/F= 5.13497 %FUEL= 16.300000 R,EQ.RATIO= 0.986407 PHI,EQ.RATIO= 0.965065

	CHAMBER	THROAT	EXIT	EXIT
Pinf/P	1.0000	1.7711	758.97	1939.01
P, BAR	20.000	11.292	0.02635	0.01031
T, K	2352.31	2141.58	668.23	538.96
RHO, KG/CU M	2.3404 0	1.4514 0	1.0855-2	5.2680-3
H, KJ/KG	-5185.76	-5652.09	-8520.69	-8725.73
U, KJ/KG	-6040.33	-6430.10	-8763.45	-8921.53
G, KJ/KG	-31723.3	-29812.3	-16059.3	-14806.0
S, KJ/(KG)(K)	11.2815	11.2815	11.2815	11.2815
M, (1/n)	22.887	22.887	22.887	22.887
Cp, KJ/(KG)(K)	2.2336	2.1910	1.6194	1.5532
GAMMAs	1.1942	1.1988	1.2892	1.3053
SON VEL,M/SEC	1010.2	965.7	559.4	505.5
MACH NUMBER	0.000	1.000	4.616	5.263

PERFORMANCE PARAMETERS

Ae/At	1.0000	50.000	100.00
CSTAR, M/SEC	1426.8	1426.8	1426.8
CF	0.6768	1.8100	1.8648
Ivac, M/SEC	1771.3	2676.6	2734.4
Isp, M/SEC	965.7	2582.6	2660.8

MOLE FRACTIONS

*CO	0.00434	*CO2	0.11209	*H	0.00019
*H2	0.00455	H2O	0.67733	*NO	0.00171
*N2	0.18568	*O	0.00014	*OH	0.00544
*O2	0.00853				

* THERMODYNAMIC PROPERTIES FITTED TO 20000.K

PRODUCTS WHICH WERE CONSIDERED BUT WHOSE MOLE FRACTIONS
WERE LESS THAN 5.000000E-06 FOR ALL ASSIGNED CONDITIONS

NOTE. WEIGHT FRACTION OF FUEL IN TOTAL FUELS AND OF OXIDANT IN TOTAL OXIDANTS